Photophysical Studies of Beta Phase Formation in Poly(9,9-di-n-alkylfluorenes)

BRIGHT, DANIEL,WILLIAM

Photophysical Studies of Beta Phase Formation in Poly(9,9-di-*n*-alkylfluorenes)

Daniel William Bright

Abstract

The photophysical changes that take place in Poly(9,9-di-*n*-alkylfluorenes) upon formation of the beta phase in methylcyclohexane solution are observed by optical spectroscopy. The equilibrium absorption spectra as a function of temperature show that conformational changes occur for all five polymers studied, from the hexyl (PF6) to decyl (PF10) side chains. The spectroscopic indicators of beta phase formation are not observed in PF6, and the trend of beta phase formation efficacy shows an optimal side chain length of 8 carbons. The beta phase formation in PF8, PF9 and PF10 is modelled using a previously reported aggregation model, with limited success.

A mechanism for the beta phase formation is proposed, where the interactions between the alkyl side chains provide the chemical energy to overcome the activation energy barrier to planarise the polymer backbone, leading to the extended conjugation length that characterises the beta phase. Excitation spectra show that the beta phase can occur reversibly in dilute solution, most likely by chain folding leading to side chain interactions. The presence of side chain interactions is confirmed by evidence of a PF7-PF9 alternating structure formed in a mixed solution.

The same trend of beta phase formation is observed in thin films of these polymers after thermal cycling and warm toluene vapour exposure, showing that side chain interactions are also required for beta phase formation in the solid state. Spectra of PF8 films with controlled keto content show that the energy transfer to the keto sites is mediated by migration, indicating that the beta phase is formed in domains rather than isolated chains, a result which is consistent with the side chain interaction model and other published results. The fraction of beta phase formed is shown to decrease linearly with a greater content of dibenzothiophene (DBT) co-monomer units, up to a cut-off limit of 20%. A statistical model of the distribution of DBT units in the chain is used to find a conjugation length of 9 monomer units, in contrast to a previous estimate but in agreement with the persistence length of PF8 in toluene.

These results characterise the beta phase formation mechanism and its effects on the photophysical properties of Poly(9,9-di-*n*-alkylfluorenes), which is under widespread investigation for more use in efficient blue and white organic LED applications.

Photophysical Studies of Beta Phase Formation in Poly(9,9-di-n-alkylfluorenes)

Daniel William Bright

Department of Physics

Durham University

A thesis submitted to the Faculty of Science at Durham University for the degree of Doctor of Philosophy

January 2011

Declaration

All material contained in this thesis is original and is the result of my own work except where explicit reference is made to the work of others.

This thesis has not been submitted in whole or in part for the award of a degree at this or any other university

Acknowledgements

Grateful thanks go to the assistance of: Prof. Andy Monkman for wisdom and guidance, Dr Fernando Dias and Dr Konstantinos Bourdakos for help and advice, Helen and Ed for putting up with my jokes, and Norman and Davey for knowing how to fix everything. Thanks also to Kieran Kamtekar, Katy Moss, and Prof. Martin Bryce for making most of the compounds used in this work.

Thanks most of all to my lovely wife Aimée, just for being her.

Publications

Work from this thesis has been published by the author:

Bright, D. W.; Dias, F. B.; Galbrecht, F.; Scherf, U.; Monkman, A. P. "The Influence of Alkyl-Chain Length on Beta-Phase Formation in Polyfluorenes" *Advanced Functional Materials* **2009**, 19, (1), 67-73.

Bright, D. W.; Galbrecht, F.; Scherf, U.; Monkman, A. "β Phase Formation in Poly(9,9-di-n-decylfluorene) Thin Films" *Macromolecules* **2010**, 43, (18), 7860-7863.

Bright, D.W.; Moss, K. C.; Kamtekar, K. T.; Bryce, M. R.; Monkman, A. P. "The β Phase Formation Limit in Two Poly(9,9-di-n-octylfluorene) based Copolymers" *Macromolecular Rapid Communications* DOI: 10.1002/marc.201100221

Index of Figures and Tables

Glossary

DBT: dibenzothiophene (see chapter 7.2 p139).

Exciton: an excited state formed by a bound electron-hole pair before recombination to release the excited state energy. See chapter 2.3 p9.

Fluorescence Lifetime: the time taken for the intensity of emission from a sample to decay to (1/e) or 36.8% of its initial value after excitation has ceased.

HOMO: the Highest Occupied Molecular Orbital.

Keto: fluorenone (figure 3-2), an oxygen defect formed on the bridging atom of the fluorene unit.

LUMO: the Lowest Unoccupied Molecular Orbital.

MCH: methylcyclohexane, an aliphatic organic solvent.

PF8: Poly(9,9-dioctylfluorene), a fluorescent blue semiconducting polymer. See figure 3-1 p28.

S unit: dibenzothiophene-*S,S*-dioxide (figure 7-1 p140).

Saturated blue: a blue colour with narrow spectral width that can be used as part of a red-green-blue display to show the entire range of visible colours.

TCSPC: Time-Correlated Single Photon Counting, a method for determining fluorescence lifetimes.

1 Introduction

Modern lifestyles and technologies are dependent upon electric lighting, and increasingly dependent upon emissive displays, such as televisions, computer monitors, and mobile telephones. The increasing popularity of mobile devices in particular has made efficiency of displays a particularly important goal, and the goal of efficiency now also applies to lighting due to concerns about the impact of energy consumption on the environment.

Advances in lighting efficiency from its origins of the filament light bulb have come in the form of the invention of the sodium lamp and fluorescent tube lighting. However, these light sources suffer from a lack of spectral bandwidth, leaving colours oddly altered by this illumination. The filament bulb still maintains popularity for its ability to render colours in a similar fashion to sunlight, the obvious standard against which lighting quality is compared. Research now targets an efficient lighting source that provides a good quality light, measurable by scales such as the colour rendering index (CRI), in order to produce a spectrum close to sunlight.

A recent and promising research area for both efficient displays and efficient white lighting is that of organic light-emitting diodes (OLEDs). The field became prominent after the discovery of efficient organic electroluminescence from small molecules by Tang and van Slyke in 1987.[1] They used a two-layer structure of *tris*-(8-hydroxyquinolinato)aluminium (Alq_3) as the emission layer and 1,10-bis(di-4-tolylaminophenyl) cyclohexane (TAPC) as a charge transport layer. Electrons were injected though a 10:1 magnesium-silver alloy electrode and holes were injected through a transparent layer of conductive indium-tin oxide (ITO), leading to green emission at operating voltages above 2.5V, with up to 1% quantum efficiency (the ratio of emitted photons to injected electrons). This was a great improvement over the previous emission from anthracene where driving voltages of up to 10000V were required for bright emission.[2]

The use of disordered organic polymers followed in 1990 from Cambridge, by Burroughes et al.[3] They used a single layer of a conjugated polymer formed *in situ* from a spin-coated solution of chemical precursor, between an aluminium cathode and a glass substrate coated with indium oxide, a transparent conductor. However, in this polymer device the quantum efficiency was just 0.05% and it required 14V to emit visible light.

Since the initial demonstrations of the technology, research in this field has expanded dramatically, with many discoveries made about the underlying physics of both the small molecules[4-5] and polymers.[5-6] Polymers are potentially superior to small molecules based on their suitability for use solution-based manufacturing methods such as ink-jet printing as opposed to thermal evaporation of small molecules which is less easily implemented in manufacturing.[7] Both these approaches are still being pursued, as small molecules currently hold an advantage in terms of device efficiency over the more easily manufactured polymer devices.[8-9]

Development of a deeper understanding of the device physics proceeded swiftly. The importance of charge recombination became apparent; early devices with a single organic layer often displayed higher charge mobility for electrons than for holes, resulting in a high “dark current” of electrons which did not produce light emission. A critical factor for efficient devices is balancing the transport of positive and negative charges.[10] The use of multiple layers was soon adopted, which allows the energy levels of intermediate conductive layers to be suitably selected so as not to impede the motion of the charges. This allows control of the motion of the charge carriers to an interface in the emissive layer, where high charge densities are built up and the probability of charge recombination is greatly enhanced.[11]

Even when charge carriers meet, the emission of light is still not certain. Bound excitons are created when holes move into the Coulomb capture radius of excited state electrons, which can pair with parallel and anti-parallel spins, and these excitons may migrate through the material before finally

recombining to release the energy. Ultra pure materials are therefore needed to prevent the excitons migrating to impurities and releasing heat rather than light.

Once durable emissive materials had been developed, and the understanding of device physics had proceeded sufficiently far, development of commercial displays began. Manufacturing processes have progressed to the point that excellent results can be obtained, and small commercial screens are already in use for mobile devices such as mobile phones, digital cameras and mp4 players. A sample 11-inch Sony television using Organic Light Emitting Diodes (OLED) was also recently sold, but the production run was limited and served mostly to promote the potential of the technology.[12]

In order to be commercially successful, the requirements for OLED displays are stringent. Not only must they function well as a display, but they must also offer additional advantages to displace current technologies, such as thin-film transistor (TFT) displays. It is hoped that OLED displays will achieve this by incorporating superior power efficiency with a very high picture quality through better contrast ratios, which are a result of direct emission that allows black pixels to be switched off completely. The remaining technical issues for organic displays are centred around blue light emission and large panels. Blue emitters provide two challenges: the energetic photons emitted degrade the emissive layer itself, and it has been difficult to generate the “saturated” deep blue colour which has the spectrally narrow emission in the blue region that is required to allow red-green-blue displays to render the visible range of colours. There are also difficulties with large area displays, but these are an engineering and quality control issue related to the new manufacturing technologies.

In the course of the development of OLED devices, the electroluminescent materials themselves have proven a complex and critical factor. Conjugated carbon-based chemical systems containing alternating single and double bonds can be synthesised with an extraordinary range of structures. Much work has looked at polymers incorporating phenyl rings into the polymer backbone, which tend to emit in the visible spectrum. The simplest, poly(*para*-phenylene) (PPP) is simply a group of

phenyl rings bonded by carbon-carbon bonds between rings, and is a blue emitter.[13] Poly(phenylene vinylene)s (PPV) alternate phenyl rings with carbon-carbon single and double bonds between rings, often with solubilising side chains and functional groups bonded to the main chain. These materials are emissive in the yellow-red part of the visible spectrum,[14] and show strong variations in emissive properties which depend upon the nanoscale arrangement of the polymer.[15] Another common type is poly(fluorene) (PF), which is based upon PPP but alternate pairs of phenyl rings are bonded by a carbon bridge, which can be substituted with side chains for improved solubility.[16] This is related to another type of polymer where all the phenyl rings are held planar by multiple carbon bridges, ladder-type poly(*para*-phenylene) (LPPP), which is also emissive in the blue region.[17]

Figure 1-1: Structures of some emissive conjugated polymers: a) PPV, b) PPP, c) PF8 (a variant of PF with octyl side chains) and d) a variant of LPPP, many other types have been produced with different sets of substituted side chains.

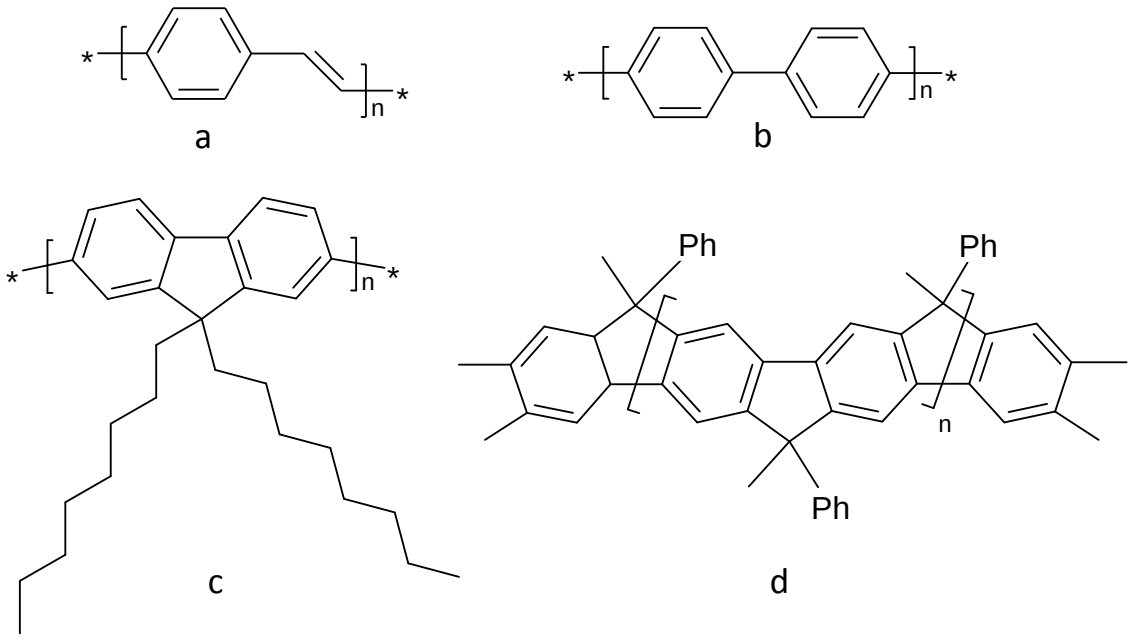

The polymers PF and LPPP show an interesting effect of the polymer microstructure on the material photophysics; whilst the PF polymer backbone is mostly planar, it is able to twist around the polymer chain axis, whereas LPPP is fixed fully planar.[18] The absorption and emission of PF are broad, while

these spectra of LPPP are narrow and sharp, with better resolution of the vibrational replicas in the spectra.

This work aims to contribute further to the understanding of device physics. It focuses on a blue emitting polymer which undergoes a phase transformation in certain circumstances which produces a more saturated blue light under electroluminescence, within the requirements for saturated blue emission in displays, and when incorporated into devices is more efficient than the normal disordered phase. Poly(9,9-di-*n*-octylfluorene) (PFO or PF8) is a well-studied polymer[19] with good stability in terms of colour emission and lifetime[16, 20] which upon slowly cooling is known to change to a more planar configuration termed the beta phase, in both solutions and thin films.[21] There are conflicting theories on how the phase change occurs, whether by an initial planarization step before aggregation[22] or by firstly aggregating and then becoming planarised.[23] By carrying out temperature controlled optical spectroscopy on a series of polymers related to PF8 but with different lengths of linear side chains, it will be shown that the formation of beta phase is dependent upon the interactions of the side chains, and that either aggregation or chain folding can lead to its formation.

Chapter two covers theoretical background to the physics of organic light emission from conjugated polymers. Chapter three describes the details of the experimental methods used in this work, from absorption spectrophotometry and photoluminescence, to time resolved spectra and fluorescence decay measurements, as well as details of sample preparation. Chapter four includes an overview of literature detailing the main investigations into the formation of the beta phase in poly(9,9-di-*n*-octylfluorene) (PF8). It gives the results of the experiments on the temperature dependence of the formation of beta phase in polyfluorene solutions with linear alkyl side chains of length n=6-10, showing that the side chains are fundamental to the formation of the beta phase. There is a trend in formation efficacy with n=8 being optimal, and the process is shown to be more complex than simple aggregation. Chapter 5 describes the results of attempting to induce beta phase in thin films of this polyfluorene series. The effectiveness of inducing the beta phase from thermal cycling and

toluene vapour exposure is investigated, and the vibrational modes within the films are characterised to show a similar trend in the efficacy of beta phase formation to that found in solution. Chapter 6 presents steady-state and time-resolved spectroscopy of PF8 with controlled concentrations of the keto oxygen defect. Investigations of the energy transfer to the keto defect from the alpha and beta phases finds that the energy transfer to the keto in films is migration controlled, and in films containing beta phase the transfer always proceeds via the beta phase as an intermediate step. Chapter 7 details work carried out on various copolymers of PF8 with a series of concentrations of different co-monomers to explore the limit at which the beta phase can form, showing an upper limit in the region of 20% of co-monomers. The conclusions of this thesis are given in chapter 8.

1.1 References

1. Tang, C. W.; Vanslyke, S. A. *Appl. Phys. Lett.* **1987,** 51, (12), 913-915.
2. Helfrich, W.; Schneider, W. G. *Phys. Rev. Lett.* **1965,** 14, (7), 229-231.
3. Burroughes, J. H.; Bradley, D. D. C.; Brown, A. R.; Marks, R. N.; Mackay, K.; Friend, R. H.; Burn, P. L.; Holmes, A. B. *Nature* **1990,** 347, 539-541.
4. Misra, A.; Kumar, L.; Kumar, P.; Dhawan, S. K.; Kamalasanan, M. N.; Chandra, S. *Indian J. Pure Appl. Phys.* **2004,** 42, (11), 793-805.
5. Mitschke, U.; Bauerle, P. *J. Mater. Chem.* **2000,** 10, (7), 1471-1507.
6. Friend, R. H.; Gymer, R. W.; Holmes, A. B.; Burroughes, J. H.; Marks, R. N.; Taliani, C.; Bradley, D. D. C.; Dos Santos, D. A.; Bredas, J. L.; Logdlund, M.; Salaneck, W. R. *Nature* **1999,** 397, (6715), 121-128.
7. Bharathan, J.; Yang, Y. *Appl. Phys. Lett.* **1998,** 72, (21), 2660-2662.
8. Reineke, S.; Lindner, F.; Schwartz, G.; Seidler, N.; Walzer, K.; Lussem, B.; Leo, K. *Nature* **2009,** 459, (7244), 234-U116.
9. Li, Y. J.; Sasabe, H.; Su, S. J.; Tanaka, D.; Takeda, T.; Pu, Y. J.; Kido, J. *Chem. Lett.* **2010,** 39, (2), 140-141.
10. Scott, J. C.; Karg, S.; Carter, S. A. *J. Appl. Phys.* **1997,** 82, (3), 1454-1460.
11. Martin, S. J.; Verschoor, G. L. B.; Webster, M. A.; Walker, A. B. *Organ. Electron.* **2002,** 3, (3-4), 129-141.
12. Sony Corporation OLED TV is Born. http://www.sonystyle.com/webapp/wcs/stores/servlet/CategoryDisplay?catalogId=10551&storeId=10151&langId=-1&identifier=S_BrandShowcase_OLED (05/10/2010),
13. Grem, G.; Leditzky, G.; Ullrich, B.; Leising, G. *Adv. Mater.* **1992,** 4, (1), 36-37.
14. Nguyen, T. Q.; Martini, I. B.; Liu, J.; Schwartz, B. J. *J. Phys. Chem. B* **2000,** 104, (2), 237-255.
15. Collison, C. J.; Rothberg, L. J.; Treemaneekarn, V.; Li, Y. *Macromol.* **2001,** 34, (7), 2346-2352.
16. Leclerc, M. *J. Polym. Sci. A-Polym. Chem.* **2001,** 39, (17), 2867--2873.
17. Grem, G.; Paar, C.; Stampfl, J.; Leising, G.; Huber, J.; Scherf, U. *Chem. Mater.* **1995,** 7, (1), 2-4.
18. Kim, D. Y.; Cho, H. N.; Kim, C. Y. *Prog. Polym. Sci.* **2000,** 25, (8), 1089-1139.
19. Neher, D. *Macromol. Rapid Commun.* **2001,** 22, (17), 1366-1385.
20. Grice, A. W.; Bradley, D. D. C.; Bernius, M. T.; Inbasekaran, M.; Wu, W. W.; Woo, E. P. *Appl. Phys. Lett.* **1998,** 73, (5), 629-631.
21. Grell, M.; Bradley, D. D. C.; Long, X.; Chamberlain, T.; Inbasekaran, M.; Woo, E. P.; Soliman, M. *Acta Polym.* **1998,** 49, (8), 439-444.
22. Winokur, M. J.; Slinker, J.; Huber, D. L. *Phys. Rev. B* **2003,** 67, 184106.
23. Dias, F. D.; Morgado, J.; Macanita, A. L.; Costa, F. P.; Burrows, H. D.; Monkman, A. P. *Macromol.* **2006,** 39, 5854-5864.

2 Theory

2.1 Bonding in Conjugated Polymers

2.1.1 Atomic Orbitals

The orbital model of electrons bound in a nucleus uses a complex wavefunction to describe the electron properties. The modulus of this wavefunction over the volume of the atom describes the probability that the electron will be found at any point in space.

A different wavefunction describes each of the electron states, characterised by four quantum numbers n, l, m_l and m_s. The number n corresponds to the energy level, whilst l (lower case L) represents the angular momentum, with integer values between n-1 and 0. The number m_l is the angular momentum z- axis projection, which can take integers between -l and +l, whilst m_s, the spin z-axis projection, can be +½ or -½ only for electrons. The Pauli Exclusion Principle states that only one electron can occupy each quantum state within the same atom or molecule, so the electrons within a many-electron atom occupy the lowest possible energy configuration by pairing up with anti-parallel spins within the lowest energy orbitals. In spectroscopic notation, orbitals with quantum number l=0 are called s orbitals and those with l=1 are called p orbitals. There are three different p orbitals corresponding to m_l=-1, 0 and +1, which are degenerate (at the same energy) and called p_x, p_y and p_z referring to the arbitrary Cartesian axes. The s and p orbitals are shown in figure 2-1.

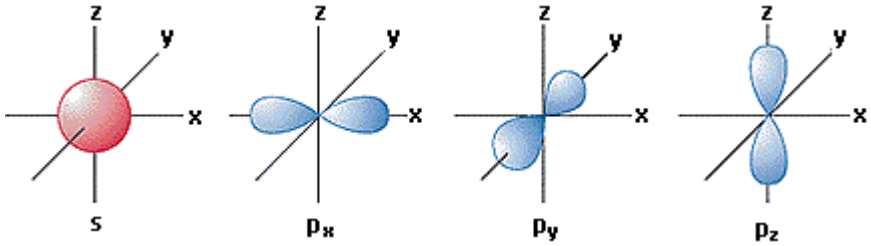

Figure 2-1: illustration of the *s* and *p* atomic orbitals for a single-electron atom.

The wavefunctions for each quantum state are spherical harmonic standing waves, which have more complex shapes and more nodal points for higher quantum numbers *n* and *l*. In the carbon atom, there are six electrons which fill the *n*=1, *l*=0 orbital ("1s" in spectroscopic notation), the *n*=2, *l*=0 orbital (2s) and partially fill the *n*=2 *l*=1 orbitals (2p). The *n*=2 electrons are distributed furthest from the atom and so are involved in bonding between carbon atoms. Each *p* orbital is lobe-shaped with opposite sign magnitudes at opposite sides of the nucleus. This has implications for bonding between carbon atoms described in section 2.1.2.

2.1.2 Symmetry and Bonding

Symmetry is used to analyse the overlap of atomic orbitals within molecules, an approach known as Linear Combinations of Atomic Orbitals. The symmetry determines the shape of the bound molecule and the shapes of the molecular orbitals.

Symmetry is characterized by symmetry operations, such as reflection, rotation and inversion, which move the atoms (or bonding orbitals) in the molecule in space to equivalent positions. If the molecule is symmetrical the net result is that the molecule appears unchanged after the operation is carried out.

The polymers used in this work, polyfluorenes, include a chain of benzene rings within the polymer backbone. This polymer is modelled as a planar poly(*para*-phenylene) (PPP) structure that is characterized by a single axis of symmetry and a single plane of symmetry, placing them in the point group C_{2h}. In the C_{2h} group the possible symmetry operations are

the identity operation (E), rotation 180° around the axis along the molecule (C_2), inversion (i), and reflection across the horizontal plane (σ_h). These elements are illustrated in figure 2-2. Note that the opposite sign in the p_z orbitals prevents the molecule from having more planes of symmetry.

Figure 2-2: Symmetry elements of poly(*para*-phenylene) used as a model for poly(fluorene).

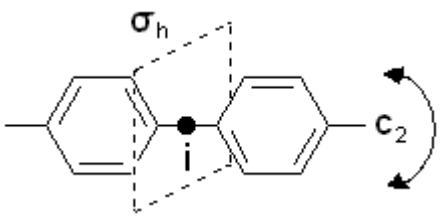

The symmetry of a molecule can be represented in a simplified form of a square matrix showing the effect of symmetry operations on a basis within the molecule. Matrix algebra can be used to reduce this matrix to its simplest possible form which is symmetrical about the diagonal, the irreducible representation. The sum of the diagonal elements of the irreducible representation is called the character of the matrix, which contains all the necessary information for calculating the molecular symmetry. The collection of these irreducible representations (the characters of each of the matrices) for any symmetry group is called its character table.

The C_{2h} point group has four one-dimensional irreducible representations (Mulliken symbols A_g, A_u, B_g and B_u) in its character table (table 2-1) that are symmetric (denoted by A) and anti-symmetric (B) with respect to rotation around the axis of symmetry C_2, and for each of these representations two are symmetric ($_g$) and two are anti-symmetric ($_u$) with respect to inversion at the centre of symmetry.

Table 2-1: The character table of the C_{2h} point group. In columns 2-5, a value of 1 denotes symmetry with respect to the operation in the column header, whilst -1 shows the operation is antisymmetric. Column 6 shows the irreducible representations for which the vectors of rotations (R) and translations (T) provide a basis. Column 7 shows the representations for which combinations of x, y and z provide a basis.

C_{2h}	E	C_2	i	σ_h		
A_g	1	1	1	1	**R_z**	x^2, y^2, z^2, xy
B_g	1	-1	1	-1	**R_x, R_y**	yz, zx
A_u	1	1	-1	-1	**T_z**	
B_u	1	-1	-1	1	**T_x, T_y**	

A reducible representation can be generated using the p_z orbitals as a basis. A reducible representation Γ can be calculated by listing the number of orbitals that remain un-shifted for each symmetry operation (E, i, C_2, σ_h for C_{2h}), and multiplying this number by the known change in character for each symmetry operation (E:+1, i:+1, C_2:-1, σ_h:-1). The elements of the irreducible representation Γ_p are then calculated by:

$$a_p = \frac{1}{g}\sum_R \chi(R)\chi_p(R) \qquad (2\text{-}1)$$

Where *g* is the total number of symmetry operations in the point group [for C_{2h} (1×E) + (1×i) + (1×C_2) + (1×σ_h) = 4)].The term $\chi(R)$ refers to the character of the symmetry operation in the reducible representation (the elements of the reducible representation Γ) and $\chi_p(R)$ is the corresponding element in the irreducible representation.

A projection operator is used to derive symmetry-adapted linear combinations of the basis vectors (for molecular bonding the molecular orbitals are used). The combinations are then required to have the same symmetry as the orbitals of the basis vectors. The derived linear combinations show the approximate shapes of the resulting molecular orbitals.

The process is illustrated by the example of the π orbitals of *trans*-butadiene, shown in figure 2-3. This molecule is in the same point group C_{2h} as PPP which is used to model polyfluorene.

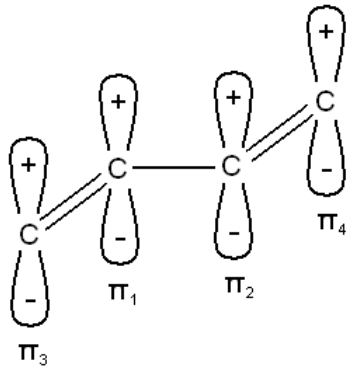

Figure 2-3: The p_z orbitals of *trans*-butadiene with arbitrary atom labels. Hydrogen atoms are present (two at C_3 and C_4 and one at C_1 and C_2) but excluded from the diagram. This molecule adopts the C_{2h} point group.

The molecule is σ-bonded using the *s*, p_x and p_y orbitals of the carbon atoms. The remaining p_z orbitals labelled π_1 to π_4 are used as the bases for generating the reducible representation in table 2-2.

Table 2-2: calculating the symmetry of the reducible representation.

C_{2h}	E	C_2	i	σ_h
unshifted π	4	0	0	4
Γ	4	0	0	-4

Using equation 2-1 for each Mulliken symbol in the C_{2h} point group:

a_g: (1/4)×[(1×4)+(1×0)+(1×0)+(1×-4)] = 0/4 = 0

a_u: (1/4)×[(1×4)+(-1×0)+(1×0)+(-1×-4)]= 8/4 = 2

b_g: (1/4)×[(1×4)+(1×0)+(-1×0)+(-1×-4)]= 8/4 = 2

b_u: (1/4)×[(1×4)+(-1×0)+(-1×0)+(1×-4)]= 0/4 = 0

This gives $\Gamma_p = 2a_u+2b_g$ as the symmetry of the reducible representation. The Symmetry-Adapted Linear Combinations (SALC) can be deduced using the orbitals π_1 and π_3 which are symmetrically distinct from each other. Applying a_u and b_g as projection operators to these orbitals gives:

a_u : $\pi_1 + \pi_2$ and $\pi_3 + \pi_4$

b_g : $\pi_1 - \pi_2$ and $\pi_3 - \pi_4$

These linear combinations show the shapes of the π orbitals. There are two bonding orbitals with electron density between the carbon atoms, and two anti-bonding orbitals with nodes between the atoms. The lowest energy orbital has electron density delocalised across the whole molecule, encompassing several alternating single and double bonds.

2.2 Molecular Orbitals in Conjugated Polymers

The combined orbitals of the electrons in a small molecule are determined by the Coulomb interactions of the electrons with the nuclei of the whole molecule. Electrons in the core n=1 orbital adjacent to the nucleus are strongly bound and screened from the other nuclei, but the higher energy are delocalised and occupy orbital regions that can cover most of the volume of the molecule, as illustrated previously. For a molecule such as anthracene, each molecule acts as a chromophore; interacting with photons to absorb and emit light.

In a polymer, a long chain of carbon atoms can form with alternating single and double bonds between neighbouring carbon atoms, known as conjugation, for example in poly(acetylene) which is the simplest example. The π bonds can join together over many double bonds to form a delocalized region over many repeat units of the chain, the length of which (in monomer units) is called the conjugation length, which in poly(9,9-dihexylfluorene-2,7-diyl) has been measured at 5 structural repeat units,[1] and these make up the chromophores of the polymer system. These regions are separated by imperfections, twists and bends in the polymer chain. The weakly bound electrons are able to move between the delocalized regions on the same chain and adjacent chains by Dexter transfer, or the energy of the excited state may be transferred by Förster transfer (see section 2.8).

The electrons in the delocalized π orbitals of conjugated polymers that interact with light occupy the Highest Occupied Molecular Orbital (HOMO). The second energy level of importance to conductivity and the emission of light is the Lowest Unoccupied Molecular Orbital (LUMO), the π^* orbital. Conjugated polymers that have an energy level spacing in the

optical region typically include aromatic rings in the monomer unit.[2-4] These energy levels had previously been thought of as an approximation to the valence and conduction bands seen in inorganic semiconductors. However, there are many significant differences between these and organic semiconductors and the physics of semiconducting crystals does not strictly apply to the disordered polymer system. Conventional solid state band theory works on the assumption of uncorrelated charges that are free to move freely through the ordered environment of a crystalline material, whereas in polymeric systems the charges can exist in electron-hole pairs that have significant binding energy (on the order of 0.4eV [5]) and are confined to molecular orbitals. The presence of charges also distorts the local nanoscale environment to a much greater extent than in a bulk crystal (see section 2.9).

The input of energy (excitation) can promote an electron from the HOMO into the LUMO. This can occur the absorption of a photon with sufficient energy to excite an electron to a higher energy orbital (see section 2.5), or via direct injection of electrical charge into the HOMO and LUMO from electrical contacts. Doping the polymer with charges causes it to become electrically semiconducting when some of the π electrons are removed, allowing charge motion by Dexter transfer (see 2.8.2).

Excitation creates a quasi-particle, a hole; a positively charged vacancy in the HOMO, created by the departure of the negatively charged electron, which other nearby electrons in the HOMO can move into. When another electron nearby in the HOMO moves into the location of this hole, it effectively moves the hole itself through the material to the point where the electron originated. Thus the hole can move as a quasi-particle through the HOMO of the bulk material, often remaining correlated to the excited electron in the LUMO. Holes have similar properties to electrons; they have spin ½, and a charge of *e*, but they are positively charged.

2.3 Singlets and Fluorescent Emission

When an electron and a hole meet at the same point in space, their electrostatic charges create a mutual attraction and they bind to form a neutral quasi-particle: an exciton.[6] This is a localized bound state with a binding energy of the order of 0.4eV.[5] From this bound state recombination can take place, whereby the excited electron loses its energy and fills the empty hole in the HOMO. However, this process is more complex than such a simple picture would indicate, because of the spins of the electrons.

As described earlier, each electron orbital exists at a specific energy and has a specific angular momentum and spin, and two electrons can coexist in the same orbital as long as their spins are aligned anti-parallel. Therefore in order for an excited state electron to be able to decay, or relax, into a hole, the excited electron and the lone electron in the available ground state orbital must have anti-parallel spins for the transition to take place.

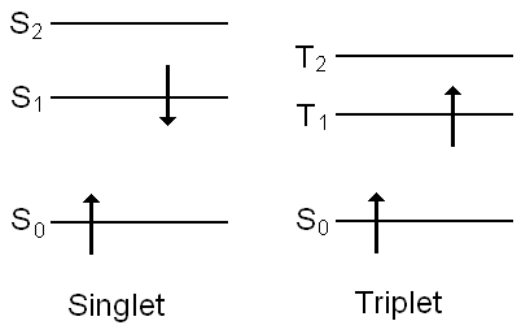

Figure 2-4: Simplified energy-level diagram of singlet and triplet exciton states. Arrows represent the electron spin orientation. S_0 is the ground state of the exciton.

The scenario in which these electron spins are anti-parallel is called a singlet exciton, because there is only one possible quantum state corresponding to it. This state has a total spin of zero, shown in equation 2-2, where arrows indicate the electron spin directions. The singlet can quickly relax in a radiative transition, where the energy of the excited electron is converted into a photon or to heat as the hole is filled.

$$|0,0\rangle = \frac{1}{\sqrt{2}}(|\uparrow\downarrow\rangle - |\downarrow\uparrow\rangle) \tag{2-2}$$

This is permitted by quantum mechanics because the initial state, the singlet exciton, has a total spin of zero, and the final state, a photon and the anti-parallel paired electrons, also has a total spin of zero and spin is conserved in the interaction. Thus the radiative decay probability is high and the lifetime of the singlet is extremely short; of the order of picoseconds to nanoseconds, dependent upon the polymer.

The exciton ground state is represented as S_0 in figure 2-3, where the S describes the singlet character and the 0 indicates the energy level above the ground state. It is important to note that the HOMO and LUMO do not simply correspond to S_0 and S_1; the marked energy levels S_1 and T_1 are the energies of the bound excitons with singlet and triplet character. The terms HOMO and LUMO refer to the free orbitals, and the states are the arrangement of the electrons within the orbitals. When the excited electron is bound in an exciton, it exists at an energy level below the unbound orbital, with the difference equal to the binding energy.

2.3.1 Exchange Interaction

The electron and hole in the exciton are bound by the Coulomb charge. But as fermions in close proximity, their wavefunctions overlap leading to a second interaction energy term, the exchange interaction. The Pauli Exclusion Principle is a result of the requirement for fermions to have an anti-symmetric wavefunction, which includes terms for the orbital and particle spin. In order for this to be satisfied, the exchange interaction must be a positive energy for singlet excitons (symmetric spatial wavefunction) and negative for triplets (anti-symmetric spatial wavefunction), implying triplets are a lower energy state than singlets because the two electrons interact less. The result is a relatively lower energy level for triplet excitons, which is shown in figure 2-3.

2.4 Triplets and Phosphorescent Emission

When the spin of the excited electron and the HOMO electron are parallel, the exciton is called a triplet, because there are three different quantum mechanical states that correspond to a total spin of 1 (equations 2-3 to 2-5).

$$|1,0\rangle = \frac{1}{\sqrt{2}}(|\uparrow\downarrow\rangle + |\downarrow\uparrow\rangle) \tag{2-3}$$

$$|1,1\rangle = |\uparrow\uparrow\rangle \tag{2-4}$$

$$|1,-1\rangle = |\downarrow\downarrow\rangle \tag{2-5}$$

Radiative transitions from excited triplet state to the singlet ground state are spin forbidden, as the initial state has a total spin of one and so spin is not conserved. In order for the radiative transition to take place, there must be an interaction to change the angular momentum of the excited electron and flip its spin to the anti-parallel alignment. This can be achieved by angular momentum exchange with atomic nuclei. However, in a pure polymer system the heaviest atom present is often carbon, and so from equation 2-6 the exchange interaction is small and the probability of angular momentum exchange is low. This results in the triplet exciton having a relatively long lifetime, from nanoseconds to seconds depending on the polymer. The radiative transition from the initial triplet state, phosphorescence, is therefore less likely than fluorescence (in an un-doped system), since within its lifetime it is more likely that the energy will be lost as heat.

Triplet excitons may be allowed to decay radiatively with high efficiency in an environment where there is strong spin-orbit interaction. The spin-orbit interaction is of the form: [7-9]

$$H_{SO} = \alpha_{fs}^2 \sum_{\mu}^{N} \sum_{i}^{n} \frac{Z_\mu}{r_{i\mu}^2} \overrightarrow{L_i} \overrightarrow{S_i} \tag{2-6}$$

Where α_{fs} is the fine structure constant, Z_μ is the effective charge on nucleus μ, L and S are the Orbital and Spin moments of the electron. The coupling occurs between electron *i* and the nuclear field of nucleus μ. Other terms from electron-electron interactions could be included in H_{so} for completeness but are neglected as being far smaller in magnitude.

The presence of the effective nuclear charge Z_μ shows that this effect is stronger in the presence of large nuclei. This interaction has been widely exploited by using molecular dopants which contain a heavy atom such as iridium or platinum.[10] These molecules efficiently produce phosphorescence from triplet excitons, which are of great importance to light emitting applications since a simple statistical view of exciton formation shows that there are four possible states to be formed by exciton formation, three of which are triplets. This gives a ratio of singlets to triplets of 1:3, assuming that they have an equal probability of formation, an assumption that has been questioned.[11]

2.5 Absorption and Photoluminescence

2.5.1 Absorption

The transition of an electron from HOMO to LUMO may be excited by the absorption of a photon with energy equal to or greater than the energy gap between the two orbitals. The electron is excited to a higher energy state, where the energy gap corresponds to the photon energy.

The optical absorption of an incident light intensity I_0 by a thickness *l* of a material with a molar absorption coefficient ε at concentration *c* can be simply stated by the Beer-Lambert Law, showing exponential intensity drop:

$$I = I_0 \cdot 10^{\varepsilon l c} \tag{2-7}$$

The optical density (OD) of a material, also known as the absorbance, is calculated by:

$$A = -\log_{10}\left(\frac{I}{I_0}\right) \tag{2-8}$$

This is a standard unit used in the measurement of the absorption spectrum of a sample. Comparing equations 2-6 and 2-7 shows that the absorption is linear with path length and concentration.

2.5.2 Molecular Vibrations and Rotations

Covalent molecules can absorb photons in the infrared region, at energies well below the main optical absorption, giving a spectrum that shows the direct excitation of molecular vibrations and rotations. Molecular rotations are very low energy states, of tens of milli-electronvolts, which are not prevalent in polymers due to their large size preventing most rotations. Molecular vibrations are of the order of hundreds of milli-electronvolts, and involve the stretching-relaxing of the molecular bonds, twisting, and even larger scale motions such a ring "breathing" in benzene rings. The different classes of molecular vibrations, and vibrations involving different component atoms, exhibit characteristic energy spectra in the infrared region, allowing certain functional groups or dominant vibrational modes to be identified.

Thus a molecule may absorb a photon of higher energy than the energy gap to the S_1 state. The electron is excited to the S_1 state, and the excess energy corresponds to a number of activated vibration modes. By Kasha's rule, the excited electron rapidly drops to the lowest vibronic (no activated vibrations) of the first excited state (S_1) by internal conversion, where the excess energy is dissipated as heat to the surrounding medium.[12-13] For the higher-lying energy levels (S_2 or T_2 and above) with large spatial overlap and small energy separation, this happens swiftly, but upon reaching the larger energy separation between the S_1 (or T_1) and S_0 this process is no longer fast.[14] This leaves the electron with a high probability of relaxation from the S_1 level by photon emission.

2.5.3 Photoluminescence

The schematic Jablonski diagram, in figure 2-4, shows all the types of transitions that take place in an organic system with discrete energy levels and vibronics. Thick lines denote the principal energy levels, starting at the ground state (S_0), and thin lines show multiples of a single dominant molecular vibration. Absorption is an electronic transition from a low lying state to higher energy states promoted by interaction with a photon. Absorption occurs from the lowest lying vibrational state, because the vibronic energy level occupation is determined by the Boltzmann factor. For a typical vibronic energy level of over 50meV, almost all electrons at room temperature will be in the lowest vibronic of the S_0 level, although some electrons may occupy very low energy ring-torsion modes. The electron may then relax to the ground state resulting in a photon or in heat, or undergo spin flip (intersystem crossing or ISC) and enter the lower-lying triplet level.

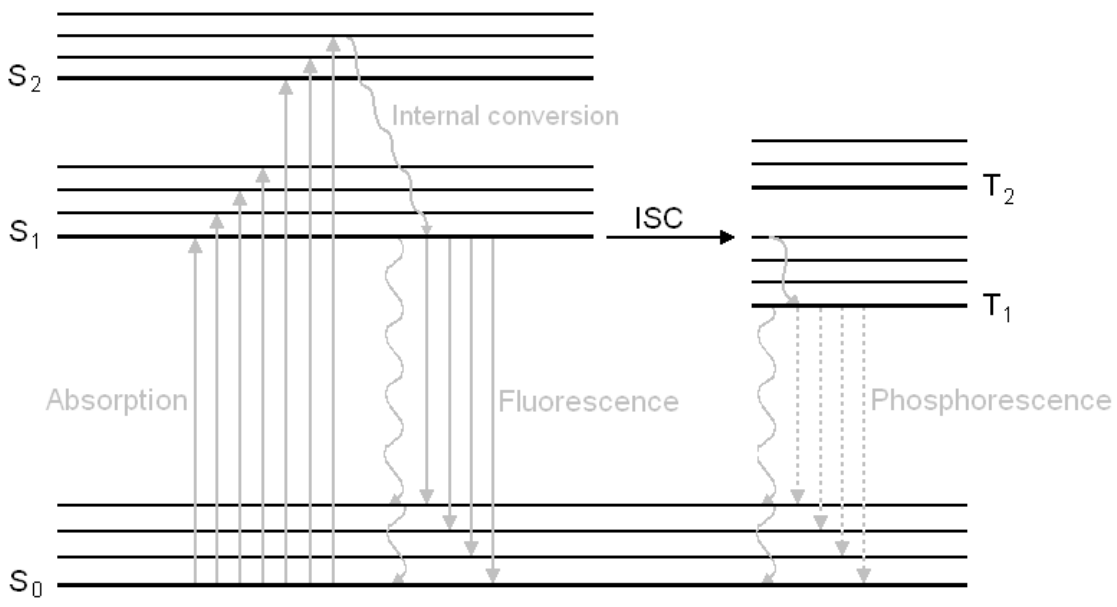

Figure 2-5: The Jablonski diagram showing the possible energetic transitions between energy levels (thick black lines). Thin black lines show the first three vibrational modes of each energy level. Curving lines represent internal conversion (to thermal energy) and ISC refers to Inter-System Crossing.

The vibrational energy levels are seen in the emission spectra as replicas of the main emission peak measured at lower energy, shown in figure 2-5. These are known as vibronic replicas. Since the fluorescence (produced by recombination of an exciton) initiates from the lowest vibronic of the S_1 level and can terminate in any vibronic of the ground state, the fluorescence in organic molecules often shows two or more vibronic replicas, and appears to be a mirror image of the absorption spectrum, but offset by a small amount of energy, the Stokes shift. A large Stokes shift indicates a significant amount of structural re-organization occurs once the molecule enters the excited state, in order to lower the total energy of the system. The emission then occurs from the lower-lying energy level of the new molecular arrangement.

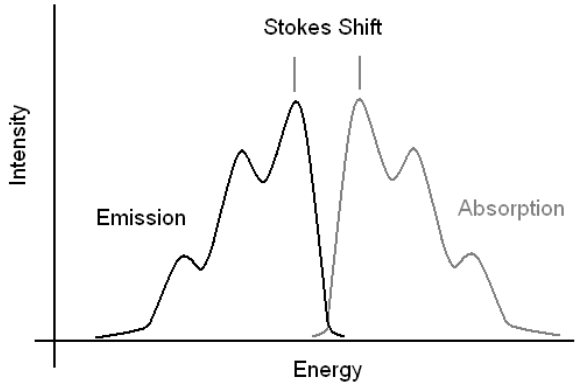

Figure 2-6: Ideal molecular optical spectra showing mirror-image absorption and emission, with a large Stokes shift.

The optical transitions are further affected by the spatial overlap of the different excited state wavefunctions of each of the vibronics with the ground state. Where there is a large overlap, the probability of the transition is high, and where the overlap is low, little absorption is seen. This is illustrated in figure 2-6, which shows an absorption transition from (n=0, v=0) to (n=1, v'=2) where there is strong spatial overlap of the wavefunctions of the two states. The offset parabolas indicate a change in the spatial configuration of the molecule upon reaching the excited state. This shows why only a few vibrational replicas are seen in spectra, as the higher molecular vibrations states have a smaller overlap.

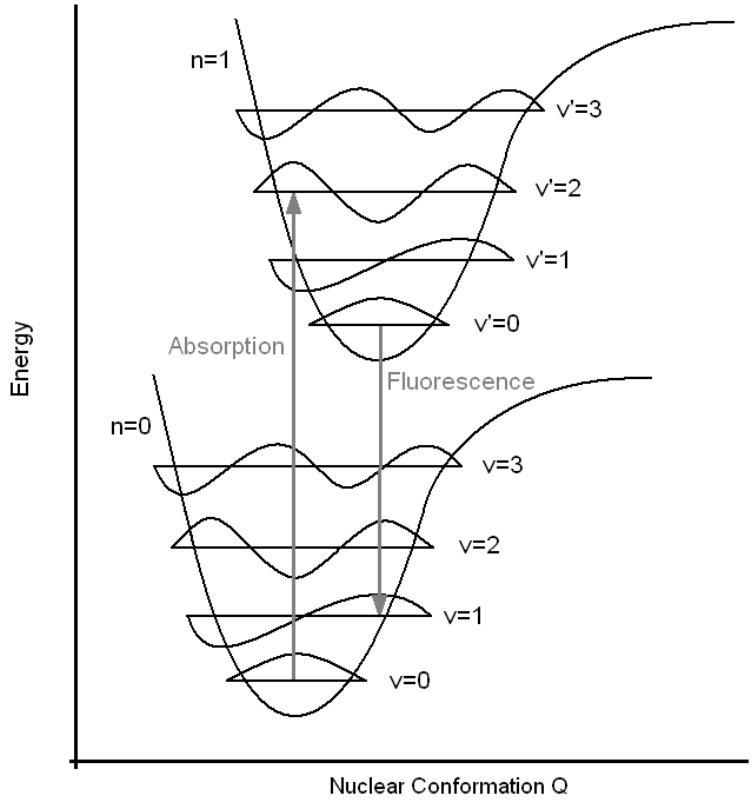

Figure 2-7: Vibronic wavefunctions illustrated on the potential energy levels of a simple diatomic molecule. Adapted from Lakowicz[15]

The extent of wavefunction overlap further explains the absorption and emission spectra in figure 2-5. Once an electron is excited into the n=1 parabola, very fast internal conversion allows the energy of the v'=2 vibronic to be lost as heat, with the result that the emission always begins from the n=1, v'=0 level. The vibronic peaks in the emission spectrum of a molecular system are often therefore a mirror image of the absorption spectrum, as the peaks in the emission spectrum corresponding to each of the vibronics will be replicated by the emission spectrum: v'=0 to v=2 compared to v=0 to v'=2 for absorption, as the amount of overlap of the wavefunctions will be the same due to the symmetrical nature of the parabolic energy surface in figure 2-6 for small changes in *r*. In disordered polymers the absorption spectrum rarely shows the mirror image vibronic peaks, since the conjugated regions have a distribution of lengths, each with different vibronic levels, and the net effect

of this is to average out many energy levels to form a broad, smooth absorption band. Structured fluorescence is still observed, as energy transfer ensures that the emission always originates from the lowest-energy subset of conjugated regions.

2.5.4 Symmetry Selection Rule

The significance of the symmetry groups in the spectroscopy of conjugated polymers becomes apparent through selection rules, which permit and forbid transitions based on the symmetry of the states involved.

Direct products, in terms of symmetry, refer to the multiplication of the characters of each of the symmetry operations corresponding to each representation. Using simple multiplication rules allows the resulting symmetry of the product to be quickly known just by using the Mulliken symbols of the representations.

The probability of an optical transition occurring is proportional to the integral:

$$\int \psi_i^* \mu \psi_f d\tau \tag{2-9}$$

where μ is the transition dipole moment between the initial state ψ_i and the final state ψ_f of the transition. The direct product $\psi_i^* \mu \psi_f$ must contain the completely symmetric representation, in which all the characters are +1, in order for the integral to be non-zero. The transition dipole moment has the same symmetry type as translations within the symmetry group, which are of symmetry A_u for translations in z and B_u for translations in x and y. The symmetry of an electron state is given by the direct product of the symmetry of all the electrons in their orbitals. If any of the products have a completely symmetric representation (A_g in this point group) then the transition between the initial and final states is permitted. For the polyfluorenes in this work the transitions are only permitted between energy levels with opposing symmetry; from A_g (the symmetry of the ground state) to B_u (the first excited state S_1).

2.5.5 Huang-Rhys Parameter

The offset of the two energy-separation parabolas determines the amount of overlap between the wavefunctions of the different vibrational modes, and hence the relative intensity of each transition which is observed in the absorption and emission spectra. The relation between the intensity of successive replicas of the same vibrational mode is given by the Huang-Rhys parameter *S*:

$$I_{0\to n} = \frac{e^{-S}S^n}{n!} \tag{2-10}$$

Where

$$S = \frac{m\omega}{2\hbar}\Delta Q^2 \tag{2-11}$$

For a coupled oscillator of total mass *m*, vibrational frequency ω, and offset in parameter space ΔQ between ground and excited states. Experimentally, *S* can be determined by the first vibronic peak intensity ratio I_1/I_0. A smaller offset in the parabolas leads to smaller intensity vibrational replicas. This gives a measure of the number of energy quanta needed to distort the excited state (the Stokes shift).

2.6 Fluorescence Lifetime

The fluorescence lifetime is a characteristic defining the time in which the fluorescence intensity of an initially excited ensemble of states will decay to 1/e of its initial value. For a simple system the intensity of the emission is described by an exponential decay after excitation has ceased:

$$I = I_0 e^{-\frac{t}{\tau}} \tag{2-12}$$

For a system of several different emitting species the decay may be the sum of two or more exponential terms with different time constants τ_i. The lifetime of a decaying species is determined by the rate of decay to radiative (k_r) and non-radiative (kn_r) processes:

$$\tau = \frac{1}{k_r} + \frac{1}{k_{nr}} \tag{2-13}$$

An increase in either of the decay rates will reduce the time taken for the intensity to drop by the same fraction. A high non-radiative decay rate will reduce the number of decays that result in photon emission. This is related to the quantum efficiency ϕ of a material:

$$\phi = \frac{photons\ re{-}emitted}{photons\ absorbed} = \frac{k_r}{k_r + k_{nr}} \tag{2-14}$$

2.7 Chain conformation and redshifted emission

The size of the delocalized regions on a conjugated polymer is limited by kinks and defects in the chain. If there are many imperfections, the average size of the delocalized region is reduced. Correspondingly, the energies of the molecular orbitals, as well as their energy gaps, are increased. This occurs because the more an electron is confined in a smaller space, the higher its energy, and the greater the spacing between energy levels, a scenario analogous to the quantum-mechanical 'particle in a box.' Therefore when the delocalized regions increase in size, the energy of the emitted photons is reduced, making the emitted light occur at a lower, redshifted frequency. This has been modelled and observed in experiment.[16-17] An increase in average conjugation length may occur if the polymer changes to a more ordered phase, most typically observed by going from solution to solid state.

2.8 Energy Transfer

2.8.1 Förster Transfer

Förster energy transfer is a radiation-less energy transfer mechanism that does not involve the physical movement of electrons. In a system involving two constituent parts, where a donor molecule or chromophore has an emission spectrum that overlaps at least partially with the absorption spectrum of an acceptor, the energy may be transferred from the donor to the acceptor via dipole interactions if the two are sufficiently close in space. This mechanism primarily applies to singlet transfer. The transfer rate constant is:

$$k_{D\to A} = \frac{1}{\tau_D}\frac{R_0^6}{r^6} \tag{2-15}$$

Where τ_D is the radiative lifetime of the donor. The transfer efficiency *E* depends upon the distance *r* between the chromophores:

$$E = \frac{1}{1+(r/R_0)^6} \tag{2-16}$$

The Förster radius R_0 is defined as the distance at which the efficiency is 50%, which depends upon the overlap integral between the donor and acceptor chromophores:

$$R_0 = \frac{9\ln(10)\kappa^2 e^4}{128\pi^2 n^4 N_A \tau_e r^6}\int f_D(\lambda)\epsilon_A(\lambda)\lambda^4 d\lambda \tag{2-17}$$

Where κ is an orientation factor (κ^2 = 2/3 for random dipole orientations), *e* is the electron charge, *n* is the refractive index of the medium, N_A is the Avogadro number, and τ_e is the average dwell time of the donor in the excited state in the absence of the acceptor. The term f_D is the fluorescence of the donor (normalized to a total area of 1), and ε_A is the molar absorption coefficient of the acceptor.[10] Typical Förster radius values are in the range 1 to 5nm.

2.8.2 Dexter Transfer

Dexter energy transfer is an electron exchange mechanism that acts over shorter ranges than Förster transfer (<1nm) because it requires an overlap in the spatial wavefunctions of the electrons in adjacent molecules. Spin is conserved in the exchange, allowing singlet-singlet or triplet-triplet transfer. The transfer rate constant k_{ET} is given by:

$$k_{ET} \propto \frac{h}{2\pi} P^2 J e^{\frac{-2r}{L}} \tag{2-18}$$

Where P and L are constants and J is the overlap integral from equation 2-17. Dexter transfer allows excitons to migrate through the material.[18-21]

2.8.3 Photon Self-Absorption

The emission and absorption spectra of a conjugated polymer often overlap significantly, allowing the polymer to re-absorb the photons emitted within the higher energy tail of its spectrum. It may also permit energy transfer from a donor to an acceptor where there is spectral overlap. This process is independent of distance between the emitting and absorbing chromophores, but the rate of energy transfer resulting from this process is lower than for either Dexter of Förster transfer when the chromophore separation is small enough for them to become effective. In the cases of dilute solutions and thin films, the effect of self-absorption is often insignificant. In thicker films, it may lead to a distortion of the high energy tail of the emission spectrum.

2.9 Excitons in Polymer Systems

An exciton in a real polymer system may often have significantly different properties depending upon its local molecular environment. The properties are largely determined by

the electron-hole separation. In a Frenkel exciton, the separation is small (<0.5nm), and both the electron and hole are localized on the same conjugated region of the same chain. This gives the highest-energy emission from the polymer, often seen in photoluminescence studies of polymer solutions where correlated electron-hole pairs are generated.

Charge-transfer excitons often occur in polymers where there is a permanent dipole moment on part of a monomer unit, and the local electric field causes a separation of the charges in the exciton, leading to a broad redshifted emission peak relative to the Frenkel exciton. These separated charges are still correlated. The binding energy of the excited state electron level is slightly below that for a Frenkel exciton, and the energy of the hole is slightly above that of the ground state, which arises from the induced conformational changes in the polymer created by the presence of the charge.

In solid polymer films or aggregates, the exciton can form where the electron and hole are weakly bound across two adjacent polymer chains, leading to large separation of the electron-hole pair of ~4-10nm, called a Wannier-Mott exciton or excimer, which also gives a more red-shifted emission relative to the Frenkel exciton. Such excitons are commonly encountered in electroluminescent devices where the transport of charge through the bulk film makes exciton formation from well separated charges far more likely. Thus, emission from electroluminescent devices is often very different to the dilute solution case and is strongly affected by film morphology.[22-25]

2.10 Polarons and Geminate Pairs

Chemical dopants, charge injection and dissociation of excitons within the polymer system can all produce free charges, without a nearby correlated opposite charge. These charges,

and the local distortions of the molecular environment they produce, are known as polarons.

An uncorrelated charge in a semiconducting crystal leads to a change in the local electric field and a slight misalignment of the positions of the nearby atomic centres. In a polymer system the positions of the constituent atoms are not stabilised by a rigid crystalline lattice, and the presence of a charge on the polymer chain can lead to significant distortion of the local polymer backbone, altering the molecular orbitals and their energies.

There is also an intermediate state between the exciton and the polaron, where the separation is large enough that the wavefunctions of the electron and hole no longer overlap, and there is no longer an exchange interaction. This state is called a geminate pair. All these states may contribute to the optical spectra of a sample.

2.11 Summary

This work makes use of the fluorescent polymers of the type poly(9,9-di-*n*-alkylfluorene), a conjugated polymer with a π-π* transition corresponding to the blue part of the visible spectrum and a useful polymer for organic light-emitting diodes. Through phase changes that alter the planarity of the polymer backbone, this polymer exhibits changes in its photophysical spectra that allow the phase changes to be easily tracked, and morphological changes to be inferred. The focus of this work is to contribute further to understanding the effects of the morphology of the polymers on their emission properties, which also impacts upon device efficiency. A phase change in poly(9,9-di-*n*-octylfluorene) is known to occur and to significantly improve both device efficiency and colour purity.[26]

This work builds on the physics of conjugated polymers, absorption and emission spectroscopy, but also on the modifications of the photophysical behaviour of these polymers that result from a change in phase in both solution and in thin films. These changes will be observed by optical spectroscopy, tracking the absorption and photoluminescence as

a function of the polymer phase. An understanding of energy transfer is critical in the interpretation of the photoluminescence data.

2.12 References

1. Wasserberg, D.; Dudek, S. P.; Meskers, S. C. J.; Janssen, R. A. J. *Chem. Phys. Lett.* **2005,** 411, (1-3), 273-277.
2. Burn, P. L.; Kraft, A.; Baigent, D. R.; Bradley, D. D. C.; Brown, A. R.; Friend, R. H.; Gymer, R. W.; Holmes, A. B.; Jackson, R. W. *J. Am. Chem. Soc.* **1993,** 115, (22), 10117-10124.
3. Li, Y. F.; Cao, Y.; Gao, J.; Wang, D. L.; Yu, G.; Heeger, A. J. *Synth. Met.* **1999,** 99, (3), 243-248.
4. Liu, B.; Yu, W. L.; Lai, Y. H.; Huang, W. *Chem. Mater.* **2001,** 13, (6), 1984-1991.
5. Deussen, M.; Scheidler, M.; Bassler, H. *Synth. Met.* **1995,** 73, (2), 123-129.
6. Bassler, H.; Gailberger, M.; Mahrt, R. F.; Oberski, J. M.; Weiser, G. *Synth. Met.* **1992,** 49, (1-3), 341-352.
7. Zahlman, A. B.; Androes, G. M.; Hameka, H. F.; Heineken, F. M.; Hutchison, C. A.; Jr., R., G. W.; van der Waals, J. H., *The Triplet State*. Cambridge University Press: Cambridge, 1966.
8. Lower, S. K.; Elsayed, M. A. *Chem. Rev.* **1966,** 66, (2), 199-&.
9. Beljonne, D.; Shuai, Z.; Pourtois, G.; Bredas, J. L. *J. Phys. Chem. A* **2001,** 105, (15), 3899-3907.
10. Cleave, V.; Yahioglu, G.; Le Barny, P.; Friend, R. H.; Tessler, N. *Adv. Mater.* **1999,** 11, (4), 285-288.
11. Rothe, C.; King, S. M.; Monkman, A. P. *Phys. Rev. Lett.* **2006,** 97, (7).
12. Kasha, M. *Discussions of the Faraday Society* **1950**, (9), 14-19.
13. Kasha, M. In *From Jablonski to femtoseconds. Evolution of molecular photophysics*, Jablonski Centennial Conference on Luminescence and Photophysics, Torun, Poland, Jul 23-27 Jan, 1998; Polish Acad Sciences Inst Physics: Torun, Poland, 1998; pp 15-36.
14. Elsaesser, T.; Kaiser, W. *Annu. Rev. Phys. Chem.* **1991,** 42, 83-107.
15. Lakowicz, J. R., *Principles of Fluorescence Spectroscopy*. 2nd ed.; Kluwer Academic / Plenum Publishers: New York, 1999.
16. Heeger, A. J.; Kivelson, S.; Schrieffer, J. R.; Su, W. P. *Rev. Mod. Phys.* **1988,** 60, (3), 781-850.
17. Monkman, A. P.; Burrows, H. D.; Hamblett, I.; Navarathnam, S.; Svensson, M.; Andersson, M. R. *J. Chem. Phys.* **2001,** 115, (19), 9046-9049.
18. Jang, S.; Jung, Y. J.; Silbey, R. J. *Chem. Phys.* **2002,** 275, (1-3), 319-332.
19. Pogantsch, A.; Wenzl, F. P.; Scherf, U.; Grimsdale, A. C.; Mullen, K.; List, E. J. W. *J. Chem. Phys.* **2003,** 119, (13), 6904-6910.
20. Murphy, C. B.; Zhang, Y.; Troxler, T.; Ferry, V.; Martin, J. J.; Jones, W. E. *J. Phys. Chem. B* **2004,** 108, (5), 1537-1543.
21. Dias, F. B.; Knaapila, M.; Monkman, A. P.; Burrows, H. D. *Macromol.* **2006,** 39, (4), 1598-1606.

22. Cadby, A. J.; Lane, P. A.; Mellor, H.; Martin, S. J.; Grell, M.; Giebeler, C.; Bradley, D. D. C.; Wohlgenannt, M.; An, C.; Vardeny, Z. V. *Phys. Rev. B* **2000,** 62, (23), 15604--15609.
23. Nguyen, T. Q.; Martini, I. B.; Liu, J.; Schwartz, B. J. *J.Phys. Chem. B* **2000,** 104, (2), 237-255.
24. Shi, Y.; Liu, J.; Yang, Y. *J. Appl. Phys.* **2000,** 87, (9), 4254-4263.
25. Kulkarni, A. P.; Tonzola, C. J.; Babel, A.; Jenekhe, S. A. *Chem.Mater.* **2004,** 16, (23), 4556-4573.
26. Lu, H. H.; Liu, C. Y.; Chang, C. H.; Chen, S. A. *Advanced Materials* **2007,** 19, (18), 2574.

3 Materials and Experimental Methods

3.1 Materials

3.1.1 Linear side-chain Polyfluorenes

Poly(9,9-di-*n*-alkylfluorene)s, with the general structure shown in figure 3-1a, with linear alkyl chains of n= 6, 7, 8, 9, and 10 carbon lengths were synthesised at high molecular weight (molecular weights given in table 3-1) using Yamamoto coupling by the Scherf group at Wuppertal in Germany[1] and the Durham university chemistry department. The weight-average (M_w) values for each polymer were calculated by:

$$M_w = \sum_N w_N M_N \qquad (3\text{-}1)$$

Where w_N is the weight fraction of molecules with mass M_N in the sample.

The octyl variant (PFO or PF8) has been intensively studied as a promising efficient emitter for organic light-emitting diode applications,[2-5] and is known to undergo a distinct reversible phase transition in both films and certain solvents to a phase known as the beta phase. The monomer units are normally twisted with respect to each other by an angle of approximately 135° in the amorphous phase, but after the phase transition the monomer units become more planarised and are rotated to angles approaching 180° with respect to each other (figure 3-1b).[6-11] This is in part inferred from the strong similarity between the beta phase emission spectrum and that of fully planarised ladder-type PPP. The variants studied have similar molecular structure and molecular weights, differing only in the length of the solubilising linear side chains. The different polymers are referred to as PF6, PF7, PF8, PF9 and PF10.[12-13]

Table 3-1: The number-average (M_n) and weighted-average (M_w) molecular weights of the poly(9,9-di-n-alkylfluorene)s used in this work.

Polymer	M_n	M_w
PF6	84	200
PF7	63	144
PF8	73	258
PF9	109	221
PF10	86	236

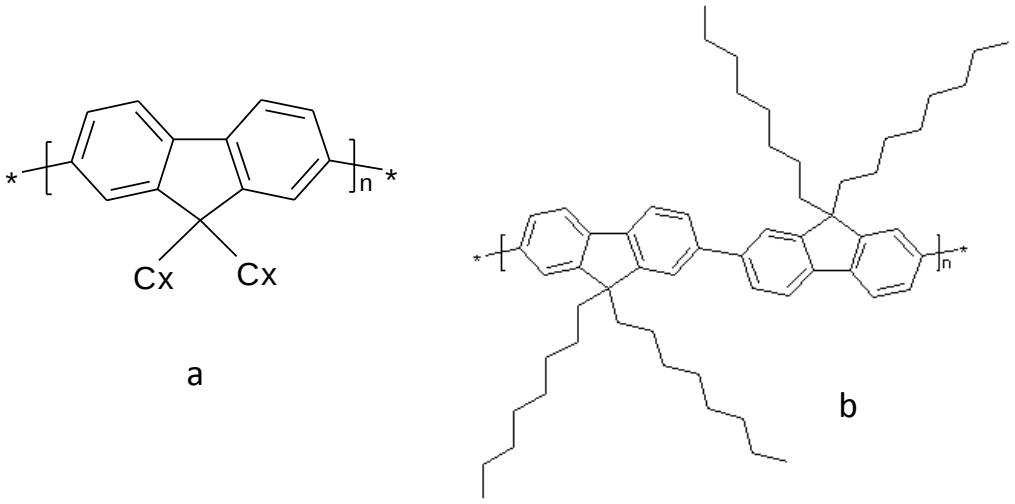

Figure 3-1: a) the general structure of poly(9,9-di-*n*-alkylfluorene)s, with substituted components at the C_x positions, and b) the idealised alternating planar backbone structure assumed for the β phase of PF8 (side chains are not in the same plane).

3.1.2 Polyfluorene Copolymers with Fluorenone Monomers

The main degradation pathway that occurs in the polyfluorenes is the gradual oxidation of fluorene units over time to form fluorenone, also known as the keto defect.[1, 14-18] To investigate the effect of this on the photophysics of the beta phase of PF8, several random copolymers were synthesised at Durham University Chemistry department using palladium-catalysed Suzuki polycondensation, with fluorenone concentrations of 0.05%, 0.1%, 0.5%, 1.0%, 1.5% and 2%. The general chemical structure of the copolymer is shown in figure 3-2, and the molecular weights are given in table 3-2.

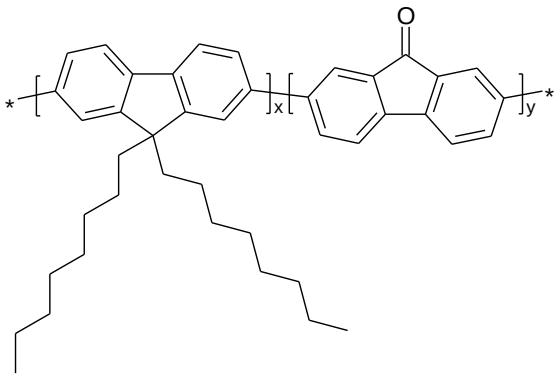

Figure 3-2: The chemical structure of the random copolymer PF8-keto.

Table 3-2: The number-average (M_n) and weighted-average (M_w) molecular weights of the PF8-keto copolymers used in this work.

PF8-keto y%	M_n (kDa)	M_w (kDa)
2.0	52	221
1.0	48	165
0.5	31	166
0.2	28	152
0.1	45	148
0.05	42	163
PF8	73	258

3.1.3 Polyfluorene Copolymers with Sulphur-Containing Units

Figure 3-3b shows a new copolymer synthesised at Durham University Chemistry department, again using palladium-catalysed Suzuki polycondensation. The polyfluorene monomers are randomly copolymerised with concentrations of 2%, 5%, 8%, 12%, and 15% SO_2 containing monomer units dibenzothiophene-*S*,*S*-dioxide (S unit). The inclusion of the highly polar S units is anticipated to promote the formation of charge transfer complexes.[19-21]

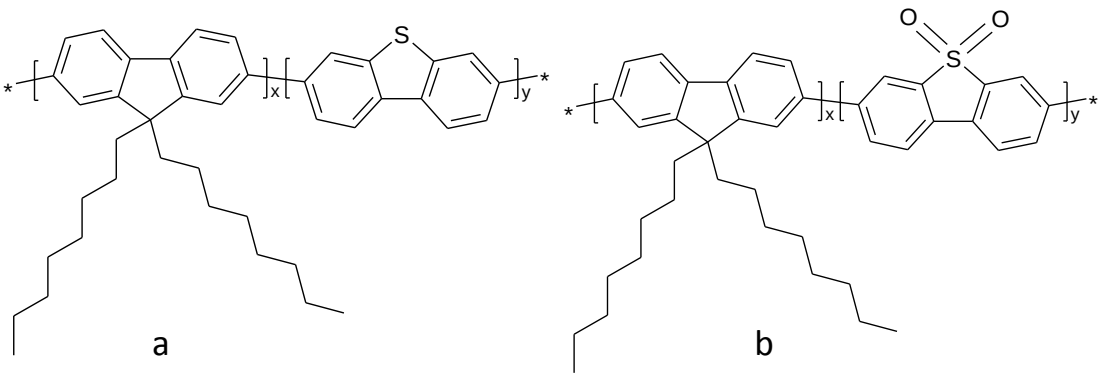

Figure 3-3: Structures of the random copolymers PF8-DBT (a) and PF8-S (b)

Further copolymers were synthesised using the same synthesis route with dibenzothiophene (DBT) (figure 3-3a) with 8%, 12%, 15% and 20% DBT content. Polyfluorene-DBT copolymer is known to improve colour purity of electroluminescent devices.[22] The molecular weights are given in table 3-3.

Table 3-3: The number-average (M_n) and weighted-average (M_w) molecular weights of the PF8-DBT and PF8-S-unit copolymers used in this work.

Polymer	S-unit %	DBT %	M_n kDa	M_w kDa
PF8	0	0	73	258
PF8-S 2%	2	0	57	220
PF8-S 5%	5	0	50	177
PF8-S 8%	8	0	54	210
PF-S 12%	12	0	35	131
PF-S 15%	15	0	39	124
PF8-DBT 8%	0	8	47	157
PF8-DBT 12%	0	12	40	140
PF8-DBT 15%	0	15	55	181
PF8-DBT 20%	0	20	53	158

3.2 Experimental Methods

3.2.1 Solution mixing

All solutions for spin-coating thin films or spectroscopic study of the Poly(9,9-di-*n*-alkylfluorene)s were dissolved in pure solvent, either spectroscopic grade toluene or methylcyclohexane (MCH). Pure polymer solids were added to a new glass vial and weighed to an accuracy of 0.1 mg, and the required concentration was made up by weight of solvent using the known density to calculate the added volume. Solutions for spin-coating films were usually made to a concentration of 3-5 mg mL^{-1} w/v, and solutions for spectroscopic study were made to concentrations between 1 µg mL^{-1} (for absorption spectra) and 10 ng mL^{-1} (for dilute excitation and fluorescence spectra) by dilution of a more concentrated solution. Initial polymer weights added to the vials was a minimum of 0.5 mg, giving an uncertainty of up to 20% in the final concentrations. Other sources of uncertainty from the volume of added solvent in the initial and secondary dilutions were below 0.1 % from the use of a calibrated pipette.

Mixing was aided by magnetic stirring and heating, with the temperature regulated by a temperature controlled hotplate. In most cases the solution was heated in a beaker of water held at or just below boiling point. To check that no degradation of the polymers would be induced by heating the thermal decomposition temperature of the polymers PF6 to PF10 was measured in the Durham University chemistry department by thermal gravimetric analysis and found to be over 340°C. The temperature of boiling water is also above the known temperature threshold for the beta-phase transition of 75°C,[7] ensuring that the polymer was dissolved in a random and non-aggregated initial solution state.

The importance of heating the solutions to ensure that they were fully dissolved is demonstrated by showing the absorption spectra for solutions of 15 µg mL^{-1} stored in a cold laboratory, where the temperature during winter cycles from -2°C at night to +20°C during the day. Figure 3-4 shows the absorption spectra for solutions stored in the laboratory for a period of 3 weeks. The solutions were

all found to have formed the beta phase (see chapter 4.3 for details of the beta phase spectra) showing that the polymer had aggregated from solution.

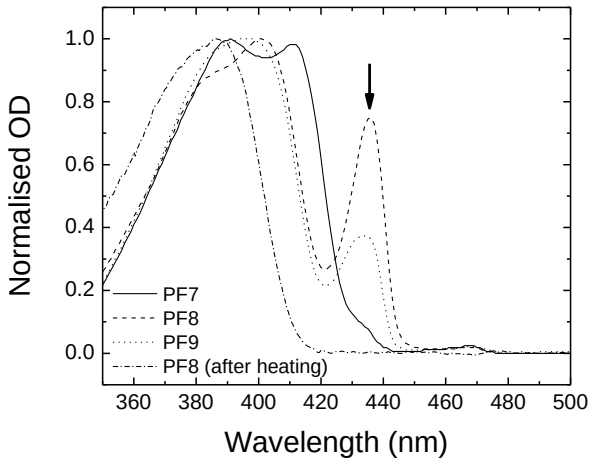

Figure 3-4: Absorption spectra of 15 ug mL^{-1} solutions of PF7, PF8 and PF9 stored for 3 weeks of thermal cycling from 20°C to -2°C. PF8 solution after heating to fully dissolve is included for comparison. An arrow marks the beta phase absorption peak.

3.2.2 Absorption Spectra

Absorption spectra were measured on thin films and freshly prepared solutions of Poly(9,9-di-*n*-alkylfluorene)s to monitor phase changes to films after thermal cycling and vapour exposure, and solution phase changes with temperature. The solution samples were measured at room temperature in a quartz cuvette with 1 cm path length, or at low temperatures in a long cryostat cuvette with 1 cm path length mounted in a Janis Research VNF-100 liquid nitrogen variable temperature cryostat with quartz windows, and the temperature was set and maintained using a LakeShore Model 332 temperature controller. Films were measured in the same manner, but the sapphire disc substrates were mounted on a copper mount in the cryostat and indium wire was used to create good thermal contact with the edges of the disc.

This cryostat was mounted in a Perkin-Elmer Lambda-19 spectrophotometer or a Shimadzu UV-3600 spectrophotometer, which were used to measure the absorption spectra. The cryostat is shown mounted in the Shimadzu UV-3600 in figure 3-5. A quartz cuvette of pure solvent, or a blank

substrate, was put in the second beam path to provide the differential spectrum, but a large offset is still seen due to the presence of the cryostat, where it was used. A spectrum of the empty cryostat was subtracted from the raw spectra to account for this.

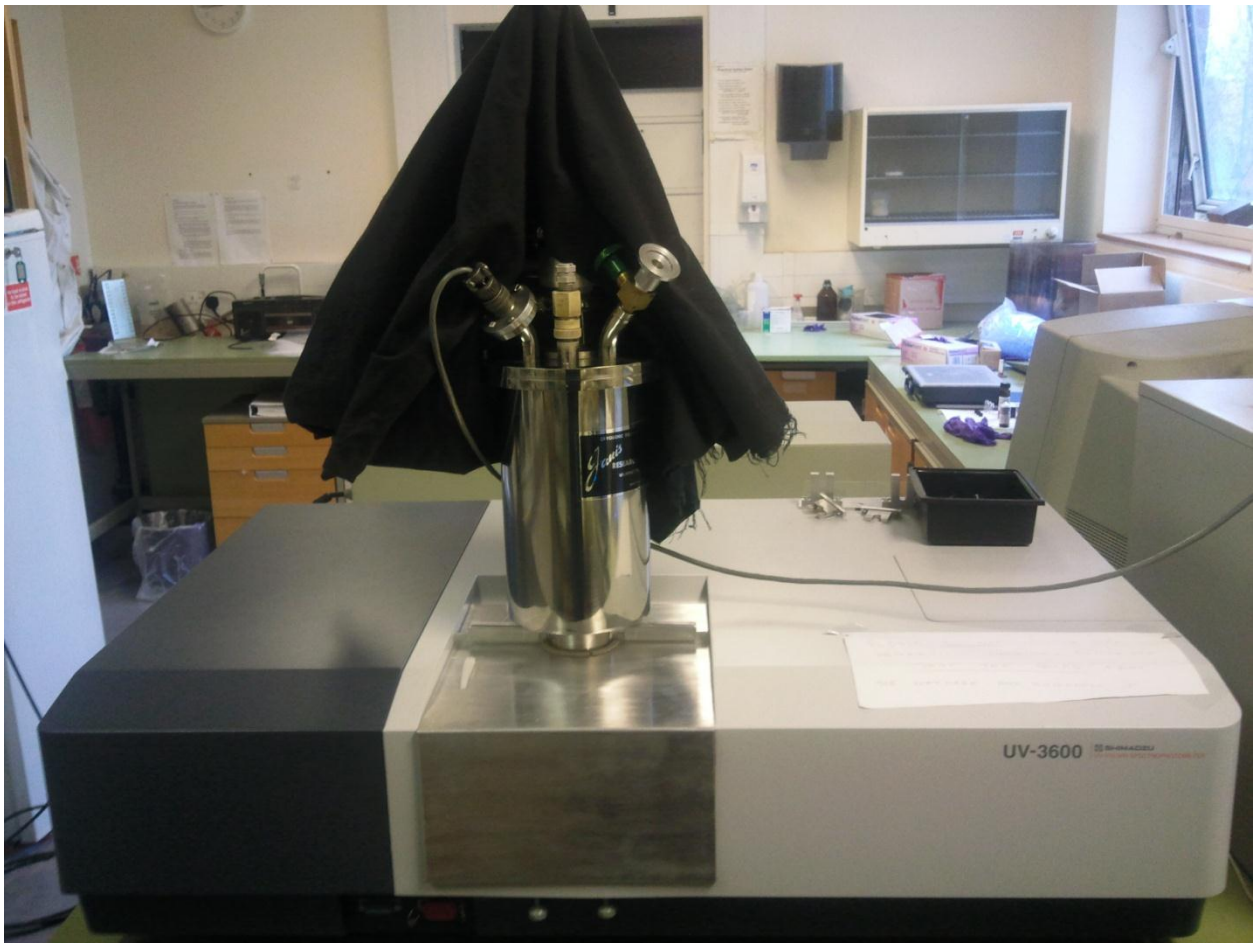

Figure 3-5: Picture of the liquid nitrogen cryostat mounted in the Shimadzu UV3600 spectrophotometer with a black cloth over the top of the glass sample cuvette to prevent stray light entering.

The spectrophotometer uses two lamps, one for visible and infrared wavelengths, and another for ultraviolet wavelengths (less than 400 nm). There are also two diffraction gratings for wavelength control, one for visible and ultraviolet wavelengths, and one for deep red and near infrared (>800 nm). The emission from the lamp is reflected by the diffraction grating onto an adjustable slit to select the wavelength and spectral width for the measurement. The beam at this selected transmission window is then split and sent down two equal paths through the sample chamber, where the sample and reference are placed. The transmitted light is then measured alternately by a

photomultiplier tube or photodiode, depending on the wavelength. The optical density is calculated from the difference in absorbed light between the sample and reference beam over the set spectral range, using equation 2-7.

A baseline scan is taken initially in order to correct for the variation in the lamp emission intensity over the wavelength range. The lamp change-over point can be manually adjusted over a range of wavelengths, in order to shift the change outside of the measurement area where possible.

Spectra collected from the same polymers using the two different instruments were found to be the same, giving a high degree of confidence in both the accuracy of each of the instruments, and the validity of the measured data.

The instrument software for both spectrophotomters automatically calculates the optical density of the sample as a function of wavelength over the range, and displays it directly. A screenshot of the UV-Probe software that runs the Shimadzu UV3600 spectrophotometer is shown in figure 3-6.

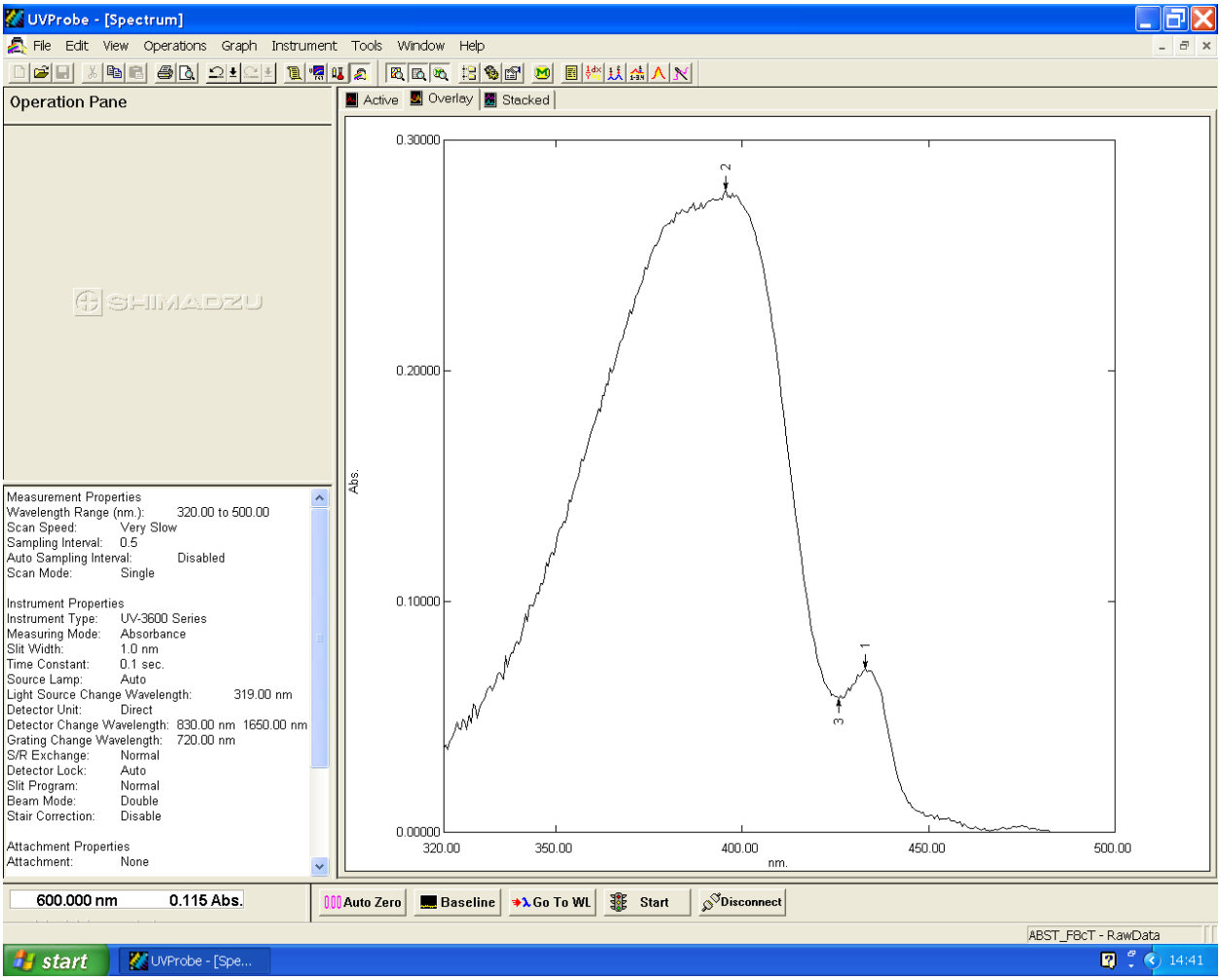

Figure 3-6: Screenshot of UV-Probe software for collecting absorption spectra on the Shimadzu UV3600 spectrophotometer, showing an example absorption spectrum of a beta phase PF8 thin film.

3.2.3 Excitation Spectra and Photoluminescence Spectra

Photoluminescence spectra are measured by optically exciting the sample at a fixed wavelength in the main absorption band, whilst scanning a range of wavelengths and observing the luminescence. Excitation spectra are measured by observing the luminescence from a sample at fixed wavelength in the sample emission spectrum, whilst scanning the excitation beam across a range of frequencies. The resulting spectra usually strongly resemble the absorption spectra of the sample, since a stronger absorption will lead to greater emission from the sample over its whole spectrum. However, excitation-energy dependent migration processes or the presence of more than one

emitting species may cause the excitation spectrum of a sample to differ significantly from its absorption.

The samples were measured in either a Jobin Yvon HORIBA Fluromax-3 or Fluorolog-3 spectrofluorimeter, with single- (for the fluoromax) or double-monochromated (for the fluorolog) excitation and emission beams for spectral control of the excitation beam and the sample emission. The sample chambers were also large enough to accommodate the liquid nitrogen cryostat used in the absorption spectra, which was available for cooling solutions when required. Film samples were cooled in a dedicated helium-loop cryostat mounted above the Fluorolog.

Both fluorimeters use the monochromated outputs from a xenon arc lamp to excite the sample. The incident slit width can be adjusted to trade resolution for signal strength, and the emission from the sample passes a second monochromating chamber and slit, which can be likewise adjusted. The emission from the sample is collected perpendicular to the excitation beam, allowing extremely low emission intensities to be measured. In excitation mode, the absorption spectrum can be approximated for a far higher range of optical densities than can be measured through direct absorption measurements, as only the sample emission is counted rather than very small differences in intensity between two light beams.

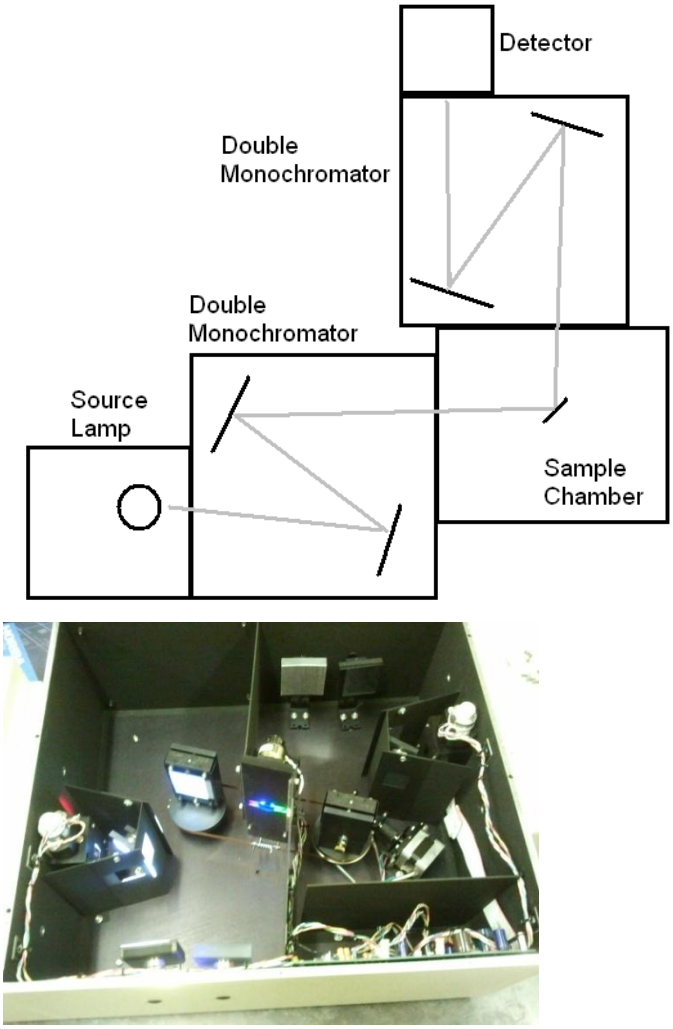

Figure 3-7: (Left) Schematic of the Flourolog-3 spectrofluorimeter for the collection of photoluminescence and excitation spectra. Light grey lines indicate approximate light paths from source to detector. (Right) Photograph of the inside of the excitation double-monochromator unit, with source lamp excitation arriving from the left of the image.

The control software used was the Instrument Control Centre which is supplied with both instruments. A screenshot is given in figure 3-5 showing the main configuration window for setting up a simple emission spectrum, adjusting the excitation and emission slit widths as well as the major scan parameters.

Spectra were collected from samples using real-time processing to output the processed spectrum rather than the raw counts. Displayed spectra are counts divided by the intensity of the excitation lamp at the same wavelength measured by a reference detector to correct for variations in lamp intensity across the measurement range.

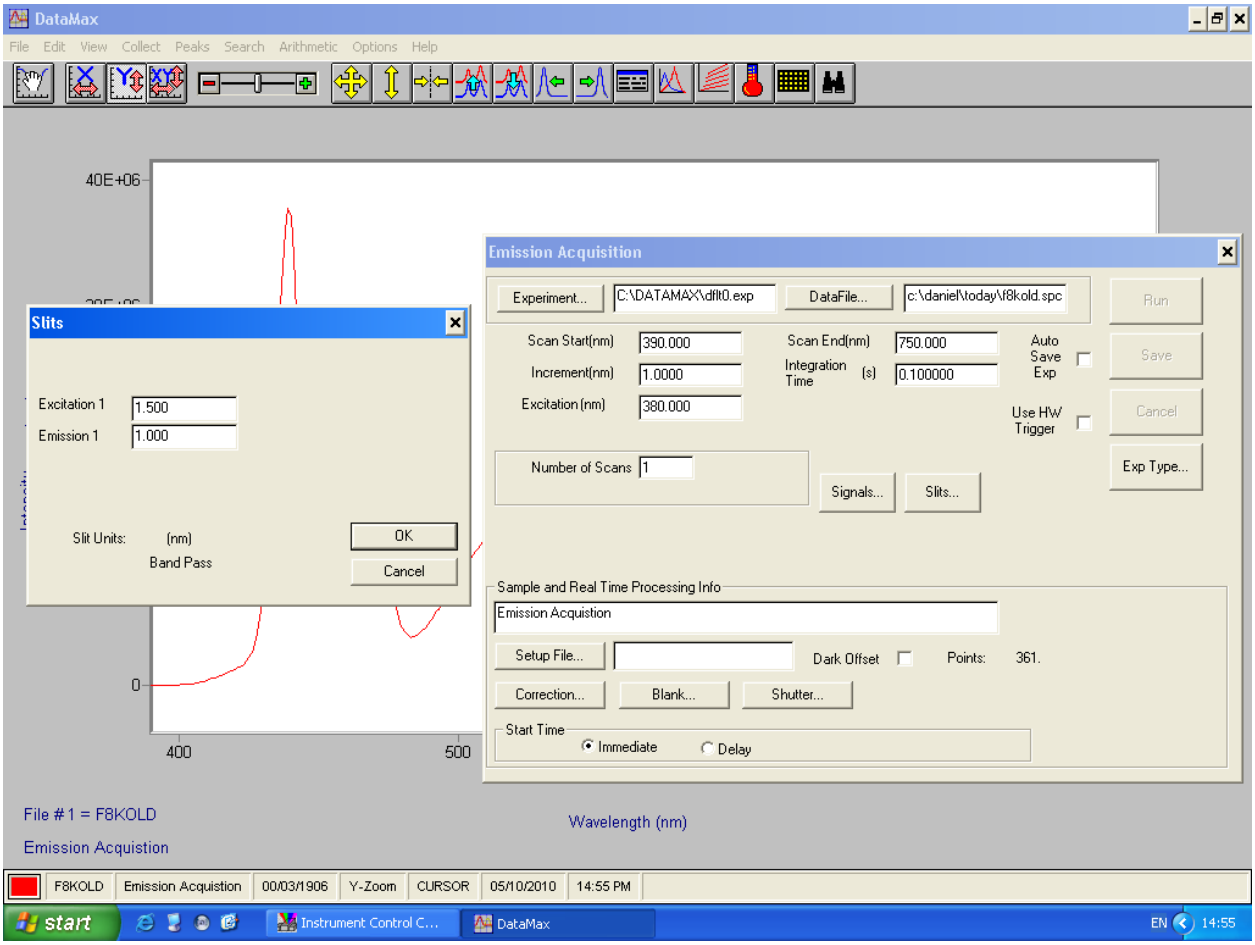

Figure 3-8: Screenshot of the Instrument control software used for both the Fluorolog and Fluoromax spectrometers, showing the configuration options windows.

3.2.4 Thin Films from Spin Coating

Film samples for beta phase formation studies in Poly(9,9-di-*n*-alkylfluorene)s were spin-coated from solutions of approximately 3 mg/mL in toluene. A clean quartz or sapphire 12mm disc, with 1mm thickness, was used as the substrate in all cases. A large drop was added to the centre of the disk by pipette to the surface before spinning at 500 rpm for 10 seconds, followed by 2000 rpm for 60 seconds. This resulted in thin films with an optical density (OD) of about 0.3 (from 3 mg/mL) at the absorption peak. However, significant variability in the film thickness was found from changes in constituent polymers, the temperature of the solution, and small variations in concentration.[23]

Extensive experience showed the critical importance of the preparation method for producing PF8 films of pure alpha-phase from solution. Alpha phase films were required for this work because it is a

relatively simple process to induce the beta phase in an alpha phase thin film (See chapter 5.4), but far more difficult to carry out the reverse process. Heating the film on a hotplate in air past the transition point (~80°C) will induce the change, but a vacuum oven is required to avoid producing significant quantities of fluorenone that will greatly disrupt the emission from the film (see chapter 6). Care must also be taken to avoid forming other phases during heating of films – thermal annealing for example will produce a different, crystalline phase with altered spectroscopic properties, as will quenching the film from high temperature.[24] Thus this method was avoided in order to prevent unwanted confounding variables to the results from complex processing histories.

The chemical preparation laboratory and fume cupboard used in this work were usually at a temperature of between 5 and 15°C. In order to produce films of PF8 in the alpha phase, a solution with a concentration of less than 5 mg mL^{-1} is required (a concentration below 1 mg mL^{-1} will yield films that are too thin for accurate absorption spectra). Secondly, the solution must be protected from sharp drops in temperature during all steps of the spinning process. Heating the solution to over 80°C before spinning is necessary to break up any small aggregates that may have formed during storage, but this alone is insufficient to produce a pure alpha-phase film, as drawing this solution into a glass pipette at 10°C with a 1 mm tip causes small beta-phase precipitates to be formed in the solution before deposition. A similar process occurs if the substrate is cold, and so all components that will be in contact with the solution must be heated on a hotplate before spinning if the environment is cold. The concentration of beta phase chromophores formed by these small precipitates is of the order of 0.1 % (estimated from the absorption spectrum), but this is sufficient to exhibit a beta phase peak in the emission spectrum near 438 nm that is of similar magnitude to the alpha phase emission, shown in figure 3-9. Spinning onto a cold substrate often leads to spectra where the first vibronic replica is of higher intensity in the emission spectrum than the 0-0 transition, indicating that the polymer microstructure is no longer fully amorphous.

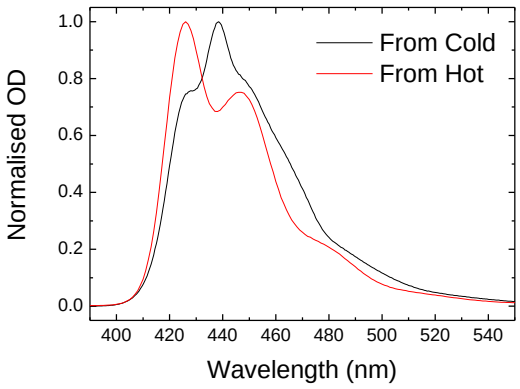

Figure 3-9: Emission spectra from a film spun from cold solution (black) and hot solution (red) at 5 mg/mL

For simple emission and absorption spectroscopy an OD of approximately 0.5 or less is preferable in order to reduce the influence of self-absorption on the emission spectrum, especially for polyfluorenes where there is significant spectral overlap which is further increased by the formation of the beta phase.

3.2.5 Toluene Vapour Exposure of Thin Film Samples

The method of toluene vapour exposure, first discussed by Grell et al.[25] was used to induce beta phase formation in thin films of PF6 to PF10, although little detail is provided in the paper for accurate replication of their method. Initial attempts to induce this phase involved enclosing the sample with a reservoir of toluene under an upturned glass enclosure, but this method yielded no significant changes even after several days. In order to produce a high density of toluene vapour, the method shown in figure 3-10 was adopted. A hotplate is set to 120°C indicated temperature, which corresponds to a lower temperature of 65°C for the toluene in a beaker upon it. This hotplate heats a pool of toluene at the bottom of a large beaker, providing a strong vapour flow out of the beaker which is shielded from the lateral airflow introduced by the fume cupboard. A clamp stand is used to suspend the film sample in a metal sample holder, face down and 5 cm above the solvent surface.

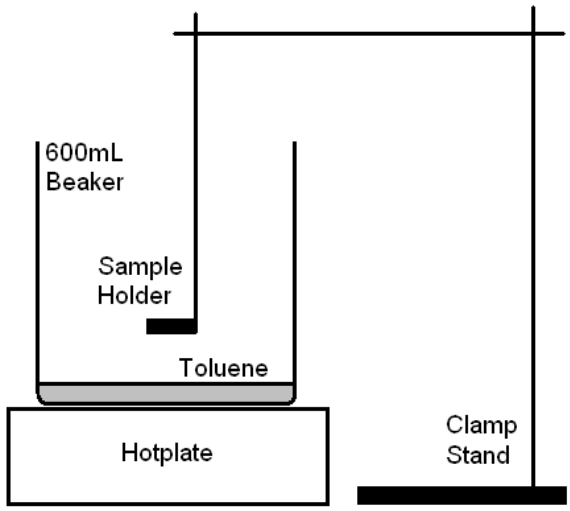

Figure 3-10: Arrangement for toluene vapour treatment of thin films to induce beta phase formation. The hotplate is set to 120°C giving a solvent temperature of 65°C. This is set inside a fume cupboard.

The high temperature of the solvent creates a very high vapour density, which is sufficient to saturate the film to the maximum supported beta phase content within 10 minutes (see data in chapter 5.4). This is dramatically less time than others have used (from 3-4 hours to even 3 days), but more controllable than the method of dipping the film in toluene used by Lu et al.[26] In this way a large number of samples could be prepared within the course of this work, in order to ensure that scientifically repeatable data had been obtained.

3.2.6 Single Photon Counting

Further to the use of steady-state emission spectra, samples were also studied with Time-Correlated Single Photon Counting. The sample is excited by a pulsed laser comprising a Verdi V8 green diode laser which pumps a picosecond Mira 9000 Ti:Sapphire mode-locked tuneable oscillator cavity. This cavity is tuned to 780 nm and produces a stream of pulses with a mean power of 0.7-1.2 W, dependent upon the precise cavity conditions. These pulses are passed through a beta-barium borate crystal aligned on a micrometer support to provide frequency doubling to 390 nm. The mixed 780 nm/390 nm beam is then split at a layered dielectric mirror that reflects the longer wavelength component onto a photodiode to trigger the streak camera start time. The 390nm component is directed through alignment irises and onto the sample. The sample emission is collected through a

filter to remove the laser scatter, and focused into a broad bandpass monochromator. The resulting frequency-separated light is directed into the single photon counting detector.

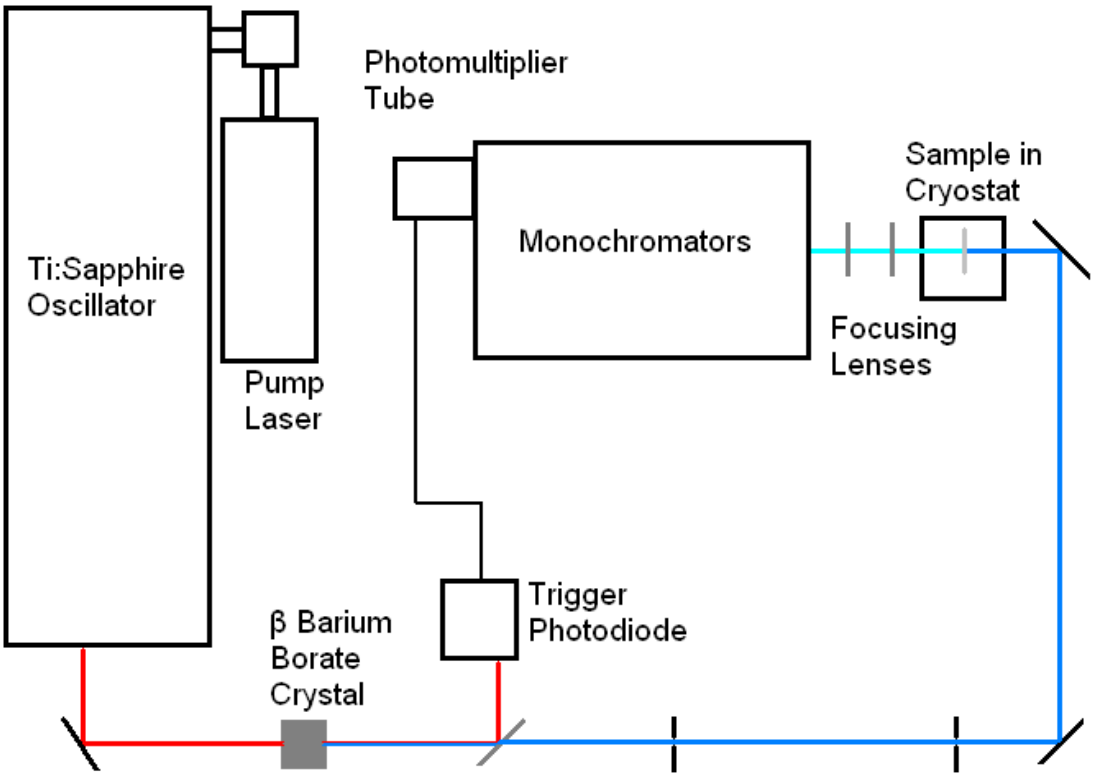

Figure 3-11: experimental arrangement for collection of TCSPC decays. Coloured lines indicate light paths through the system outside of the instruments.

The detector is a water-cooled high resolution Hamamatsu E3809U-50 MCP photomultiplier tube for single photon detection attached to the double-monochromator assembly. The computer attached to the detector has a Becker & Hickl SPC-630 Time-Correlated Single-Photon Counting (TCSPC) card, which has a maximum of 4096 channels, with adjustable time window resolution with a minimum of 814 fs. This allows photoluminescence decays to be measured both on ultra-short timescales as well as on longer time domains up to 10 ns not accessible to the streak camera. The laser pulses measured by the system (incorporating the detector response characteristics) have a full width half maximum of 21-23 ps. With deconvolution of the decays, components with lifetimes of several

picoseconds can be fitted, although the accuracy and validity of fitting such short lifetime components is at best uncertain.

The TCSPC module builds up a profile of the decay by repeated measurements of the same experiment. The incident laser beam that excites the sample passes through a beam-splitter that passes a small part of the laser pulse to a Becker & Hickl PHD-400N fast photodiode that provides the trigger pulse to the TCSPC card. This trigger pulse stops the charging of a capacitor within the card, which is started when a photon, emitted from the sample through the monochromators to the detector triggers a second pulse. This reverse mode of operation ensures that only real events are counted. The charge stored on the capacitor is read out and binned in the appropriate time channel. The probability of the photon from the sample arriving within a certain time bin is determined by the sample lifetime, and after a large number of repeats, of the order of 10^6 for an average sample, the profile of the integrated counts across the time bins represents the decay profile of the sample in the time domain. The laser repetition rate is 76 MHz, and with a low gain preamplifier on the MCP this allows most decay profiles to be collected within a few minutes.

3.2.7 Deconvolution of Fluorescence Decays

The fluorescence decay profiles collected from the streak camera and TCSPC provide little information about the dynamics of the sample decay. To extract quantitative information from the profile, the fluorescence decay must be fitted with a model of the decay, and from the model parameters the lifetimes of the various decay components can be derived.

The sample decay profile analysis is further complicated by the need to take account of the excitation profile. A crude analysis technique would be to take account of the full width at half maximum of the scattered laser pulse passing into the system, which would set a lower limit for the accuracy with which the decay can be fitted. Unfortunately, since the samples measured in this work are solid films whose lifetimes are recorded as a function of temperature, the samples must be measured within a cryostat, and there are strong scatter signals generated by the quartz windows.

These reflections of the original laser pulse provide additional excitation to the sample at later times than the initial pulse. The separation between the various windows and other nearby optics is of the order of a few centimetres, leading to time offsets between the main pulse and the scattered pulses of the order of 100 s of picoseconds. This leads to distortions of the smooth decay of the light from the sample as more energy is fed into the system, and these distortions occur at the timescales of the decay which are the most critical for accurate fitting for the fluorescence lifetime of polyfluorenes, which are in the region of 200 ps. This issue rules out the possibility of using direct exponential fitting of the decay for providing an accurate value of the lifetime components.

To take account of the complex laser excitation profile arriving at the sample, the laser scatter was recorded in every case for every sample along with its emission profile. This allowed the decay to be more accurately fitted with global parameter analysis using Globals WE fitting software. Multiple decays from different samples of alpha and beta phase films were recorded, yielding similar results each time to an accuracy of 10% including sample-to-sample variation. It was found that in some circumstances the scatter profile was not very similar to the excitation profile arriving at the sample. Before proceeding with the measurement, the film samples were tilted in the horizontal axis by a small angle to greatly reduce the scattered laser pulse intensity reaching the sample, since this caused the specular reflections to reflect off the cryostat windows at an angle sufficient to avoid the returning beam from hitting the film surface. Further experimentation suggests that the sample angle to the incident beam must not be too steep, as this causes the scattered pulses reaching the detector to be reduced more than the true scattered pulses reaching the sample, and the deconvolution gives poor results. An angle of approximately 10° gave the most acceptable results.

Globals software is used to fit the data. This builds a decay profile of the sample using the laser scatter profile and a multiple-exponential decay model where each component represents one of the sample species. The resulting modelled profile was then minimised to the recorded data using

the PORT3 algorithm in the program, and the resulting lifetimes were taken to be the exponential lifetime decay parameters. An example of a fit is shown in figure 3-12.

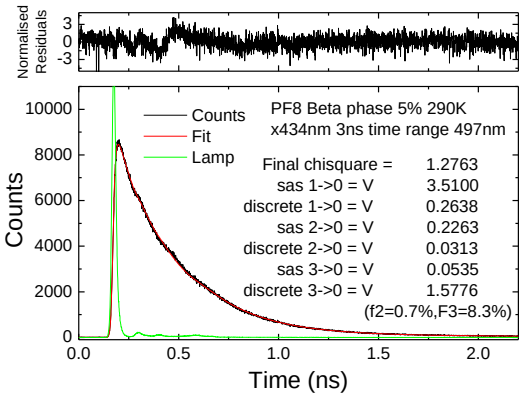

Figure 3-12: Example deconvolution fit to a fluorescence decay profile with the laser scatter profile and the 3-exponential fit using the components listed in the graph.

It is immediately obvious that there is a discrepancy between the laser profile recorded and the true excitation of the sample, since there are deviations in the residuals that show where the recorded scatter intensity is not sufficiently large to force the modelled data to fully track the measured decay. This example data is average in terms of the quality of the fit amongst the measured samples. For shorter lifetimes the fit often deviates slightly more from the measurement, and for longer lifetimes, especially for samples measured at the keto emission wavelength, the fits are extremely precise.

The samples were fitted with single exponentials initially, and more components were added if necessary to improve the fit up to the maximum of four permitted by the software. Where too many components are being used, the fit will often fail, with the error returned that there is a singular point, or two components will collapse to the same lifetime. It will also be observed in these situations that there is no significant reduction in the chi-square value when this extra fitting parameter is added.

3.3 References

1. de Freitas, P. S.; Scherf, U.; Collon, M.; List, E. J. W. *e-Polymers* **2002**, 7.
2. Leclerc, M. *J.Polym.Sci. A-Polym.Chem.* **2001,** 39, (17), 2867-2873.
3. Liu, B.; Yu, W. L.; Lai, Y. H.; Huang, W. *Chem. Mater.* **2001,** 13, (6), 1984-1991.
4. Monkman, A. P.; Rothe, C.; King, S. M.; Dias, F. D., Polyfluorene Photophysics. In *Polyfluorenes*, Scherf, U.; Neher, D., Eds. Springer: 2008; pp 187-226.
5. Becker, S.; Ego, C.; Grimsdale, A. C.; List, E. J. W.; Marsitzky, D.; Pogantsch, A.; Setayesh, S.; Leising, G.; Mullen, K. *Synth. Met.* **2001,** 125, (1), 73-80.
6. Grell, M.; Bradley, D. D. C.; Inbasekaran, M.; Woo, E. P. *Adv. Mater.* **1997,** 9, (10), 798.
7. Grell, M.; Bradley, D. D. C.; Long, X.; Chamberlain, T.; Inbasekaran, M.; Woo, E. P.; Soliman, M. *Acta Polym.* **1998,** 49, (8), 439-444.
8. Grice, A. W.; Bradley, D. D. C.; Bernius, M. T.; Inbasekaran, M.; Wu, W. W.; Woo, E. P. *Appl. Phys. Lett.* **1998,** 73, (5), 629-631.
9. Ariu, M.; Lidzey, D. G.; Bradley, D. D. C. *Synth. Met.* **2000,** 111, 607-610.
10. Cadby, A. J.; Lane, P. A.; Mellor, H.; Martin, S. J.; Grell, M.; Giebeler, C.; Bradley, D. D. C.; Wohlgenannt, M.; An, C.; Vardeny, Z. V. *Phys. Rev. B* **2000,** 62, (23), 15604-15609.
11. Kitts, C. C.; Vanden-Boot, D. A. *Polymer* **2007,** 48, 2322-2330.
12. Knaapila, M.; Dias, F. B.; Garamus, V. M.; Almasy, L.; Torkkeli, M.; Leppanen, K.; Galbrecht, F.; Preis, E.; Burrows, H. D.; Scherf, U.; Monkman, A. P. *Macromol.* **2007,** 26, 9398-9405.
13. Knaapila, M.; Almasy, L.; Garamus, V. M.; Ramos, M. L.; Justino, L. L. G.; Galbrecht, F.; Preis, E.; Scherf, U.; Burrows, H. D.; Monkman, A. P. *Polymer* **2008,** 49, (8), 2033-2038.
14. List, E. J. W.; Guentner, R.; de Freitas, P. S.; Scherf, U. *Adv. Mater.* **2002,** 14, (5), 374-378.
15. Zojer, E.; Pogantsch, A.; Hennebicq, E.; Beljonne, D.; Bredas, J. L.; de Freitas, P. S.; Scherf, U.; List, E. J. W. *J. Chem. Phys.* **2002,** 117, (14), 6794-6802.
16. Hintschich, S. I.; Rothe, C.; Sinha, S.; Monkman, A. P.; de Freitas, P. S.; Scherf, U. *J. Chem. Phys.* **2003,** 119, (22), 12017-12022.
17. Dias, F. B.; Knaapila, M.; Monkman, A. P.; Burrows, H. D. *Macromol.* **2006,** 39, (4), 1598-1606.
18. Lupton, J. M.; Craig, M. R.; Meijer, E. W. *Appl. Phys. Lett.* **2002,** 80, (24), 4489-4491.
19. Perepichka, I. I.; Perepichka, I. F.; Bryce, M. R.; Palsson, L.-O. *Chem. Commun.* **2005**, (27), 3397-3399.
20. Li, H.; Batsanov, A. S.; Moss, K. C.; Vaughan, H. L.; Dias, F. B.; Kamtekar, K. T.; Bryce, M. R.; Monkman, A. P. *Chem.Commun.* **2010,** 46, (26), 4812-4814.
21. Li, Y. Y.; Wu, H. B.; Zou, J. H.; Ying, L.; Yang, W.; Cao, Y. *Organ. Electron.* **2009,** 10, (5), 901-909.
22. Yang, W.; Hou, Q.; Liu, C. Z.; Niu, Y. H.; Huang, J.; Yang, R. Q.; Cao, Y. *J.Mater. Chem.* **2003,** 13, (6), 1351-1355.
23. Hintschich, S. I. Picosecond Studies of Excited States in Conjugated Polymers. Durham University, Durham, 2007.
24. Chen, S. H.; Su, A. C.; Su, C. H.; Chen, S. A. *Macromol.* **2005,** 38, (2), 379-385.
25. Grell, M.; Bradley, D. D. C.; Ungar, G.; Hill, J.; Whitehead, K. S. *Macromol.* **1999,** 32, 5810-5817.
26. Lu, H. H.; Liu, C. Y.; Chang, C. H.; Chen, S. A. *Adv.Mater.* **2007,** 19, (18), 2574.

4 Beta Phase Formation in Linear Alkyl Chain Polyfluorene Solutions

4.1 Introduction

An early-developed and widely used polymer for stable blue-light emission is poly(9,9-di-*n*-octylfluorene) (PF8). The carbon numbering for the fluorene molecular unit is shown in Figure 4-1: the monomers are bonded on the 7 and 2 positions to form the polymer, and the side chains are both bonded at position 9. The length between adjacent 7-position carbon atoms (the periodicity of the polymer chain) is 8.38 Å. PF8 has long been known to exhibit spectral changes as a result of a change in the conformation of its polymer chains. However, there is still uncertainty as to the precise nature of the physics behind this change. This chapter will cover some of the relevant physics, and then review the important literature that shows the progress leading to this work. The experimental results will then be presented that show clearly the critical role of the side chains in the formation of the beta phase in PF8 solutions in MCH, and from the detailed analysis of this data a mechanism for the formation of the beta phase will be presented.

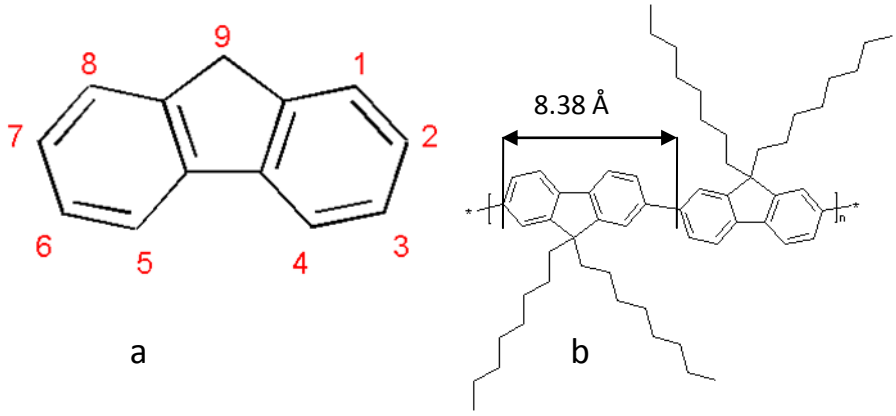

Figure 4-1: a) the carbon numbering on the fluorene unit, and b) diagram showing the repeat unit length.

4.1.1 Van der Waals Interactions

The polymer poly(9,9-di-*n*-octylfluorene) and its close analogues are uncharged, non-polar hydrocarbons, and so there are no intermolecular interactions resulting from permanent dipole attractions or hydrogen bonds. Electrons within molecular materials are confined to specific orbitals, which may be defined as time-averaged probability density distributions of the electron's location in space. At any point in time there may be an imbalance in the distribution of the electrons within the molecule, leaving temporary small net dipoles at one or more positions on the molecule. Where two molecules come into close proximity, an uneven distribution in the electrons on one molecule induces a corresponding opposite uneven electron distribution in the other, with the result that a temporary dipole-dipole attraction occurs between them. The magnitude of the attraction between the molecules scales with the number of electrons and the surface area in contact.

The van der Waals interactions are short range interactions, so are only likely to be active between nearest neighbor molecules. The attractive force is often modeled by the Lennard-Jones potential energy (V):[1]

$$V = 4\varepsilon\left[\left(\frac{\sigma}{r}\right)^{12} - \left(\frac{\sigma}{r}\right)^{6}\right] \qquad (4\text{-}1)$$

Where ε is the depth of the potential well, σ is the distance at which the inter-particle potential is zero, and r is the distance between the particles.

4.1.2 Solubility and solvent quality

The major factors affecting the solubility of these polymers in organic solvents are temperature, the presence of phenyl rings in the solvent, the presence of hydrogen bonding, and polarity of either polymer or solvent.

In the absence of specific interactions, the polymer solubility can be predicted on the basis of cohesive energy densities of the polymer and solvent, described by the Hildebrand solubility parameter, δ. [2-4]

$$\delta_i = \left(\frac{\Delta E_i^V}{V_i}\right)^{1/2} = \left(\frac{\Delta H_i^V - RT}{V_i}\right)^{1/2} \quad (4\text{-}2)$$

Where ΔE_i^V is the energy of vaporization of species *i* and V_i is the molar volume of species *I*, ΔH_i^V is the enthalpy of vaporization of species *i* under standard conditions (293.15 K, 101.325 kPa), *R* is the ideal gas constant and *T* is the temperature. The enthalpy change upon mixing is:[3, 5]

$$\Delta H_m = V(\delta_1 - \delta_2)^2 \phi_1 \phi_2 \quad (4\text{-}3)$$

where ϕ_i is the volume fraction of each component in the mixture. Dissolution is determined by the Gibbs free energy change upon mixing:

$$\Delta G_m = \Delta H_m - T\Delta S_m \quad (4\text{-}4)$$

where ΔS_m is the entropy change upon mixing.[3, 5] Spontaneous mixing occurs when this energy is negative, and when this is not the case two or more phases will result from the mixing process.[3] For high molecular weight polymers, the increase in entropy is relatively small, leaving the enthalpy change as the main determining factor of the free energy.[3]

Another theory for quantifying solubility is the Hansen solubility parameter. This considers the total solubility to be a combination of several factors corresponding to hydrogen bonding, δ_h, dipole interactions, δ_p, and dispersive interactions, δ_d.[6] For systems where there is no hydrogen bonding or strong dipoles, such as the solvents and polymers used in this chapter, the Hansen dispersive parameter is similar to the Hildebrand solubility parameter.[6]

The units of the solubility parameter are conventionally used in non-SI units of $cal^{1/2}\ cm^{-3/2}$, which simply converts to the SI units of $MPa^{1/2}$ by multiplying by a factor of 2.05. The values of δ used for the solvents in this work are 8.9 $cal^{1/2}\ cm^{-3/2}$ for toluene,[4] and 7.5 $cal^{1/2}\ cm^{-3/2}$ for methylcyclohexane. Values of δ near 9.3 $cal^{1/2}\ cm^{-3/2}$ are optimal for PF8.[7]

4.1.3 The Flory-Higgins Equation for Polymer Solutions

The Helmholtz free energy of mixing for a simple polymer solution is defined by the Flory-Higgins Equation: [5]

$$\Delta F_{mix} = kT\left[\frac{\phi}{N}\ln\phi + (1-\phi)\ln(1-\phi) + \chi\phi(1-\phi)\right] \quad (4\text{-}5)$$

Where ϕ is the volume fraction of the polymer and N is the number of polymer units in the chain. The Flory interaction parameter is defined empirically [5]

$$\chi \cong A + \frac{B}{T} \quad (4\text{-}6)$$

Where A represents the contribution from entropy change and B represents contributions from enthalpy change. This demonstrates the dependence of the solubility on the polymer chain length, the concentration, and the temperature.

4.2 Literature Review

The beta phase of poly(9,9-di-*n*-octylfluorene) (PF8) was first reported by Grell et al. in 1997, who noted the formation of a solid gel in concentrated solutions and a change in the optical spectra of the polymer upon thermal treatment and the use of poor solvents to make solutions and films. [8-9] They applied computer modeling to a single di-*n*-ocltylfluorene molecule as well as coupled Gel Permeation Chromatography/Light Scattering measurements of the polymer to determine a Kuhn length (see 5.2.2) of 17.1±2.1 nm, much larger than the monomer unit at 0.83 nm. They concluded that the polymer is not a completely rigid 'hairy rod' but a 'wormlike chain.' [10] Spectrophotometry revealed the appearance of a small absorption peak at 436 nm, redshifted with respect to the broad

main absorption band centred at 385nm. This band appeared and increased to a maximum over a timescale of about 48hrs in poor solvent, whilst the solution (10 mg mL^{-1}) formed an infinitely viscous gel. The phase was attributed to simple aggregation effects driven by poor solubility, leading to sites with a lower energy gap for optical transitions.[10] Photoluminescence of the aggregated films showed a redshifted and well-resolved emission spectrum with peaks at 438 nm, 467 nm, 500 nm and 536 nm, which are the main band of the beta phase (at 438 nm) and its vibrational replicas. This was observed independent of independent of the excitation wavelength, implying that efficient energy transfer takes place between the disordered bulk and the lower energy aggregated chains. This was later confirmed by more detailed measurements of the photoluminescence spectra as a function of beta phase content by Khan et al.[11] and by time-resolved microwave conductivity of the beta phase by Prins et al.,[12] that showed charge trapping takes place.

Grell et al. then went on to study the structure of the polymer upon forming this new phase.[13] They produced beta phase in samples by thermal cycling of samples to low temperatures and by exposure to saturated toluene vapour over 3 days, and concluded that mechanical stress, from a mismatch in the thermal expansion coefficients of polymer and substrate or from solvent swelling of the film, led to elongation of the polymer chain and hence extended planarization of the chain, from which the redshifted emission occurs. They measured the intrachain correlation length in the alpha phase to be 15 nm (18 monomer units) and for beta phase to be 22 nm (26 monomer units), indicating that the effective conjugation length changes from being conformationally limited to intrinsically limited. They proposed that this extended planarization conformation approaches a 'planarised zig-zag' producing extended conjugation over many monomer units, because the optical spectra of the planarised chains closely resemble those of the fully planarised ladder-type poly(*para*-phenylene). They concluded that the intra-chain ordering produced by the stress governs the optical properties, and that the beta phase formation in films is entirely an intrachain process.[13]

Cadby et al. then studied the beta phase using electroabsorption spectroscopy in 2000, confirming the 'extended conjugation' nature of the phase, with redshifted absorption and higher polarisability.[14] They also studied the Photo-Induced Absorption (PIA) spectrum and found that the amorphous α phase is dominated by triplet excitons, but the beta phase PIA spectrum showed features from both triplets and polarons. Ariu et al. went on to study the Photo-Luminescent Quantum Yield (PLQY) of poly(9,9-di-*n*-octylfluorene) in the alpha phase, and beta phase.[15] The PLQY in films measured in each of the 'as-spun', crystalline and quenched nematic glass phases to be around 85% at 10 K, and it decreased at higher temperature to around 50-75%. The beta phase film PLQY at room temperature is intrinsically less efficient at 55%, which decreased to 40% at 10 K due to the greater population of polarons at lower temperatures. The lower energy beta phase sites act as traps for the polarons and quench the singlet emission, reducing the PLQY of the beta phase. However, their results may have been influenced by the presence of fluorenone (or keto defect).

However, it is interesting to note that for real electroluminescent (EL) device performance, the efficiency of devices which contain some beta phase as opposed to purely α phase is actually much higher, since the lower energy beta phase sites act as traps for electrons and increases the recombination probability of charges.[16] The hole mobility is also increased, leading to a better balance of charges, since the large imbalance between electron and hole mobilities in α phase polyfluorene is reduced. Lu et al. reported an increase in EL device efficiency from 1.26 cd A^{-1} to 3.85 cd A^{-1} (at 3.8 V and a useful brightness of 176 cd m^{-2}), which gave an External Quantum Efficiency (EQE) increase from 1.08% to 3.33%. At publication in 2007 this was the highest efficiency yet achieved for pure blue emission, with CIE coordinates of (0.168, 0.115) at 4 V.

Winokur et al. carried out extensive studies on the phase transition in thin films from beta phase to α phase, termed the Order-Disorder Transition (ODT).[17] Absorption, emission and X-ray scattering spectra as a function of temperature show that the formation of beta phase during thermal cycling from 293K to 77K then back to 293K actually occurs upon slowly warming past 260K, and that

cooling below 250K is unnecessary. Upon starting the transition, the appearance of the characteristic beta phase spectroscopic peaks follows an Avrami type expression; exponentially approaching the maximum value after several hours.[17] They fitted the emission spectrum at low temperature to find a Huang-Rhys parameter of 0.75. They conclude that the beta phase is an intra-chain relaxation process which can be followed by aggregation.

Khan et al. made detailed studies of the energy transfer to the beta phase.[11] They cast films from different solvents to control the relative amounts of beta phase chains present. They used Franck-Condon analysis with distinct contributions from the two phases to model the luminescence at 8K. The Huang-Rhys parameter for the beta phase is shown to be 0.6, or approximately half the value obtained for the glassy phase, in agreement with a more delocalized exciton in the beta phase. Time-resolved photoluminescence measurements on a film with (they estimate) ~25% of beta phase show a fast transfer of excitons from the glassy to the beta phase, indicating that the two phases are well intermixed. Assuming the transfer dynamics to be governed by dipole-dipole coupling, they obtained a Förster radius of 8.26±0.6 nm, significantly larger than that typically found in the glassy phase. These results are consistent with the large spectral overlap between the emission of the glassy phase and the absorption of the beta phase. This explains why the latter dominates the emission, even from films containing only a small fraction of beta phase chains.

Rothe et al. used time-resolved emission spectra and photo-induced absorption to show that the beta phase is not simply an extended intra-chain conjugation, but that inter-chain effects are also important.[18] This is demonstrated by significant differences between the PIA spectra of PF8 and MeLPPP, which both have planar intra-molecular configurations. The beta phase also acts as an energetic trap for both singlet and triplet excitons initially created on amorphous chain segments, with the triplets being trapped more effectively due to their longer lifetime. Triplet migration is shown to be via thermally activated hopping, possibly competing with Förster mechanisms for energy transfer. In beta-phase containing films, the segregation time, between dispersive and

thermally activated migration, is strongly dependent on the separation between beta-phase domains and indicates that beta-phase content grows in via further nucleation of sites as opposed to growth of larger domains.

Becker and Lupton attempted Single-Molecule Spectroscopy (SMS) on PF8 polymers dispersed at a concentration of 10^{-6} in a Zeonex matrix.[19] The spectra show beta phase emission claimed to be from single molecules, and they claim the effects are entirely from intra-molecular interactions. However, they cite as their evidence against aggregation the monotonic scaling behaviour with molecular weight and surface density in 'very similar' polymeric systems. However, PF2/6, most commonly cited as a similar comparison, has completely different aggregation properties. It has been shown that the aggregation and beta phase formation of linear alkyl-substituted polyfluorenes varies very strongly over tiny changes in chain length and aggregation does not occur with branched chains.[20-21]

Chunwaschirasiri et al. then approached the modeling aspect of the polymer conformations in the different phases.[22] They carried out Frenkel-type tight-binding band structure calculations of the single chain absorption and photoluminescence spectra, including a full Franck-Condon vibronic progression, which matched the measured spectra very well, although there were notable discrepancies with the α phase 110K spectra. They classified distinct classes of conformation (C_α C_{beta} and C_γ) corresponding to different torsional angles between adjacent fluorene units. The C_{beta} isomer is characterized by a mean angle of ~165° between monomer units, whilst the C_α is twisted by an angle of ~135°. Their model assumed that the side chains fold over and interact with the phenyl backbone when the beta phase forms. They neglect the effect of the solvent on the polymer and side chains.

Following the work of Chunwaschirasiri et al., Arif et al. studied the morphology differences between alpha and beta phase PF8 by Raman spectroscopy.[23] They found that the major vibrational modes of the alpha phase and beta phase are very similar, with small-scale shifts in the 1300 cm^{-1} vibration position correlating with the presence of the beta phase. Significantly, they found that the beta

phase was characterized by low-energy vibrational modes in the region below 500 cm^{-1} that match to modelled vibrations of the side chains in a specific extended conformation (all-anti-gauche). These measurements were replicated in Raman studies of beta phase PF8 by Khan et al.[24] and Arif et al.[23].

Dias et al. studied the behaviour of PF8 in dilute solution in methylcyclohexane (MCH), including a model of the thermodynamics of the phase formation.[25] The fraction of beta phase formed in solution was found to be independent of the concentration in the range studied (3-23 μg mL^{-1}). The absorption spectra as a function of temperature show that α and beta phases coexist in equilibrium. Further excitation spectra in dilute solution show the beta phase formation is reversible over 24 hrs. The relative fraction of beta phase present as a function of temperature is modelled using a 2-step process; firstly the planarization of individual chains, then the aggregation of these chains. From the temperature dependence of the 437-438 nm peak intensity, the transition temperature T_{beta} = 261 K, enthalpy ΔH_{beta} = -18.0kcal mol^{-1}, and entropy ΔS_{beta}=-68.4 cal K^{-1} mol^{-1} were obtained.

Kitts et al. studied the effects of solvent quality on the formation of beta phase PF8 in solutions, which strongly influences the fraction of the phase that forms.[26] This work followed on from some initial studies in work by Grell et al. mentioned earlier.[13] Detailed spectroscopy and Differential Scanning Calorimetry of the phase formation highlighted a trend in the transition temperatures and enthalpies. There is a large hysteresis in the formation and dissolution of beta phase upon cooling and warming the sample. This was attributed to the aggregation of collapsed chains stabilizing the phase at higher temperatures. Other studies have shown that the presence of beta phase can affect properties of the material such as refractive index.[27]

Caruso and Anni studied the real-time effect of solvent swelling in thin films leading to beta phase formation using confocal microscopy, showing that the majority of the beta phase formation occurs within the first five minutes.[28] The beta phase formation is dependent upon the solvent; those which interact with the phenyl rings on the polymer backbone cause the phase change, but those which

interact with the side chains do not. They also noted that the beta phase occurs in initial seed clusters followed by growth of these clusters.

Anni et al. have further studied the beta phase in thin films by confocal microscopy, showing that the beta phase within the films showed local variations in the emission spectra, which highlighted a non-uniform beta phase distribution, with some domains of high beta phase concentration and others without.[29] The regions of variation in the fluorescence spectra correlated with microscopic irregularities in the morphology.

The Förster radius of the transfer of energy between the alpha phase and the beta phase in PF8 has been measured to be 5.4 nm by Shaw et al.[30] They use a line-dipole approximation to model the dipole-dipole interactions for the energy transfer. They use the assumption that the beta phase chromophores are uniformly dispersed, which does not fully match up to their data and conflicts with the findings of the confocal microscopy studies by Anni et al.

Recent work by Knaapila et al. used Small Angle Neutron Scattering (SANS), Small Angle X-ray Scattering (SAXS), Wide Angle X-ray Scattering (WAXS), Absorption spectroscopy and PL to study a closely-related family of linear alkyl-substituted polyfluorenes with chain lengths of 6, 7, 8, 9 and 10 carbons (Termed PF6-PF10).[20] The data revealed that at concentrations of ~10 mg mL^{-1}in MCH the polymer chains in PF6-PF9 form sheet-like aggregates with a thickness of ~2 polymer chains. There is also an odd-even effect in which the PF6 and PF8 sheets are broader and thinner than their PF7 and PF9 counterparts. PF10 remains as solvated chains. Emission from beta phase was observed for PF7, PF8 and PF9 only, and PF8 exhibited the highest degree of such emission, implying an optimal linear side-chain length for this phase formation. Follow-up work on these polymers at the same concentration in toluene showed thick (6 nm) sheet-like aggregates for PF6 and PF7, whilst PF8-PF10 showed fully solvated chains.[31] No evidence for beta phase formation in toluene was found.

This work aims to further analyse the formation efficiency of beta phase in solutions and films of the polymers PF6-PF10 to obtain more detail about the formation mechanism. By following the optical absorption, emission and excitation spectra, this chapter will show for the first time the characteristics of beta phase formation in PF7-PF10 in MCH solution.[32] This provides more conclusive evidence that the β phase is not an intra-molecular process, but dependent upon the interactions between side chains of adjacent chain segments in order to form.[32] From the data collected, a mechanism is proposed for the physical interactions that lead to the formation of the beta phase in MCH solution. In Chapter 5, beta phase is shown to occur in PF10 thin films,[33] a result not predicted by the model of Winokur et al.[22]

4.3 Results

4.3.1 Absorption Spectra in MCH solution

MCH is a poor solvent for polyfluorenes, because it is a saturated hydrocarbon whilst the polymer backbone consists of benzene rings with delocalised electrons. The solubility of polyflourenes in MCH arises primarily from the intermolecular interactions between the alkyl side chains and the solvent molecules via van der Waals interactions. Precipitation can occur upon reducing the temperature, even at quite low concentrations.[34] However, the data collected using very dilute samples is unaffected by this since smaller aggregates are formed which are not sufficiently large to drop out of solution, and an isobestic point could be clearly seen in the absorption spectra of PF8 taken as a function of temperature in dilute solution.[34]

Dilute solution absorption spectra were collected at equilibrium as a function of temperature for the purposes of establishing the isobestic points for the different polymers. Representative data for PF9 at a concentration of 0.6 μg/mL is given in figure 4-2. The curves are not scaled. An increase in optical density above 397nm is matched by a drop in the optical density below this wavelength, indicating a transfer of oscillator strength to a new phase in part of the material.[9-10]

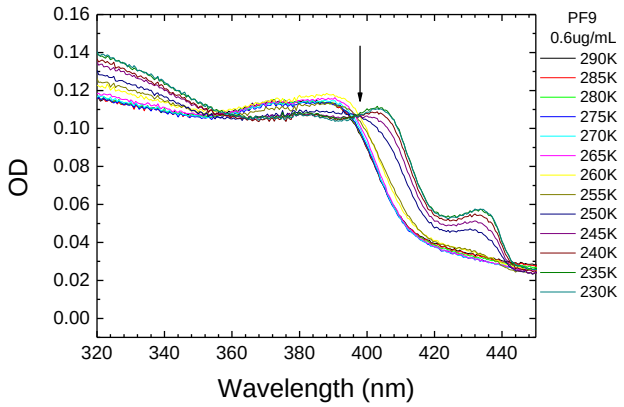

Figure 4-2: Equilibrium absorption spectra at different temperatures for PF9 at a concentration of 0.6 µg mL^{-1} in MCH. The arrow marks the isobestic point.

The spectra at wavelengths below 350 nm are clearly being obscured by the rising scattering as the solution is cooled and the beta phase particles form small aggregates. The data collected from more concentrated solutions is far less affected by this and shows much less noise. The arrow marks the isobestic point at 397 nm. The isobestic points identified for all the polymers are given in table 4-1.

The absorption spectra at higher concentrations (~10 µg mL^{-1}) are given in figure 4-3. The curves at lower temperatures were normalised at the isobestic point identified previously in PF8,[34] to correct for precipitation effects in the more concentrated solutions used to provide less noisy data.

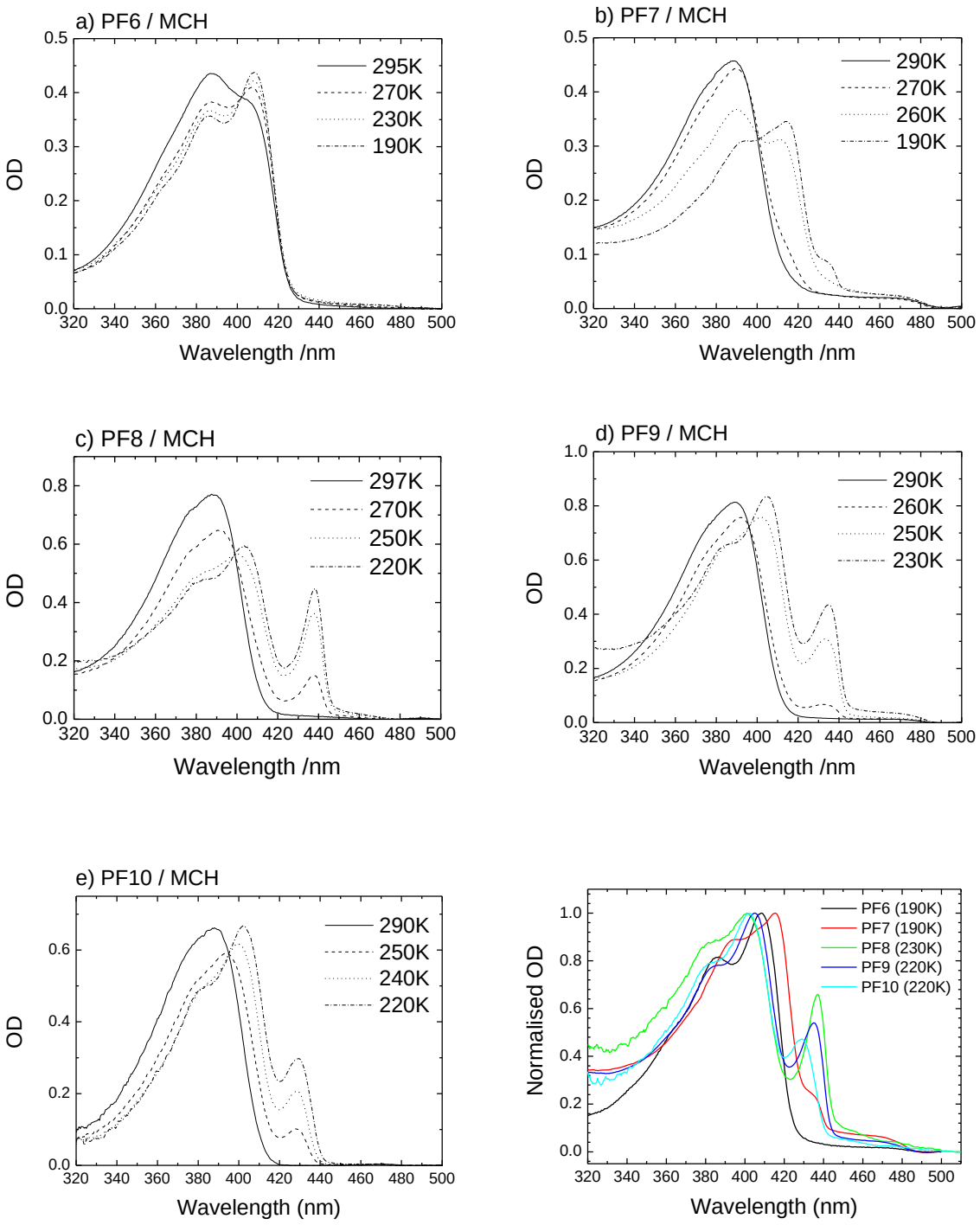

Figure 4-3: Temperature dependent absorption spectra in MCH solution for the polyfluorenes a) PF6 (6 µg mL^{-1}), b) PF7 (6 µg mL^{-1}), c) PF8 (23 µg mL^{-1}), d) PF9 (7 µg mL^{-1}) and e) PF10 (10 µg mL^{-1}). f) the final-state spectra of PF6-PF10 at low temperature (marked in legend).

Table 4-1: Isobestic points derived from the dilute solution spectra, and details of the beta-phase feature from the concentrated solution spectra. [a]shoulder location [b]peak location.

n	Isobestic point (nm)	Beta Phase Feature
6	402	none
7	400	435 nm[a]
8	399	439 nm[b]
9	397	435 nm[b]
10	395	429 nm[b]

In PF6 at room temperature, the main band shows a peak at 387 nm and a shoulder at 408 nm. This 408nm shoulder dominates over the peak at lower temperatures, but no peak corresponding to the presence of beta phase is observed at ~437 nm. In PF7 the main band is redshifted significantly by the appearance of a new peak at 414 nm, and a small shoulder around 435 nm indicates the formation of beta phase in this polymer at very low temperatures. Note that this new absorption band starts to be observed only below 200K and no further growth is detected down to the freezing point of the solvent (160K). There is also unusual behaviour in that the main band shift is much larger than for the other polymers in the series, a result that may be related to its aggregate thickness measured in MCH solution by x-ray and neutron scattering, which was smaller than for the other polymers in this series.[20] The PF8 main band is redshifted by a new peak appearing at 408nm, and a strong absorption band at 437nm which appears below 280K and grows stronger with decreasing temperature. PF9 shows very similar behaviour to PF8; a new main band absorption appears at 405 nm, along with strong absorption at 435 nm, similar to that seen in the PF8 but of lower height relative to the main absorption band. PF10 shows similar behaviour again to that seen in the PF8 but of lower height relative to the main absorption band, but also the beta phase peak is located at significantly shorter wavelength.

Figure 4-3 clearly shows that the length of the linear alkyl side chain has a strong influence on the formation of beta phase, and that formation is most favourable for (but not restricted to) a chain

length of 8 carbon atoms. The decrease in solvent action at lower temperatures, with concomitant increase in polymer-polymer interaction, is not sufficient to explain this favourability. In fact, PF6 is affected the most by solvent action because it is the least soluble of the polymers, yet no beta phase is observed.

PF6 shows spontaneous aggregation at room temperature. After heating to 100°C, the spectrum is the same as that of the PF10, but over the course of 6 hours at 295K the absorption spectrum shifts to become structured (figure 4-4a), indicating the presence of an aggregate. PF6 has the shortest side chains of the group, and is therefore expected to have the least interactions with the solvent. From equation 4-5 the solvent quality is expected to drop at lower temperatures, with the result that the free energy of mixing will drop or even become positive, and so the solution will separate into separate phases of liquid solvent and solid aggregates. At this point it is more energetically favourable for the polymer to interact with other polymer chains or fold upon itself than it is for the polymer to interact with the solvent molecules.

The presence of an aggregate is supported by the data in figure 4-4b, where the OD at the location of the shoulder rises smoothly to the new equilibrium. The structured absorption in figure 4-4a is not seen in solutions of poly(9,9-di(ethylhexyl)fluorene) (PF2/6) in MCH,[35] which has branched side chains.

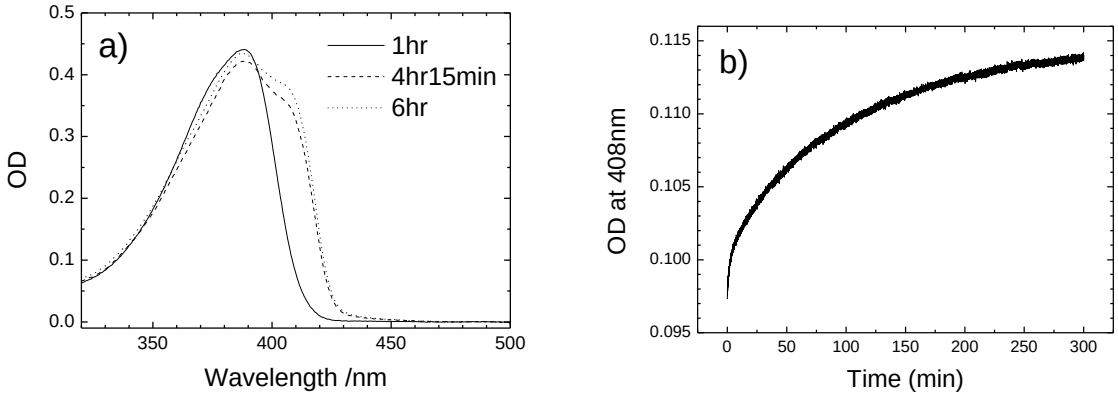

Figure 4-4: a) The absorption spectrum of (6 µg mL^{-1}) PF6/MCH, taken at intervals after boiling the solution then returning to 295K. b) The absorption at 408 nm of a 2 µg mL^{-1} solution of PF6/MCH as a function of time.

This structure in the main absorption band, which becomes more pronounced upon cooling, is very similar to the structure in the absorption spectra of the other polyfluorenes (Figures 4-3a-e) at low temperature, indicating that they too are forming aggregates. These data are consistent with previously mentioned x-ray scattering studies by Knaapila et al.[20] which found sheet-like aggregates formed by PF6, PF7, PF8 and PF9 but only trace levels for PF10.

4.3.2 Emission and Excitation Spectra in Dilute MCH

Fluorescence spectra are far more sensitive than absorption spectra, and can be used to investigate the reversibility of beta phase formation in very dilute solutions (~10 ng mL^{-1}) in order to avoid as far as possible the effects of aggregation and precipitation. Figure 4-5 shows excitation spectra with emission collected at 460 nm. For each sample, an excitation spectrum was initially collected at 295 K, then it was cooled sufficiently to induce beta phase formation, and a second spectrum was taken. Then the sample was returned to 295 K and spectra were recorded as a function of time. The sharp peak observed at 404 nm is due to Raman scattering from the solvent. The spectra for all the solutions and especially PF6 show that the main absorption band drops to below its original amplitude, and in the case of PF6 the signal almost disappeared after 24 hrs. PF10 shows no such drop as testing was stopped after only two hours after returning to room temperature, since the sample had already completed the phase change back to the original spectrum. For PF6 to PF9, the signal intensity was not restored upon boiling of the solutions, which would have indicated that the drop in signal was due to precipitate falling to the bottom of the cuvette. The reason for this loss is not clear, but it is likely to be either photodegradation, because the samples were tested repeatedly and so were continuously subject to intense UV and blue light, or adsorption onto the cuvette walls, which is likely to occur after such an extended duration. However, the forms of the spectra are in excellent agreement with those in the absorption spectra in figure 4-3.

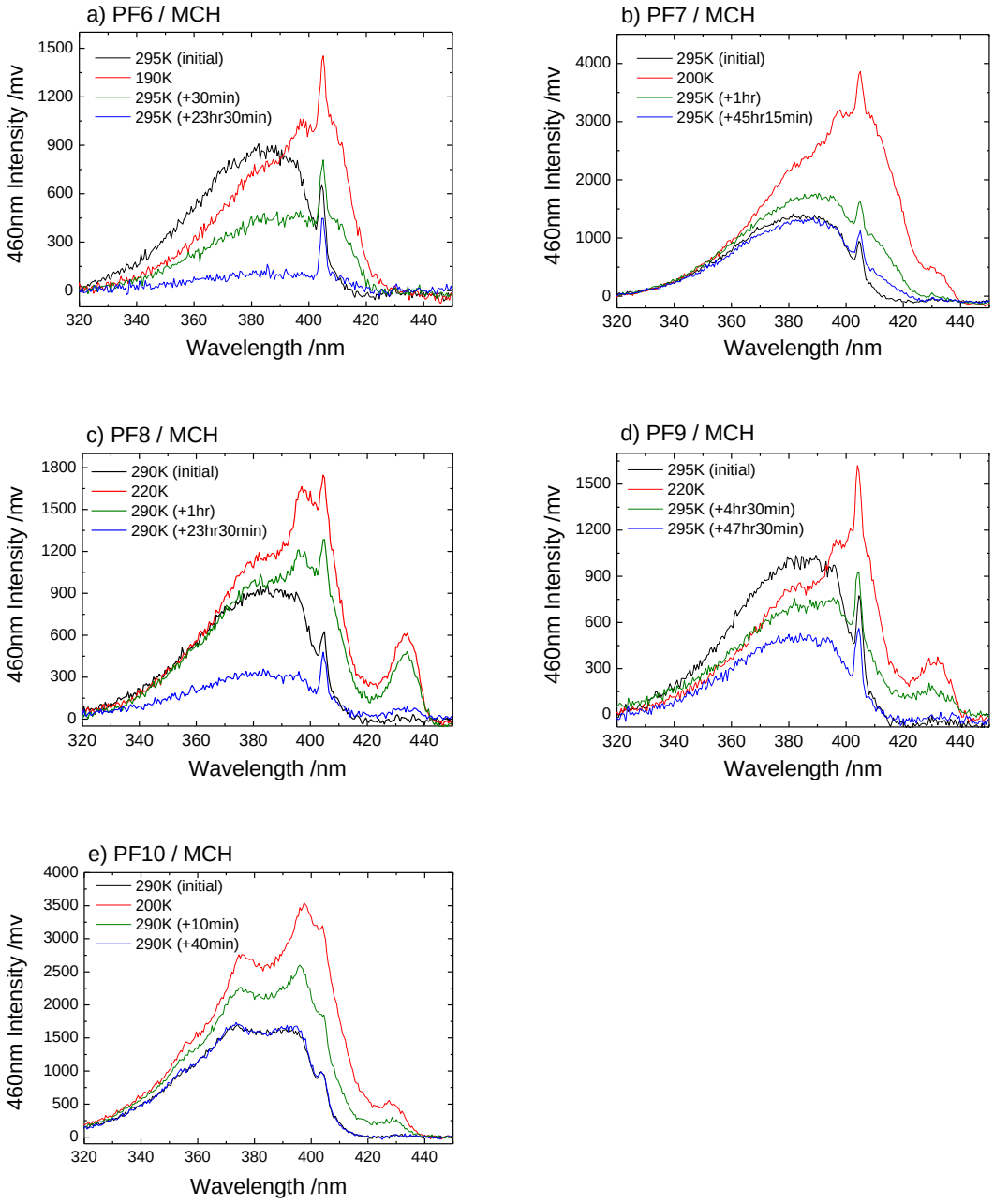

Figure 4-5: Excitation spectra of a) PF6, b) PF7 c) PF8 d) PF9 and e) PF10 dilute solutions in MCH during a cooling – warming cycle. All solutions were of concentration ~10 ng mL^{-1}. Spectra were recorded as follows: at 295K; after cooling to sufficiently low temperature to induce the beta phase, and as a function of time after returning to 295K.

There also appears to some form of odd-even effect occurring in the rates of the signal degradation; the even-chained PF6 and PF8 signal amplitudes decay almost entirely within 48 hours of measurement, whereas the odd-chained PF7 and PF9 retain over 50% of their intensity over the same period.

The PF6 does not display any beta phase peak even at 190K, which is concurrent with the absorption spectrum in figure 4-3a. The initial emission spectrum at 295K (Figure 4-5a) appears blue-shifted with respect to the equilibrium absorption, as the sample was only left at 295K for ~1.5 hours before taking the first excitation spectrum and cooling, whereas 6 hours are required to reach equilibrium (Figure 4-3). The data after cooling are then fully consistent. The PF7 spectrum at 200K shows the same shoulder that is seen in its absorption (Figure 4-3b), as well as the redshifting of the main band. The beta phase shoulder disappears almost entirely within an hour of returning to 295K, but the redshifted shoulder returns to the original profile over a much longer timescale; it has still not fully recovered after 48 hrs. The PF8 (figure 4-5c) shows a very large peak at 438 nm, which is still present after 24 hrs, but dropping with respect to the main band peak height. Since there is lower noise in this data compared to the results from Dias et al,[25] a remnant of the peak (not shown in the figure for clarity) can now be seen after 40 hrs, in contrast to their findings. In the PF9 at 220K, there is again a good reproduction of the absorption spectrum profile (figure 4-5d), with a strong absorption band at 430 nm attributed to the beta phase, and a main band redshift. Both of these changes return back to the original profile at 295K within 48 hrs, and both changes occur over similar timescales. The PF10 shows a small beta phase like peak which is of the same form as the absorption trace in figure 4-3e, and it remains for less than 40 minutes after returning to room temperature.

The emission spectra (Figure 4-6) were recorded in tandem with the excitation spectra, and show the same degradation in signal over extended measurement times that is seen in those tests for PF9 and PF6. The PF6 emission spectra show an interesting redshift of the whole spectrum at 190K, with the short wavelength peak moving from 413 nm to 424 nm. Upon returning to 295K, this peak shifts back slightly to 420 nm after an hour and to 418 nm after ~24hrs. In the spectra of PF7 to PF10, there is a sharply defined peak of emission at 437-438 nm, and the broad 413 nm emission peak that dominates at 295K is suppressed. This change is fully reversible within one day. In the case of PF10, there is almost no trace of the beta phase emission peak remaining after only 25 minutes.

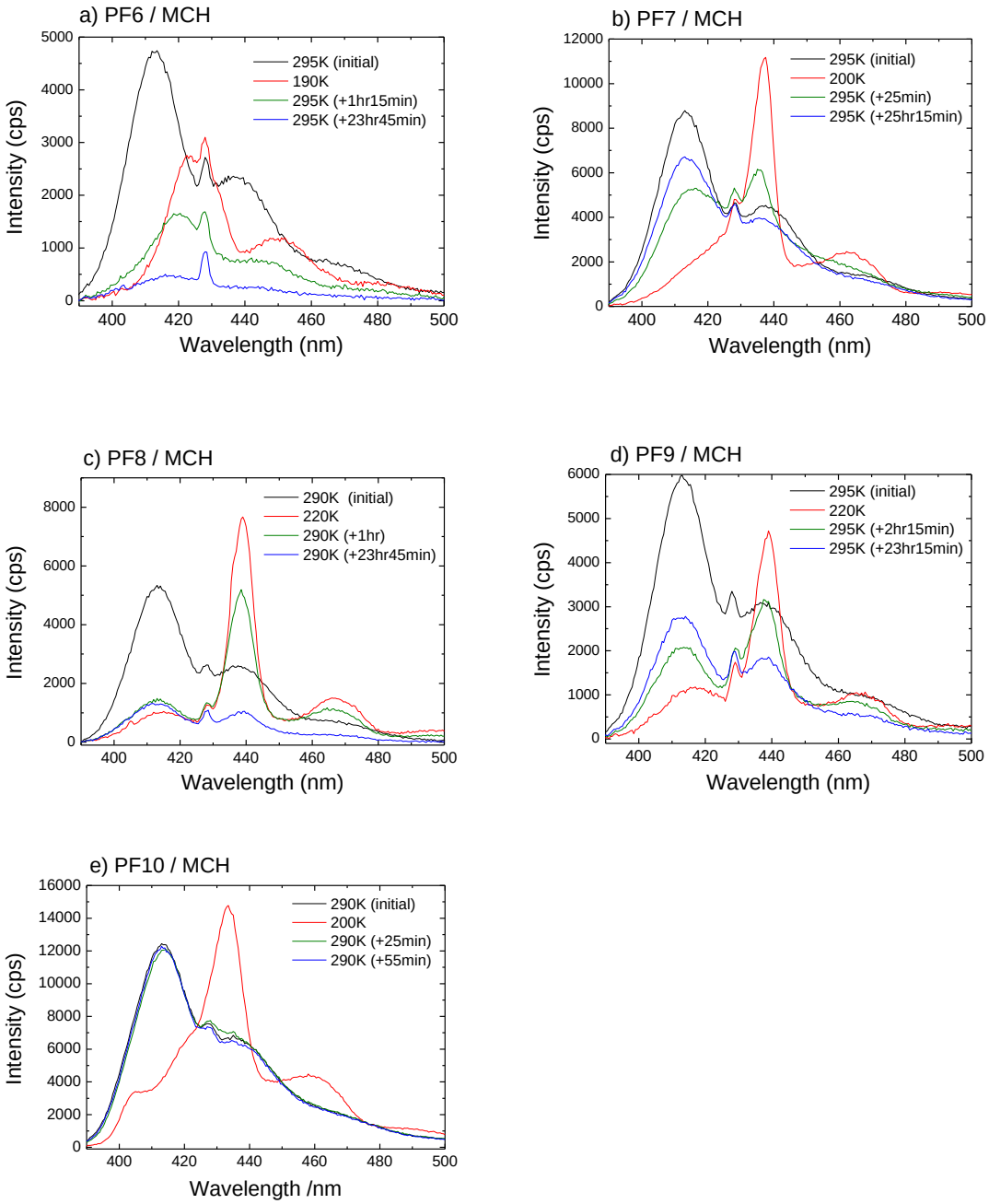

Figure 4-6: Emission spectra of a) PF6, b) PF7 c) PF8 d) PF9 and e) PF10 dilute solutions in MCH. Spectra were recorded as follows: at 295K; after cooling to sufficiently low temperature to induce beta phase formation; as a function of time after warming back to 295K. The sharp spike at 428nm is the Raman peak of the MCH.

4.4 Analysis and Discussion

4.4.1 The Issue of Deriving the Beta Phase Content

Before deriving the fraction of the beta phase present within each of the polymers, an issue now arises. It was widely accepted by workers in this field, prior to the publication of the data in chapter 4, that the peak at 408 nm is entirely composed of a vibronic replica of the beta phase. The offset from the 0-0 transition is in the region of the value indicated by the emission spectra and Raman spectra (238 meV in absorption vs. 169 meV for the emission spectra but these are within the uncertainty). In some of the recent literature,[32, 34] the fraction of the beta phase that is present in film samples has been derived using the approximate method of simply dividing the OD of the beta phase peak near 434 nm (0.30 for the data in figure 4-7a) by the sum of the OD at the peak of the main absorption band and the OD of the beta phase peak (0.30+1.0), which yields the large fraction of 23.1% beta phase content. Others subtract the alpha phase spectrum from the beta phase spectrum and calculate the area fraction of the result, a method which often requires a scaling factor for the alpha phase spectrum whose validity is uncertain.[10, 36-37] Following on from the data presented in figure 4.3a-d, the shortcomings of these methods become clear. The peak at 408nm in the main absorption band that accompanies the beta phase formation is often larger than the main band absorption at 385 nm, so for the OD intensity comparison method, to which peak should the comparison be made? Furthermore, the fractions derived by the area subtraction method are all overestimated by including the aggregation peak at 408 nm which is not due to the absorption by beta phase chains.

The chromophores in conjugated polymers exist in a range of different conjugation lengths, typically assumed to be a Gaussian density of states. Each of these contributes to the optical density at a different energy, along with its vibronic replicas. For a system of, for example, a pure polymer with only one phase, there is only one absorption band due to the $S_0 \rightarrow S_1$ transition. Then the absorption spectrum is the frequency distribution of the different conjugation lengths and the associated

vibronic replicas, convolved with a function representing the broadening due to finite lifetime and interactions with neighbouring polymer chains. The optical density of a sample at a given wavelength is proportional to a number of chromophores in the sample that can absorb the incoming photons of that particular energy, but that is not necessarily representative of the total number of chromophores of a particular phase being present. This is a shortcoming of the intensity comparison method, which neglects the large difference in peak broadness between the alpha and beta phases. The distribution of conjugation lengths makes it necessary to sum over the range of wavelengths that a given phase will absorb.

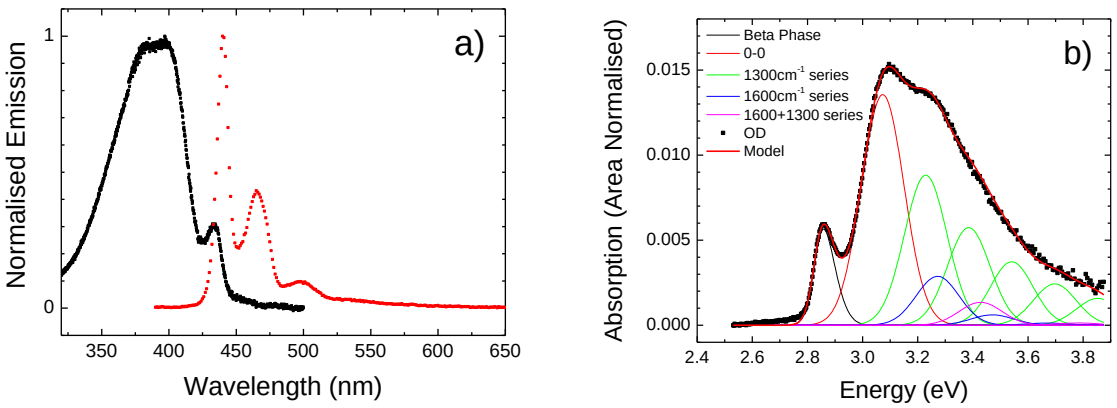

Figure 4-7: a) the normalised absorption and emission spectra of a PF8 beta phase film sample and a fit to the absorption spectrum on an energy scale using multiple Gaussian curves (b). See text for details.

For an example case of a PF8 film with equal peak intensities at 408 nm and 440 nm, the absorption band for the alpha phase with its range of vibronic replicas has a far broader width than that for the beta phase, so it is evident that there is far more than 50% alpha phase present in the sample. Therefore there is little physical basis for the application of the intensity comparison method, although it retains popularity for its simplicity. Therefore a new method of calculation is used to calculate the proportion of beta phase chromophores in the samples measured here, which uses the area of an asymmetric Gaussian peak used to fit the peak at ca. 434 nm as part of a multiple-Gaussian fit to the area-normalised spectrum on an energy x-axis. In order to be sure that the fit to

the beta phase peak area is accurate, care must be taken to ensure the multiple-Gaussian fit to the main band is sufficiently accurate. A direct single-peak fit to the beta phase section is overly simplistic and will always over-estimate the beta phase content, since the tail of the broad main band states overlap with the higher energy beta phase states (Figure 4-7b). Secondly, the smoothness and broadness of the band gives no clear evidence for any of the parameter values, so the Gaussian peaks used to fit the absorption peaks in the main band must be constrained as fully as possible with known parameters and physical constraints. This need becomes clearer when the Raman spectra of PF8 are considered. Ariu et al. demonstrated that the Raman spectra of PF8 are largely similar for all cases of morphology, be that amorphous, crystalline, quenched or beta phase.[38] The Raman spectrum of the beta phase show only small differences to that of the alpha phase, with similar peak locations but higher intensity and sharper resonances; the same vibrational modes are applicable to both phases. Taking this into account, the width of the alpha phase band (to 320 nm) could incorporate 20 Gaussian peaks at integer multiples and sums of the main three vibrational modes; 1300 cm^{-1} for a stretch vibration of the C-C bond between fluorene units, 1600 cm^{-1} for a ring breathing stretch, [23, 36] and a pair of much lower intensity modes at 735 cm^{-1} and 865 cm^{-1} for an in-plane phenyl ring deformation and a C-C stretch of the bridging carbon,[39] which were considered as a single mode for the purposes of this fit (since they produce a single low-intensity replica in the low-temperature emission, see chapter 5.3). These 20 peaks consist of the 0-0 mode, eight replicas of the 735 cm^{-1} mode, five and four replicas of the 1300 cm^{-1} and 1600 cm^{-1} modes, along with sum modes of these primary two peaks. This necessitates more than 50 free parameters if no constraints are applied, resulting in a rather unconvincingly arbitrary fit. In order to make the fit more meaningful, these were constrained as far as possible. As mentioned, the peak centres were fixed at specific multiples of the permitted vibrational modes, leaving only a variation in the 0-0 ground state transition energy. In principle the 0-0 energy should not be a free parameter, and indeed when it was allowed as a variable, the resulting fits to the absorption spectra of 30 different PF8 film samples resulted in consistent convergence on a mean 0-0 position of 3.079±0.007 eV showing that

it did not vary significantly. Secondly, the peak widths were fixed at the same value of broadening parameter *w* for all the Gaussian peaks within the main band, since the vibrational modes are all occurring within the same energy parabola in coordinate space. Simple multiple-Gaussian peak fits to the well resolved emission spectra of alpha phase solutions and films show a consistent FWHM of 120-130 meV for the 0-0 transition and its vibronic replicas. Since these values are obtained from the emission, which is a self-selecting subset of the most extended states within the film, it is expected that in the absorption a greater degree of broadening will be encountered as the whole distribution of states will contribute. The parameter *w* was permitted to vary, but the region of the fit from 2.79 eV to 3.30 eV was weighted by a factor of 10 to force the fit to track the main band edge and the asymmetry of the beta phase as accurately as possible. The parameter *w* produces an excellent fit to the slope at 3 eV (whilst also still giving an excellent fit to the entire band) at a value of the order of 80meV, giving a FWHM of around 190 meV, which is significantly larger than the values derived from the emission spectra, as expected. The region of the fit from 2.79 eV to 3.30 eV was weighted because the sum of the un-weighted squared differences between the model and data within the minimisation favours excessive broadening of the Gaussian bands at the expense of this slope fit quality, in order to better fit the region of the absorption the spectrum above 3.2 eV that is of less importance here. With these parameter constraints only the 20 Gaussian amplitudes remain variable, along with the peak centre, amplitude and two asymmetry parameters of the beta phase peak. Thirdly, the amplitudes were also fully constrained with Huang-Rhys parameters. For each series of vibrational modes (v=1, v=2 v=3 etc. for a given energy interval) the amplitudes for each subsequent replica were fixed to a multiple of the amplitude of the previous replica. This leaves only 11 parameters free: the four parameters describing the asymmetric peak, the 0-0 position and amplitude, the width parameter, and the four Huang-Rhys factors. The Huang-Rhys factor of the dominant (1300 cm^{-1}) mode of the fit is 0.66, which is in the region of the Huang-Rhys factor derived for PF8.[17]

The asymmetric Gaussian function used to fit the beta phase peak is given in equation 4-7. It uses two parameters *B* and *u* to determine the curve shape; *B* approximately determines the peak width and *u* determines the asymmetry. Variation of these parameters does not affect the normalization of the area of the peak, so the peak area is determined entirely by a prefactor. However, the precise values of the width and asymmetry depend on both these parameters and must be determined manually from the peak trace. The peak widths of the beta phase are in the region of 80 meV, which again is larger than the 30meV that is the FWHM of multiple-Gaussian peak fits to the well resolved emission spectra of beta phase solutions and films. The peak centre is at 2.824 eV (for films), and the peak intensity is at 2.857 eV. From the beta phase fluorescence spectrum, the vibrational replica intensity is of the order of 0.3, but the approximate overlap with the 0-0 of the aggregated alpha phase means it cannot be resolved, so no vibronic replicas of the beta phase peak are included. This makes the method here subject to a systematic underestimate of the beta phase content.

$$W(E') = \frac{1.13}{B} \frac{exp\left\{-\left[\frac{E\prime}{B}-\left(\frac{0.95}{1+e^{u}}-0.475\right)\right]^2\right\}}{1+exp\left\{-\left[\frac{E\prime}{B}-\left(\frac{0.95}{1+e^{u}}-0.475\right)\right]\right\}} \qquad (4\text{-}7)$$

Whilst it is possible to progress further to a more accurate physical model of the spectrum,[40-41] it is difficult to derive more detailed information from the broad shape of the main band with any confidence. The aim is to give a sufficiently accurate fit to the absorption spectrum so that the electronic 0-0 Gaussian band overlap with the beta phase absorption distribution can be accurately and reliably modelled, allowing the true beta phase content of a given sample to be reliably determined. For the representative sample, this fitting process gives a beta phase fraction of 6.2%, far lower than the fraction derived from the simple method of OD magnitudes described earlier. The parameters for the fit in figure 4-7b are tabulated in table 4-2.

Table 4-2: Free parameters for the fit to figure4-7b, using the multiple-peak fit described in the text. Vibronic energy intervals were fixed from the fluorescence data. The FWHM of the Gaussian peak corresponds to width parameter *w* × 2.355.

β Peak	Alpha 0-0	Alpha phase vibronics (fixed)	Huang-Rhys Parameter
B = 0.0838 meV	w = 82.4meV	v1 = 85 meV	<0.001
Area = 3.145×10^{-4}	Area = 2.606×10^{-3}	v2 = 156 meV	0.654
0-0 = 2.818 eV	0-0 = 3.078 eV	v3 = 199 meV	0.314
U (asymmetry) = 3.40		v2+v3	0.169

The area method used is subject to uncertainty, primarily from the broadness of the absorption spectrum and the inability to reliably resolve the beta phase vibronic replica. Other uncertainty is introduced by the slightly arbitrary cut-off of the area of the absorption band that is considered at 320 nm, which is used to avoid including absorptions due to a broad, higher-lying energy level at 295 nm, which has a substantially weaker transition probability. This cut-off may introduce a small systematic error into the calculation, but the magnitude of this uncertainty was estimated to be in the region of 5% of the result, by looking at the change in the result if the area of the absorption band was included down to 300 nm, where the absorption spectrum is already rising again due to overlap with the higher energy S_0-S_2 absorption band. It also requires the assumption that the oscillator strength of the transitions is equal in the alpha and beta phases, an assumption which is corroborated by a similar PLQY of the alpha and beta phases.[15]

4.4.2 Difference Spectra

In much previous work,[16, 38, 42-43] the absorption spectrum of the beta phase itself has been obtained by deriving the change in the absorption spectrum by subtracting the alpha phase spectrum from that of a sample containing some beta phase. This has either been carried out as-is,[25] or by subtracting an arbitrarily scaled alpha-phase spectrum from that of the beta phase.[44]

The difference spectra for the polymer group in MCH solution using the spectra from figure 4-3(a-e) are presented in figure 4-7 below. The un-scaled absorption spectra for each polymer at 290K are subtracted from the respective low-temperature spectra where the maximum phase change has taken place.

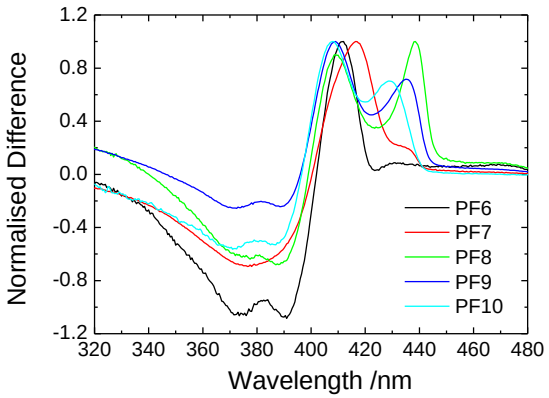

Figure 4-8: The difference spectra for PF6 to PF10 (see legend) obtained by subtracting the room temperature absorption spectrum from the lowest temperature spectrum for each polymer.

Given that the spectral changes associated with the beta phase are absent in PF6, it is clear that the peak in the difference spectrum around 410 nm is not the result of beta phase formation. In previous studies of PF8 it has been assigned as the first vibronic level of the beta phase, as a result of its appearance with the beta-phase peak at around 435 nm.[10, 25, 36-37] This data shows that, whilst the band originates from aggregation in PF6 to PF10 in solution, it is not a result of the formation of the beta phase. This is supported by the x-ray analysis by Knaapila et al. referred to earlier, which showed the beta-like aggregate sheets were present in PF6 through PF9 (along with trace levels in PF10). It is likely that there is some morphological adjustment occurring, with an increase in molecular scale ordering due to chain folding or aggregation, but the backbone planarization associated with the beta phase does not occur. Therefore any estimation of the beta phase content using such area subtraction methods has produced a significant overestimate.

4.4.3 Analysis of Absorption Spectra with Temperature in Solution

In figure 4-3, the beta phase absorption band does not form in all cases, which clearly shows that the length of the linear alkyl side chain is a critical factor in beta-phase formation in solution. A commonly held theory of beta phase formation currently postulates the formation of a planarised intra-molecular state prior to the formation of the aggregated chains,[22, 25] but it is not clear that this would explain the absence of beta phase formation in PF6.

If the backbone planarization happens within the individual polymer chains prior to aggregation, then cooling the family of closely related polyfluorenes might be expected to give the same planarization due to a drop in solvent quality, irrespective of whether or not the chains are then suited to the formation of an aggregate after this first step. The increase in backbone planarity is the accepted origin of the change in spectrum[22] so the presence of intra-chain planarised polymer would give beta-phase absorption and emission peaks in all cases of side-chain length.

From figure 4-3, it is also clear that the beta phase does not arise purely from the onset of aggregation. The poorly soluble hexyl polymer is shown to aggregate readily, and was found by Knaapila et al. to form the same sheet-like aggregates as PF8 [20], yet the red-shifted spectroscopic indicators of the beta phase are not produced in this case. The formation of beta phase is thus shown to be a complex process that does not simply result from an initial intra-chain planarization.

From the perspective of thermodynamics, it is expected that energy is required in order for the fluorene unit to be planarised against the steric repulsion that arises from the adjacent hydrogen atoms at the 2 and 7 positions on the molecule, which produce its normal twisted state. The initial state of the free polyfluorene chain is associated with the alkyl solvent by Van der Waals interactions with the alkyl side chains. In the beta phase, the alkyl side chains of adjacent polymers are interacting with each other and the solvent is excluded, and the fluorene units are planarised. Thus there is an activation energy required to disrupt the normal molecular configuration and enforce the planarization, which is supplied by the release of energy from the Van der Waals interactions

between the alkyl side chains of the polymer when it forms the aggregate. The amount of energy supplied by this weak van der Waals interaction scales with the length of the alkyl chains, in much the same way as the boiling point of linear hydrocarbons is well known to rise with chain length.

Longer alkyl side chains potentially provide more energy to overcome the activation energy and planarise the molecule, and so it is expected that beta phase spectral characteristics will not be observed in the cases where the polymer side chains do not provide sufficient energy to overcome the steric repulsion. This potentially explains why there is no beta-phase formation in the hexyl polymer, and suggests that the energy supplied by the heptyl polymer is only just sufficient to begin to planarise the polymer backbone, since only a small shoulder is seen as evidence of the beta-phase formation.

Yet for the nonyl and decyl polymers the fraction of beta phase formed is lower. As the alkyl chain increases in length, it becomes less likely that the side chains will be in an extended linear state, as they are highly flexible and interact with the disordered environment of the solvent and other polymer molecules. This leads to a reduction in the extent of aggregation and the fraction of beta phase formation, since despite the continued presence of the aggregate seen in figure 4-2, the side chains are less likely to lie next to each other in a fully interacting state, and so they are less likely to provide the necessary energy, and therefore a lower fraction of the fluorene units will be planarised compared to the case of the octyl polymer.

4.4.4 Thermodynamics

The absorption spectra as a function of temperature can be further analysed in order to investigate the thermodynamics of the beta phase. Following the work of Dias et al.[25] the aggregation of the beta phase polymer was assumed to be a multi-stage process, where a single alpha-phase domain forms a single beta-phase domain, followed by the addition of successive beta-phase domains to the aggregate. This initial stage is an important basis for the proposed model. In their paper, it is proposed that the initial stage is an intra-chain planarization, possibly brought about by the

interactions with the side chains with the polymer backbone. Here, it is proposed that the initial step is the collapse of isolated dissolved chains into folded chains, which is supported by the side-chain dependent formation of the beta phase in very dilute solution in figure 4-4. Chain folding would allow the inter-digitating side chains to drive the planarization whilst appearing to be an intra-chain effect. The nature of this step is discussed further in section 4.4.5. Further assumptions include: the alpha and beta domains are of the same length, and extend over the same number of monomer units giving a 1:1 ratio of exchange.[25]

$$\alpha \rightleftharpoons_{k_{-1}}^{k_1} \beta_1 \tag{4-8}$$

The rate constants k_1 and k_{-1} are assigned to the forward and reverse reactions, and β_i represents a beta phase domain of i chromophores. Though they proposed an intramolecular planarization step to be responsible for the first stage, on the basis of the results here it is more likely that the initial stage is that of chains folding upon themselves, with the result that the interacting side chains create the planarization. The aggregation then proceeds iteratively:

$$\beta_1 + \beta_k \rightleftharpoons_{k_{diss}}^{k_{agg}} \beta_{k+1}, \qquad k \in (1, \dots, N-1) \tag{4-9}$$

The rate constants k_{agg} and k_{diss} apply to the aggregation and dissociation processes.[25] The optical density at the beta phase peak of the absorption spectrum indicates the concentration of the beta domains, whether as single folded chains or aggregates. The aggregates contribute to the absorption with the number of beta domains they contain: β_3 will contribute $3\times\beta_1$ and so forth. The rate equations for the formation of these aggregates are then given by: .[25]

$$\frac{d\alpha}{dt} = -(k_1\alpha - k_{-1}\beta_1) \tag{4-10}$$

$$\frac{d\beta_1}{dt} = (k_1\alpha - k_{-1}\beta_1) - J_1(\beta) - \sum_{k=1}^{N-1} J_k(\beta) \tag{4-11}$$

$$\frac{d\beta_k}{dt} = J_{k-1}(\beta) - J_k(\beta), \quad 2 \leq k \leq N \tag{4-12}$$

$$J_k(\beta) = k_{agg}\beta_1\beta_k - k_{diss}\beta_{k+1} \tag{4-13}$$

Where N is the maximum number of domains assumed to be in each aggregate. Then, under equilibrium conditions ($t \rightarrow \infty$) the solutions of the equations of the aggregation steps are of the form $\beta_1^{\infty} = K_1\alpha^{\infty}$ and $\beta_p^{\infty} = K_1K_2\alpha^{\infty}\beta_{p-1}^{\infty}$, where $K_1 = k_1/k_{-1}$ and $K_2 = k_{agg}/k_{diss}$.[25] For an infinitely large N:

$$\beta_p^{\infty} = \frac{1}{K_2}(K_1K_2\alpha^{\infty})^p, \quad p \geq 1 \tag{4-14}$$

Mass conservation expressed as $\alpha^{\infty} + \sum_{p=1}^{\infty} p\beta^p = \alpha_0$ (the initial concentration) leads to:[25]

$$\alpha^{\infty} + \frac{K_1\alpha^{\infty}}{(1-K_1K_2\alpha^{\infty})^2} = \alpha_0 \tag{4-15}$$

Using y to symbolise the fraction of the initial α domains converted into β_p aggregates,

$\alpha^{\infty} = (1-y)\alpha_0$ giving: [25]

$$\frac{K_1}{(1-K_1K_2\alpha^{\infty})^2} = \frac{y}{1-y} \tag{4-16}$$

Dias et al. then simplify the equation using the order of magnitudes of the parameters to show that $K_1K_2\alpha^{\infty} \leq 10^{-4}$, with the final result:

$$K_1 = \frac{y}{1-y} \tag{4-17}$$

In the method of Dias et al. the value of *y* at any given temperature was taken to be the ratio of the optical density at the wavelength of the peak of the beta phase absorption to the absorbance at the

same wavelength at the lowest temperature where the beta phase absorption has reached its maximum value: $y = OD_\beta / OD_\beta^0$.

The transition temperature of the phase change can be shown clearly by simply plotting the value of *y* as a function of temperature for each of the polymers. The results using the OD from the isobestic-point normalised data are compared directly to the value of $y = Area_\beta / Area_\beta^0$ calculated using the beta phase fractions from the area fitting method, shown in Figure 4-9 which contains data collected from two separate experiments on each polymer. Note that the method for deriving *y* following the method of Dias et al.[25] using the OD differs subtly from the method used to determine the beta phase fraction by OD (discussed in section 4.4.1, where the OD at the beta phase peak is divided by the sum of the beta phase and main band OD) since here the OD of the main band is ignored; the spectra are scaled by the isobestic point and then the value of *y* is simply the peak beta phase scaled OD at a given temperature divided by that of the lowest temperature.

Studies of different concentrations of PF8 using this analysis method of the temperature-dependent absorption spectra have shown that the results are independent of concentration over the range 2 – 23 µg mL^{-1},[32, 46] which can be understood by clarifying the precise meaning of aggregation in use here. In conventional use, in the context of emissive molecules and polymers, aggregation means that the molecules not only physically coalesce but also that the electron wavefunctions of the two particles overlap to form an interacting state, for example with pyrene.[47] This produces a redshift in the emission, but also reduces the number of chromophores within the system, leading to a concentration dependence of the emission. Here, the two chromophores physically coalesce through side chain interactions, but the delocalised wavefunctions on the two sections of polymer backbone do not interact. The two separate conjugated regions become planarised and extended through the energy provided by the side chain interactions, resulting in two extended conjugation lengths rather than one.

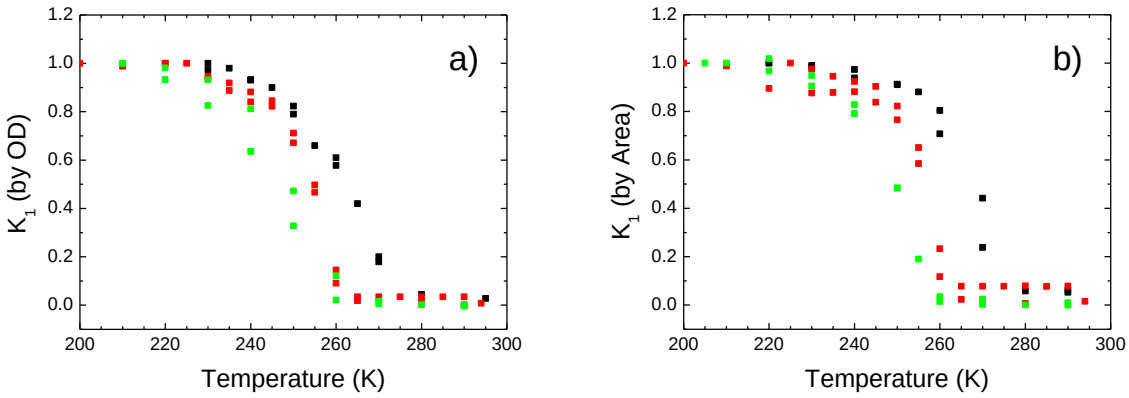

Figure 4-9: values of K_1 from equation 4-17 derived by scaled OD (a) and area fit method (b) showing the transition temperatures for PF8 (black) PF9 (red) and PF10 (green). Each series consists of two separate datasets from different experiments showing the variability of the data.

The plots show a possible trend in the transition temperature of beta phase formation towards lower temperatures for longer side-chains, which is simply a result of the greater solubility of the longer side chains, requiring a lower temperature to be reached before the solvent quality drops sufficiently for aggregation or chain folding to be induced. It can be seen that there are small differences between the plots arising from the different methods used. The OD method tends to generate a slower tailing-off at lower temperatures towards the maximum value, whereas the area fit method yields a steeper gradient and a sharper arrival at the maximum value. This arises from a weakness with the OD scaling method; since the spectra are collected as a function of temperature, rather than just as a function of self-dopant concentration, there is an inherent red-shift of the absorption bands at the temperature drops, and this effective shift in the true isobestic point causes the scaling to artificially raise the beta phase content at lower temperatures. However, there is a greater uncertainty in the absolute values of beta phase content generated by the area fit method, resulting in a greater spread of values in this data.

A van't Hoff plot is used to determine the thermodynamic quantities of the entropy change ΔS_{beta} and enthalpy change ΔH_{beta} of the beta phase transition in PF8 and PF9. The natural logarithm of the

constant K_1 (equation 4-17) plotted with the inverse temperature yields a straight line fit corresponding to equation 4-18:[25]

$$\ln K_1 = \frac{\Delta S_{beta}}{R} - \frac{\Delta H_{beta}}{RT} \qquad (4\text{-}18)$$

The plots for the data derived from the respective absorption spectra as a function of temperature at equilibrium are shown in figure 4-10 for PF8, PF9 and PF10 where y is derived by using the OD (a) and fitted beta phase peak area (b). A similar plot for PF7 is not feasible since there is too much overlap with the redshifted structure in the absorption band to accurately determine the OD present due to the absorption on the beta phase chromophores. Furthermore, it is not clear if there is any beta phase present within the sample at all but the final few data points, which would not produce sufficient data points for a reasonable linear fit.

The quantities derived using equation 4-18 are given in table 4-2, using the value of the OD at the beta phase peak in the spectra normalised by the isobestic point, and the fitted area of the beta phase peaks in the normalised spectra.

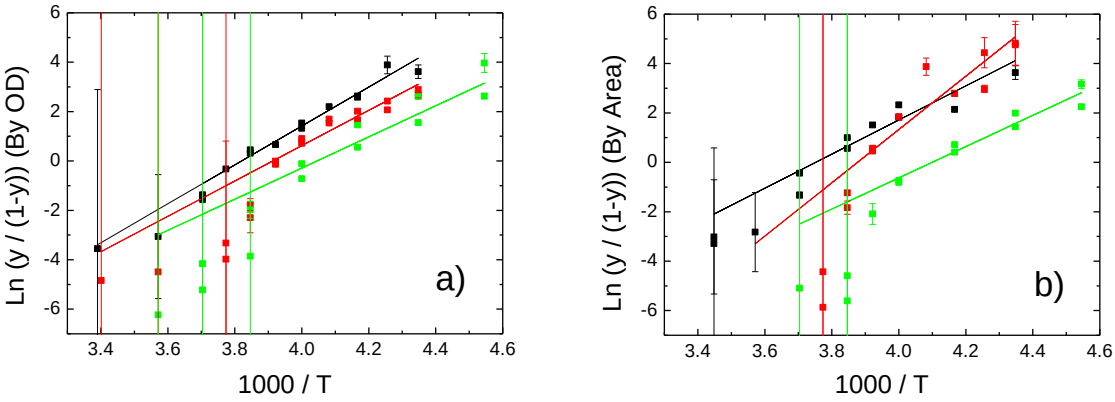

Figure 4-10: Van't Hoff plots for PF8 (black), PF9 (red) and PF10 (green) of data derived from figures 4-3 (c-e) using the OD peak magnitudes from the spectra scaled by the isobestic point (a) and the fitted area of the beta phase peak (b). Linear fits are included with matched colours.

Table 4-3: Fit parameters from a linear best fit to the van't Hoff plots in figure 4-10.

	Data By OD			
	Gradient	**ΔH_{beta} kJ mol^{-1}**	**Intercept**	**ΔS_{beta} J K^{-1} mol^{-1}**
PF8	7.9 (0.5)	-65.5(3.9)	-30.1 (1.9)	-250 (16)
PF9	7.2 (0.5)	-59.5 (3.9)	-28.0 (1.9)	-233 (16)
PF10	6.3 (0.5)	-52.4 (4.0)	-25.5 (1.8)	-212 (15)
	Data By Fitted Area			
	Gradient	**ΔH_{beta} kJ mol^{-1}**	**Intercept**	**ΔS_{beta} J K^{-1} mol^{-1}**
PF8	6.9 (0.5)	-57.4 (4.4)	-25.9 (2.0)	-215 (17)
PF9	10.8 (0.8)	-89.6 (6.3)	-41.8 (3.0)	-347 (25)
PF10	6.3 (0.5)	-52.5 (3.8)	-25.9 (2.0)	-215 (16)

The data in the region of $x < 3.9$ are subject to extremely large errors, since a ratio is being taken at higher temperature where the OD or peak area is very small, and the fraction uncertainty carried through the calculation of the reaction rate constant in equation 4-17 yields a large error bar.

It should be noted that the derived values from figure 4-9a and b in table 4-2 are subject to considerable uncertainty, especially since it can be seen that none of the polymers gives a smooth line in the van't Hoff plot. This may be related to the poor applicability of the assumption within the model that the alpha and beta phase chromophores are of the same size, as the alpha phase chromophore has been determined to be 5 repeat units,[48] and the beta phase chromophore may be as high as 30±15 repeat units.[44] There is also some ambiguity concerning the nature and the magnitudes of the figures in the table. Conventionally, the value is quoted per mole of monomer unit, but in this case the absorption spectrum is a probe of the number of absorbing chromophores, so the figures are not strictly comparable to other rigorously defined thermodynamic values. This may explain why the values of the enthalpy seem rather high for van der Waals interactions between short chains; the planarization requires many side-chain interactions along the length of the chromophore, and so the figure will be the sum of the energies of all these interactions (higher

than expected by a factor of 10 or more). The entropy values are subject to considerable uncertainty since the y intercept value will be affected by any systematic errors in the fitting that lead to either a small change in the gradient or an offset in the values.

There is considerable agreement between the values derived from the two different fitting methods for the PF8 and PF10, a result which can be understood from the similar FWHM of the beta phase peak as a function of temperature. The area will scale with the height of the beta phase peak for constant FWHM, so the relative proportion derived from the beta phase OD method will follow the trend in the peak area; an assumption that had not previously been shown to be valid. However, in the case of the PF9, the FWHM becomes significantly narrower at lower temperature, leading to disagreement between the two methods.

To lend more credibility to the values obtained, this data can be further compared to other data sources. Kitts et al. also measured the enthalpy of the phase change of the beta phase transition via Differential Scanning Calorimetry (DSC) which found an enthalpy of -21.04 kJ mol^{-1} of monomer, but assumes a chromophore length of 6 fluorene units.[26] A similar assumption with the average value of -61.5 kJ mol^{-1} derived here implies an interaction energy of -10.3 kJ mol^{-1} of monomer. These values equate to between 106 and 218 meV per PF8 unit, or 53 to 109 meV per side chain. In other work, Miyahara et al. carried out DSC on molecular systems - alkyldimethylamine oxide hydrochlorides with linear alkyl chain lengths with n=10, 12, 14, 16 and 18 and found a simple linear relationship between the chain length and the enthalpy of side chain melting of the crystalline phase.[49] Extrapolating their tabulated data back to n=8 yields a value of 19 kJ mol^{-1}, which equates to 99 meV per side chain. Interestingly, this is similar to the interaction energy of two linear octane molecules through van der Waals interactions, as has been modelled by Nelson and Hermans.[50] The minimum of the potential well depth was calculated to be -13.8 kJ mol^{-1}, which corresponds to 144 meV per interacting *n*-octane chain pair. This functions as a realistic upper limit for the energy values found by Kitts et al. in DSC experiments, and in this work. This is an upper limit as there are constraints on

the position and intermolecular separation of the alkyl side chains in the polymers, making it less likely that the side chains will be completely aligned and at the optimal intermolecular distance.

In summary, the values of enthalpy produced by this model seem physically realistic, but there is a high level of uncertainty, as well as an anomalously high value for PF9, and there are significant differences between the two fitting methods. This shows that the aggregation model of Dias et al. may not be a complete picture of the beta phase formation.

4.4.5 Optical Spectra of Dilute Solutions

In the case of more dilute solutions, it is far less likely that the polymer chains will come together to form aggregates. Yet the spectra in figure 4-5 and 4-6 show evidence of reversible beta phase formation in exceedingly dilute solution (10 ng mL^{-1}). This is unlikely to be the result of many chains interacting, but due to the very high molecular weight (M_w = 200 kDa, or over 700 monomers) the beta phase occurs as a result of individual chains collapsing and folding upon themselves, allowing the side chains to interact. The high number of monomer units per chain means that only a small angle of folding is required between adjacent units over a length of tens of monomers in order to bring the end of the chain folding back over the initial chain segments. An unrealistically high folding angle between adjacent monomer units is not required to provide the proposed side chain interactions.

The excitation spectra show that the peak indicating beta phase is very similar in both relative magnitude (to the main absorption band) and shape to the absorption spectra from figure 4-3. This indicates that the same process is happening for each polymer in both the dilute solution and the more concentrated solution, and therefore the results are still dependent upon the side chain. The process is shown to be reversible upon returning to room temperature as would be expected from the model of interacting side chains.

Further to the conclusions of the earlier data, an experiment was carried out in the same manner as section 4.3.2 on a mixed solution of PF7 and PF9 in dilute solution with the same total concentration

of polymer. There were no differences in the spectral features between the mixture and the separate polymers; the mixed-polymer spectra can be formed by adding an approximately 50-50 linear combination of the spectra of the separate polymers. However, there is interesting evidence for the formation of a more stable PF7-PF9 interlinked aggregate that has different thermodynamic properties to the pure polymers. The equivalent spectra are given in figure 4-11. The differences are not immediately apparent, but the timescale is very different – after 48 hours the spectra of the individual polymers had entirely disappeared, but in the case of the mixed polymers the beta phase characteristics are still clearly observable after 8 days, and that the spectra have not degraded in the same manner as observed for the individual polymers (note that regular spectra were stopped after 65 hours and interrupted for several hours). This suggests a different type of aggregate may have been formed; a 7-9-7-9 type with alternating PF7 and PF9 polymers interacting together. This also shows that the polymer chains are still aggregating to some extent even at this extremely dilute concentration.

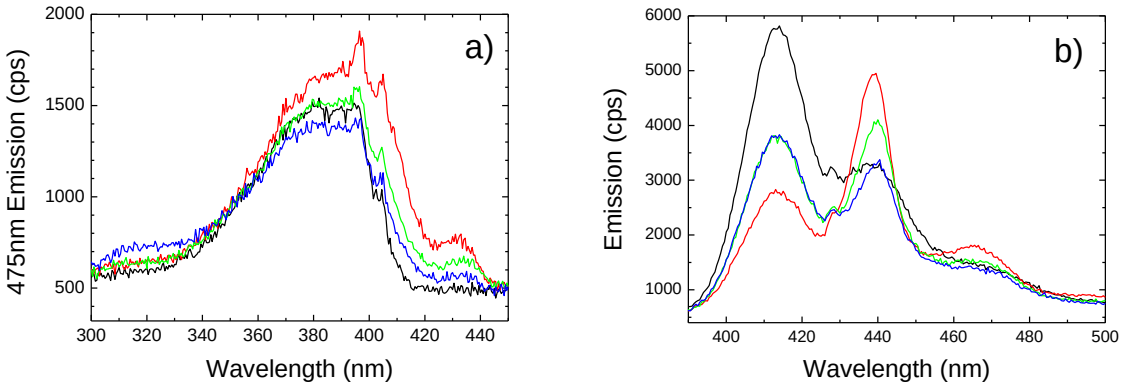

Figure 4-11: Excitation spectra (a) and emission spectra (b) for a highly dilute (10 ng mL^{-1}) solution of PF7 and PF9 mixture in MCH. Spectra are taken before the thermal cycle (black), 5.5 hours after returning to room temperature (red), 48 hours after (green) and 8 days after (blue).

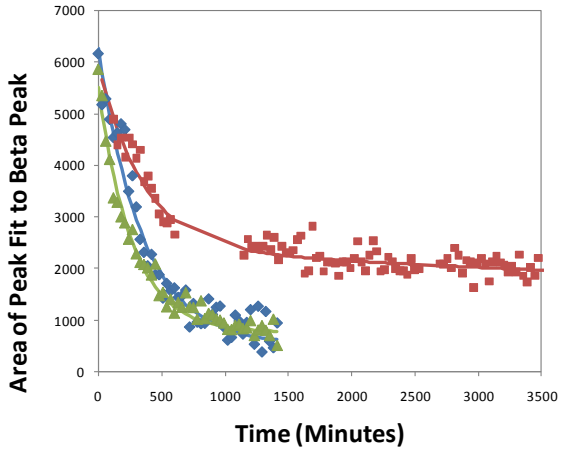

Figure 4-12: Time resolved decay of the area of the beta phase region of the excitation spectra for PF8 (blue) PF9 (green) and PF7 & PF9 50:50 mixture (red) along with exponential fits to the data (matched lines).

To give a direct comparison, the beta phase peak area is plotted as a function of time in figure 4-12 for those solutions which presented a sufficiently well-resolved beta phase peak to be fitted with reasonable accuracy; PF8, PF9 and the 50:50 mixed PF7 and PF9 solutions. This clearly shows the different behaviour of the mixed solution. The PF8 and PF9 peak areas drop almost down to the noise level after approximately 1500 minutes, with time constants of 347 minutes and 266 minutes respectively, and the PF10 reverts to the fully dissolved state almost immediately, which corresponds well to the trend of increasing polymer solubility with longer side chains. This again shows that the solvent acts to reduce the extent of aggregation for the longer side chain polymers, as discussed in section 4.4.3 within the context of the proposed formation mechanism. The mixed solution appears to show bi-exponential behaviour, with a fast drop with time constant 350 minutes, followed by a near-constant level with a time constant fit value of approximately 40 days, although it can only be said with certainty that the decay constant is longer than the measurement time.

4.5 Conclusions

Temperature dependent absorption spectra show that in PF7, PF9 and PF10 the beta phase is formed as it is in the well known case of PF8, with a trend that indicates that 8 is the optimal side chain length. Similar experiments with PF6 show no such phase is present, leading to the hypothesis that the side chains are critical in the formation of the beta phase in linear alkyl side chain polyfluorenes. Beta phase formation in dilute solution also occurs as a result of chain folding, and is reversible within 2 days at room temperature.

The conformational changes that occur within the beta phase are two-fold. The initial aggregation of the polymer in solution stiffens the polymer backbone, leading to the observation of structure within the main absorption band. Then the energy provided from the Van der Waals interactions of the side chains permits the planarization of chromophores where there are a sufficiently large number of interactions. This second stage is required to fully form the beta phase, which is why PF6 does not show the red-shifted absorption peak near 437 nm since the shorter side chains cannot provide sufficient energy.

The absorption peaks attributed to the presence of the beta phase were further analysed to derive thermodynamic constants pertinent to the process. The entropy change and the enthalpy change for beta phase formation in PF8, PF9 and PF10 are shown to be significant and negative in all cases, and there is a trend of lower magnitudes for shorter chain lengths.

Further evidence for the side chains interacting between polymers comes from a mixture of PF7 and PF9 chains, where spectra suggest that a new 7-9-7-9 aggregate may be formed, with greater stability than any of the individual polymers.

4.6 References

1. Jones, J. E. *Proc. R. soc. Lond. Ser. A-Contain. Pap. Math. Phys. Character* **1924,** 106, (738), 463-477.
2. Hildebrand, J. H. *J. Am. Chem. Soc.* **1929,** 51, 66-80.
3. Grulke, E. A., Solubility Parameter Values. In *Polymer Handbook*, 4th ed.; Grulke, E. A.; Brandrup, J.; Immergut, E. H., Eds. Wiley: New York, 1999; pp 675-711.
4. Belmares, M.; Blanco, M.; Goddard, W. A.; Ross, R. B.; Caldwell, G.; Chou, S. H.; Pham, J.; Olofson, P. M.; Thomas, C. *J. Comput. Chem.* **2004,** 25, (15), 1814-1826.
5. Rubinstein, M.; Colby, R. H., Thermodynamics of Blends and Solutions. In *Polymer Physics*, Oxford University Press: New York, 2003; Vol. 1, pp 137-165.
6. Hansen, C. M. *Industrial & Engineering Chemistry Product Research and Development* **1969,** 8, (1), 2.
7. Hintschich, S. I. Picosecond Studies of Excited States in Conjugated Polymers. Durham University, Durham, 2007.
8. Grell, M.; Bradley, D. D. C.; Inbasekaran, M.; Woo, E. P. *Adv. Mater.* **1997,** 9, (10), 798.
9. Grell, M.; Bradley, D. D. C.; Long, X.; Chamberlain, T.; Inbasekaran, M.; Woo, E. P.; Soliman, M. *Acta Polymerica* **1998,** 49, (8), 439-444.
10. Bradley, D. D. C.; Grell, M.; Long, X.; Mellor, H.; Grice, A.; Inbasekaran, M.; Woo, E. P., Influence of aggregation on the optical properties of a polyfluorene. In *Optical Probes of Conjugated Polymers*, Vardeny, Z. V.; Rothberg, L. J., Eds. Spie-Int Soc Optical Engineering: Bellingham, 1997; Vol. 3145, pp 254-259.
11. Khan, A. L. T.; Sreearunothai, P.; Herz, L. M.; Banach, M.; Köhler, A. *Phys. Rev. B* **2004,** 69, (8), 085201.
12. Prins, P.; Grozema, F. C.; Nehls, B. S.; Farrell, T.; Scherf, U.; Siebbeles, L. D. A. *Phys. Rev.B* **2006,** 74, (11), 113203.
13. Grell, M.; Bradley, D. D. C.; Ungar, G.; Hill, J.; Whitehead, K. S. *Macromol.* **1999,** 32, 5810-5817.
14. Cadby, A.; Lane, P. A.; Mellor, H.; Martin, S. J.; Grell, M.; Giebeler, C.; Bradley, D. D. C.; Wohlgenannt, M.; An, C.; Vardeny, Z. V. *Phys. Rev. B* **2000,** 62, (23), 15604-15609.
15. Ariu, M.; Lidzey, D. G.; Sims, M.; Cadby, A. J.; Lane, P. A.; Bradley, D. D. C. *J. Phys.-Cond. Matt.* **2002,** 14, (42), 9975-9986.
16. Lu, H. H.; Liu, C. Y.; Chang, C. H.; Chen, S. A. *Adv. Mater.* **2007,** 19, (18), 2574.
17. Winokur, M. J.; Slinker, J.; Huber, D. L. *Phys. Rev. B* **2003,** 67, 184106.
18. Rothe, C.; King, S. M.; Dias, F.; Monkman, A. P. *Phys. Rev. B* **2004,** 70, (19), 195213.
19. Becker, K.; Lupton, J. M. *J. Am. Chem. Soc.* **2005,** 127, (20), 7306-7307.
20. Knaapila, M.; Dias, F. B.; Garamus, V. M.; Almasy, L.; Torkkeli, M.; Leppanen, K.; Galbrecht, F.; Preis, E.; Burrows, H. D.; Scherf, U.; Monkman, A. P. *Macromol.* **2007,** 26, 9398-9405.
21. Knaapila, M.; Stepanyan, R.; Torkkeli, M.; Garamus, V. M.; Galbrecht, F.; Nehls, B. S.; Preis, E.; Scherf, U.; Monkman, A. R. *Phys. Rev. E* **2008,** 77, (5), 14.
22. Chunwaschirasiri, W.; Tanto, B.; Huber, D. L.; Winokur, M. J. *Phys. Rev. Lett.* **2005,** 94, (10), 107402.
23. Arif, M.; Volz, C.; Guha, S. *Phys. Rev. Lett.* **2006,** 96, (2), 025503.
24. Khan, A. L. T.; Banach, M. J.; Kohler, A. *Synth. Met.* **2003,** 139, (3), 905-907.
25. Dias, F. B.; Morgado, J.; Macanita, A. L.; da Costa, F. P.; Burrows, H. D.; Monkman, A. P. *Macromol.* **2006,** 39, (17), 5854-5864.
26. Kitts, C. C.; Vanden-Boot, D. A. *Polymer* **2007,** 48, 2322-2330.
27. Stavrinou, P. N.; Ryu, G.; Campoy-Quiles, M.; Bradley, D. D. C. *J. Phys.-Cond. Matt.* **2007,** 19, (46), 466107.
28. Caruso, M. E.; Anni, M. *Phys. Rev. B* **2007,** 76, (5), 054207.
29. Anni, M.; Caruso, M. E.; Lattante, S. *J. Phys. Chem. C* **2008,** 112, (8), 2958-2963.

30. Shaw, P. E.; Ruseckas, A.; Peet, J.; Bazan, G. C.; Samuel, I. D. W. *Adv. Funct. Mater.* **2010,** 20, (1), 155-161.
31. Knaapila, M.; Almasy, L.; Garamus, V. M.; Ramos, M. L.; Justino, L. L. G.; Galbrecht, F.; Preis, E.; Scherf, U.; Burrows, H. D.; Monkman, A. P. *Polymer* **2008,** 49, (8), 2033-2038.
32. Bright, D. W.; Dias, F. B.; Galbrecht, F.; Scherf, U.; Monkman, A. P. *Adv. Funct. Mater.* **2009,** 19, (1), 67-73.
33. Bright, D. W.; Galbrecht, F.; Scherf, U.; Monkman, A. *Macromol.* **2010,** 43, (18), 7860-7863.
34. Dias, F. D.; Morgado, J.; Macanita, A. L.; Costa, F. P.; Burrows, H. D.; Monkman, A. P. *Macromol.* **2006,** 39, 5854-5864.
35. Vaughan, H. L.; Dias, F. M. B.; Monkman, A. P. *J. Chem. Phys.* **2005,** 122, (1), 014902.
36. Ariu, M.; Sims, M.; Rahn, M. D.; Hill, J.; Fox, A. M.; Lidzey, D. G.; Oda, M.; Cabanillas-Gonzalez, J.; Bradley, D. D. C. *Phys. Rev. B* **2003,** 67, (19), 195333.
37. Cadby, A. J.; Lane, P. A.; Mellor, H.; Martin, S. J.; Grell, M.; Giebeler, C.; Bradley, D. D. C.; Wohlgenannt, M.; An, C.; Vardeny, Z. V. *Phys. Rev. B* **2000,** 62, (23), 15604-15609.
38. Ariu, M.; Lidzey, D. G.; Bradley, D. D. C. *Synth. Met.* **2000,** 111, 607--610.
39. Volz, C.; Arif, M.; Guha, S. *J. Chem. Phys.* **2007,** 126, (6), 064905.
40. Gierschner, J.; Mack, H. G.; Luer, L.; Oelkrug, D. *J. Chem. Phys.* **2002,** 116, (19), 8596-8609.
41. Gierschner, J.; Mack, H. G.; Egelhaaf, H. J.; Schweizer, S.; Doser, B.; Oelkrug, D. *Synth. Met.* **2003,** 138, (1-2), 311-315.
42. Scherf, U.; List, E. J. W. *Adv. Mater.* **2002,** 14, (7), 477.
43. Peet, J.; Brocker, E.; Xu, Y. H.; Bazan, G. C. *Adv. Mater.* **2008,** 20, (10), 1882.
44. Tsoi, W. C.; Charas, A.; Cadby, A. J.; Khalil, G.; Adawi, A. M.; Iraqi, A.; Hunt, B.; Morgado, J.; Lidzey, D. E. *Adv. Funct. Mater.* **2008,** 18, 600-606.
45. Tsoi, W. C.; Lidzey, D. G. *J. Phys.-Cond. Matt.* **2008,** 20, (12).
46. Knaapila, M.; Garamus, V. M.; Dias, F. B.; Almasy, L.; Galbrecht, F.; Charas, A.; Morgado, J.; Burrows, H. D.; Scherf, U.; Monkman, A. P. *Macromol.* **2006,** 39, (19), 6505-6512.
47. Birks, J. B.; Christophorou, L. G. *Spectrochimica Acta* **1963,** 19, (2), 401-410.
48. Jansson, E.; Jha, P. C.; Aren, H. *Chem. Phys.* **2007,** 336, (2-3), 91-98.
49. Miyahara, M.; Kawasaki, H.; Fukuda, T.; Ozaki, Y.; Maeda, H. *Colloids Surf. A* **2001,** 183, 475-485.
50. Nelson, D. J.; Hermans-Jr., J. *BioPhysics* **1973,** 12, (6), 1269-1284.

5 Beta Phase Formation in Films of Linear Alkyl Side Chain Polyfluorenes

5.1 Introduction

Whilst the initial work in chapter 4 using polyfluorene solutions is critical in understanding the nature of the beta phase formation in these polyfluorenes, the practical applications of these polymers use thin solid films of the polymer incorporated into a device such as a Light Emitting Diode (LED). Therefore this chapter will examine the formation of the beta phase in solid films of the polymer group PF6 to PF10.

Clearly the physics of the beta phase formation will not be identical to the solution case; the polymer chains in the solid phase are closely spaced, they are effectively in a permanently aggregated state and there is no longer a solvent to drive apart aggregated side chains. Following a review of film morphology and exciton migration in polymer films, the results in this chapter will show the trend formation of the beta phase in films of these polymers, as induced by thermal cycling and toluene vapour exposure, and provide characterisation of the beta phase in the polymers as a function of side chain length. The results show that the currently accepted picture, that local solvent-induced or thermal-expansion-induced strain on polymer chains is the cause of planarization and beta phase formation in thin films, does not tell the whole story and that the planarization is still dependent upon side chain interactions to form the beta phase.

5.2 Physical Morphology and Migration in Conjugated Polymer Films

5.2.1 Ideal Chains

A polymer chain is modelled at the simplest level as *n+1* individual atoms, which are joined by *n* bonds described by vectors r_i with bond length length *l* which join the adjacent atoms. It is called an ideal chain if atoms separated by many bonds do not interact. The end-to-end vector is the sum of the bond vectors:

$$\overrightarrow{R_n} = \sum_{i=1}^{n} \vec{r_i} \tag{5-1}$$

For a polymer with unrestricted rotations of all bonds and no steric hindrance to restrict the positions of the atoms, the ensemble average end-to-end distance is $\langle R \rangle = 0$ for isotropic chains. The ensemble average refers to all possible states of a system, which can be thought of as the average of many chains, or the average of all possible states of one chain. The ensemble average square end-to-end distance $\langle R \rangle^2$ of these chains is the sum of the products of the bond vectors r_i and r_j along the chains:[1]

$$\langle R^2 \rangle = \sum_{i=1}^{n} \sum_{j=1}^{n} \langle \vec{r_i} \cdot \vec{r_j} \rangle = l^2 \sum_{i=1}^{n} \sum_{j=1}^{n} \langle \cos\theta_{ij} \rangle \tag{5-2}$$

For a freely jointed polymer with no correlation between the bond vectors, the average $\langle Cos\theta_{ij} \rangle = 0$ for $i \neq j$ and $\langle Cos\theta_{ij} \rangle = 1$ for $i = j$, and this simplifies to:[1]

$$\langle R^2 \rangle = nl^2 \tag{5-3}$$

In a real chain nearby bond vectors are correlated by physical bond angle restrictions and the average $\langle Cos\theta_{ij} \rangle \neq 0$ for $i \neq j$, but it is assumed for ideal chains that distant bond vectors are not correlated and that this value tends to zero at the limit of infinitely separated bonds; there should be no relation between a bond vector at one end of a long polymer chain and another at the far end as the atoms are not interacting and are separated by many bonds that can bend and rotate.

In a real chain, the sum of the bond angles between a given bond vector r_i and all other bond vectors r_j in the ensemble of chains converges to a finite number C'_i since there is a correlation with the nearby bonds and no correlation for more distant bonds:[1]

$$C'_i = \sum_{j=1}^{n} \langle \cos\theta_{ij} \rangle \tag{5-4}$$

This substitutes into equation 5-2 to give:[1]

$$\langle R^2 \rangle = l^2 \sum_{i=1}^{n} \sum_{j=1}^{n} \langle \cos\theta_{ij} \rangle = l^2 \sum_{i=1}^{n} C'_i = C_n n l^2 \tag{5-5}$$

Where Flory's characteristic ratio $C_n = 1/n \sum_{i=1}^{n} C'_i$ is the average value of C'_i across the chain. For real chains, there is a limiting value in the sum in equation 5-4, at a value defined as $C_n = C_\infty$ which typically has values in the range 7 to 9 for flexible polymers such as polyethylene. This results in the approximation of the mean square end-to-end separation for long chains:[1]

$$\langle R^2 \rangle \cong C_\infty n l^2 \tag{5-6}$$

5.2.2 The Kuhn Length

An important concept in the study of the physical properties of polymers is the Kuhn Length, *b*. This compares a real polymer chain of length N, mean squared end-to-end vector $\langle R \rangle^2$ and maximum possible end-to-end vector R_{max} to an equivalent ideal chain with equivalent bond length *b*, which is capable of moving freely at the joints between the monomers without the restrictions of bond angles and steric hindrance.[1]

$$b = \frac{\langle R^2 \rangle}{R_{max}} \tag{5-7}$$

A persistence segment s_p is the number of bond lengths in the polymer chain over which the local correlations between bond vectors decay.[1]

$$s_p = -\frac{1}{\ln(\cos\theta)} \cong -\frac{2}{\theta^2} \text{ (for wormlike chains)} \tag{5-8}$$

Where θ is the bond angle between adjacent bonds. This persistence segment magnitude influences the size of the delocalised regions in conjugated polymers. Polyfluorenes are generally considered to be wormlike chains, where the chains are stiff and bonds are allowed to rotate freely for small angles of θ only, leading to the simplification shown in equation 5-8. In this case, the persistence length l_p is:

$$l_p = l \cdot 2/\theta^2 \tag{5-9}$$

For a wormlike chain, this distance is twice the Kuhn length;

$$b = l/\theta^2 \tag{5-10}$$

5.2.3 The Rouse Model

In the Rouse model, a polymer chain of N monomers is represented by N beads attached by springs with root-mean square length *b*, for a chain in solution.[2-3] Each bead is constrained by a frictional force with coefficient *ζ* and the total friction acting on the chain is *Nζ*.

The Rouse diffusion coefficient for the motion of the polymer chain is defined by an activation-type process acting against the local friction forces: [1, 3]

$$D_R = \frac{kT}{N\zeta} \tag{5-11}$$

Using this coefficient, the Rouse time τ_R is defined as the time taken for a polymer chain to move a distance of the order of its own size *R*:[1]

$$\tau_R = \frac{R^2}{D_R} = \frac{\zeta}{kT} N R^2 \tag{5-12}$$

5.2.4 Reptation in Polymer Melts

To model the behaviour of polymers in the solid state, the tube model of reptation is used, which is shown schematically in figure 5-1. It was first proposed by de Gennes for entanglement in unlinked polymers,[4] and further developed by Doi and Edwards.[5-6] This model considers the movement of a single polymer chain through a constricting tube formed by the polymer chains that surround it. The chains are entangled by being coiled around each other, forcing any one chain to adopt a configuration within the available space between them. The polymer chain is twisted and in motion inside this region as a result of thermal vibrations, such that there is a greater length of polymer chain within the tube than the shortest distance between the constriction points, called the primitive path, shown in light gray. The excess lengths of chain around the primitive path are termed entanglement strands.

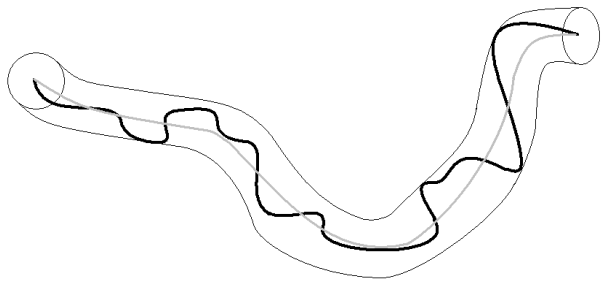

Figure 5-1: The tube model of a polymer chain (black line) confined within a region (narrow lines) of average diameter *a* formed by the surrounding medium. The primitive path is shown in light gray.

The average tube diameter, a, enforces a limit to the transverse fluctuations of the polymer chain around the primitive path. The number of monomers in an entanglement strand N_e is defined as the number of Kuhn monomers in a strand of length a. Melts of long polymer chains (above the glass transition temperature) adopt nearly ideal chain conformations,[1] and the diameter relation is:

$$a \approx b\sqrt{N_e} \tag{5-13}$$

And the number of entangled sections along the chain is N / N_e strands, each of size a.

The Rouse model is applied directly to this scenario, in the form of the curvilinear diffusion coefficient D_c of the same form as the solution case:[1]

$$D_c = \frac{kT}{N\zeta} \tag{5-14}$$

In this case the diffusion coefficient describes the motion of the chain along the primitive path of the constraining tube. This is an indication of the mobility of the polymer chains with respect to each other.

5.2.5 Swelling of Films by Solvent Vapour

When solvent is added to a film of polymer, the initial film volume V_0 is increased in a simple manner to become the total volume V of polymer plus solvent. The linear deformation λ for the unconstrained system is:[1]

$$\lambda = \left(\frac{V}{V_0}\right)^{1/3} \tag{5-15}$$

This will not strictly apply to a system of a thin film on a substrate as the underside of the film will experience frictional forces from the substrate surface. The net result will be a distribution of shear stress across the film profile. The microscopic stress on polymer chains within the thin film exerted by film deformation upon either solvent swelling or thermal expansion is hypothesised to be the source of the formation of the beta phase.[7] This swelling reduces the friction coefficient between polymer chains, reducing the friction coefficient ζ in equation 5-14. This allows the polymers to move more freely, effectively reducing the glass transition temperature. However, this extra motional freedom is moderated by the creation of tension along the polymer chains caused by the film expansion acting on intertwined chains at points of overlap.

This theoretical description is important for the understanding of the comparison between the two methods used to induce the beta phase in section 5.3, where both thermal cycling and solvent vapour exposure are trialled on the group of polymers PF6 to PF10.

5.2.6 Exciton Migration in Polymer Films

Exciton migration in polymer films occurs at a far higher rate than in solution. This is simply the result of the proximity of the chromophores within the solid phase, which provides more possible energy transfer pathways for migration to proceed to. Förster and Dexter transfer require the chromophores to be within a distance of approximately 5 nm and 1 nm respectively, which is an easily achievable separation for neighbouring polymer chains, even taking account of the side chain length of 1 nm for octyl side chains. This allows excitons to migrate effectively through the film and become localised on lower energy chromophores before emission takes place. In pure films these lower energy chromophores are the longest conjugation lengths within the distribution of energy states, and in mixed component films the lowest energy chromophores may be an oxygen defect,[8] or a dopant.

The distribution of conjugation lengths in the polymer film are also dispersed in 3-dimensional space. Therefore an exciton may not migrate directly to a lower energy state if its path between the two sites is physically blocked by higher energy states. Upon initial excitation, an exciton may be generated with a large excess of energy (by absorption of a photon on the high energy side of the absorption band) and may have sufficient energy to cross such obstructions, but within a few migration steps the exciton reaches the lower parts of the density of states and it becomes trapped once all the surrounding sites are at a higher energy. It may then cross small potential barriers of height below several kT by thermal activation, allowing thermal migration to continue. This model has been proposed because the exciton mobility is higher and time dependent for the first picosecond, but then settles to a constant level; the thermally activated regime. The time independent mobility is dependent upon the temperature.[9]

The transfer of excitons to the lower energy beta phase in thin films is fast and efficient, [10-13] but dependent upon the film morphology. The morphology has a strong effect on the quantum efficiency of film of PF8,[14] with variations from 40 % to 80 % depending upon the morphology and

the temperature of the measurement. They found that a film containing beta phase chains exhibited the lowest efficiency, which they attributed to polaron quenching and exciton trapping in the lower energy beta phase chromophores, although the presence of the keto defect in their samples is likely to have affected their results (see chapter 6). In contrast, in PLED devices under the electroluminescence scheme, the low energy trapping sites increase the exciton formation yield by increasing the charge recombination probability, leading to an increase in efficiency of beta-phase containing PLED devices by a factor of three over alpha phase PF8 devices.[13]

5.3 Results

The conjugated polymer thin films used in this work are composed of long chains of approximately 500 monomer units. The molecular arrangement in the film as spun from warm solution at concentrations below 5 mg·mL^{-1} is amorphous, giving rise to a broad single absorption band for the $S_0 \rightarrow S_1$ transition centred on 380-385 nm.[15]

Formation of the beta phase in films of PF8 can occur via four methods. Firstly, if the film is spun or drop cast from a solution in a poor solvent,[10, 16-18] then beta phase aggregates can be deposited from the solution. However, at higher concentrations (near 10 mg·mL^{-1}) it was found in this work that the film thickness becomes very inhomogeneous as large aggregates are deposited. Secondly, additives such as 1,8-diodooctane[19] into the source solution when spinning have been shown to induce controlled beta phase content.[20]

For a film already spun, two further methods have been established for inducing the formation of the beta phase; cooling the film to below the transition temperature and slowly re-warming it back to room temperature,[7, 21-22] and exposing the film to vapour of certain solvents.[7] Both these methods will be trialled for the polymer group PF6 to PF10.

5.3.1 Thermally Cycled Thin Films

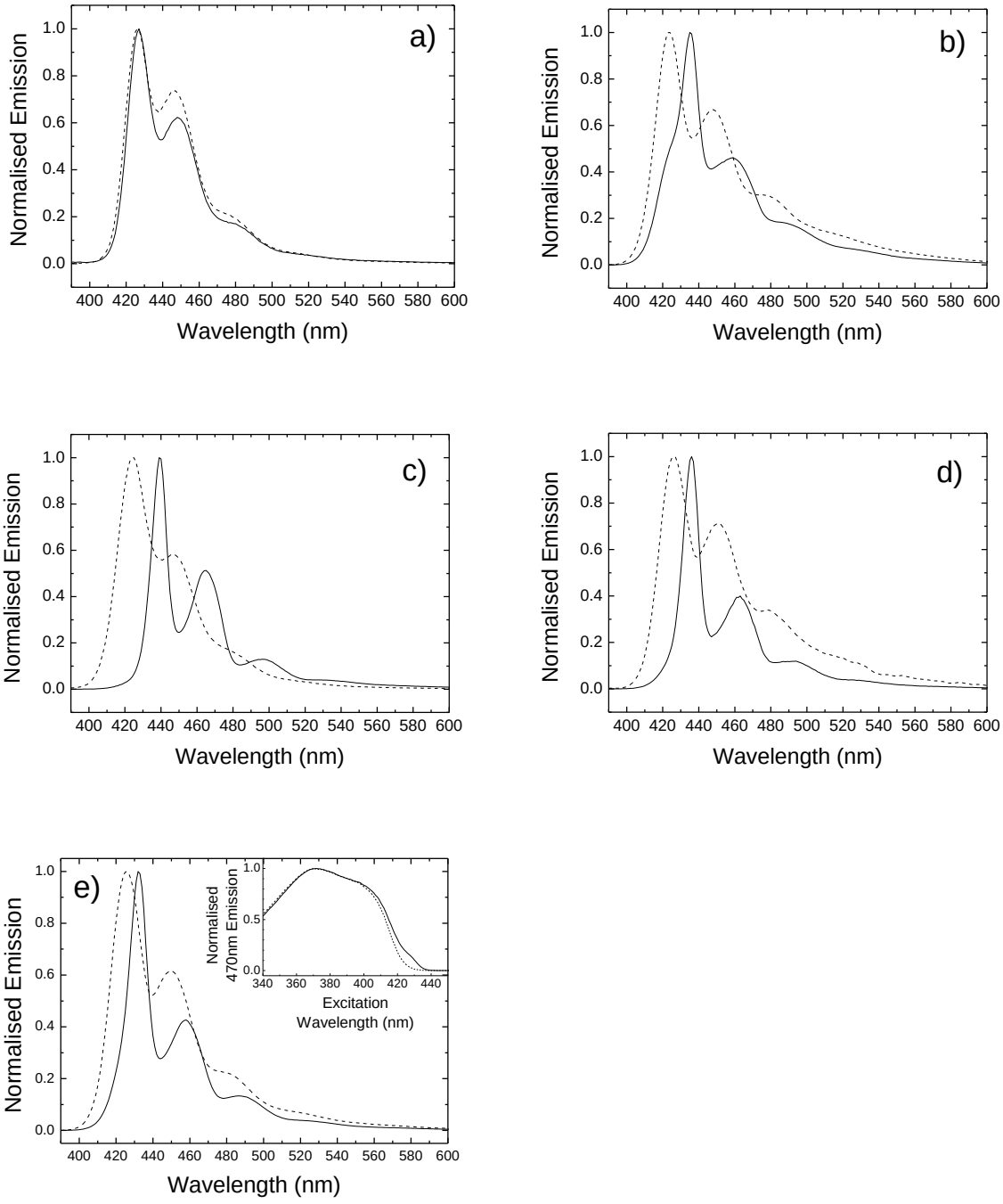

Figure 5-2: The initial (dashed line) and final (solid line) emission spectra of a) PF6, b) PF7 c) PF8 d) PF9 and e) PF10 films spin-cast from 10 mg mL^{-1} in toluene. The samples were then cooled, and reheated to room temperature at a rate of 0.6 K min^{-1}. The inset of part e) shows the excitation spectrum shift to confirm the phase change.

Thin films of these polyfluorenes with OD in the region of 0.3 were cooled to 11 K, then slowly warmed to 290 K at a rate of 0.6 K/min. The strain imposed upon the film by thermal expansion upon warming is believed to be the sole contributor to the change in phase.[7] This is backed up by the finding that if the re-warming is too fast, the polymer chains do not expand under strain with the film but slip past each other, and the phase change does not occur.

The resulting emission spectra are shown in Figure 5-2. In the solid state PF6 does not form any beta phase, in concordance with the solution sample results; the emission is characteristic of the amorphous phase, and the energy does not change after the thermal cycle. There is however a reduction in the vibronic replica intensity, suggesting a reduction in the Huang-Rhys parameter and therefore an increase in the ordering of the microstructure. In PF7, an intense, sharp beta phase emission peak is produced at 436 nm after the thermal cycle, and the final spectrum is very similar to the low temperature emission spectrum of PF7 in solution. The beta phase content is sufficient to quench the majority of the alpha phase emission at 425 nm, which remains only as a small shoulder at that wavelength. The spectrum of the PF8 thermally cycled film shows emission entirely dominated by the beta phase, which peaks at 441 nm. In the PF9, the final spectrum is a characteristic beta phase emission spectrum. The PF10 shows a relatively complete change of the emission spectrum, although the FWHM of the emission peak is not as narrow as is the case for PF7 to PF9, perhaps indicating a lower extent of ordering in this film. The phase change is confirmed by an excitation spectrum (inset) showing the build-in of the shoulder feature in a similar manner to that of PF7 in the solution phase.

The side-chain dependence of the beta-phase formation is a clear indication that the stress produced by the film expansion is not the full description of the phase formation process. There is still a need for side chain interactions to stabilise the beta phase once the stress-induced modification of the film morphology has occurred.

5.3.2 PF8 Thin Films Exposed to Toluene Vapour

Thin films of PF8 were spun with optical density in the range 0.2-0.35. A toluene vapour exposure method was then used to attempt to induce beta phase in many samples of these polymer films to establish the consistency of the method.

The films were exposed to toluene vapour by suspending them in a mount held by a clamp stand, suspended approximately 5 cm above the surface of a shallow reservoir of toluene in a large beaker, itself sitting on a hotplate set to 120 °C. The solvent itself is not in intimate contact with the hotplate surface, and the solvent evaporation provides a powerful cooling effect; the solvent temperature was measured by a thermal probe to be 65±3°C, once equilibrium had been reached. The sides of the beaker ensure that a high density of toluene vapour flows over the film surface before the vapour disperses into the strong airflow of the fume cupboard. Beta phase formation from this method was successfully induced in PF8 after only a few seconds. Previous attempts with unheated toluene, such as placing the film under an upturned beaker with a toluene reservoir, failed to produce any spectral changes indicative of beta phase formation even after many hours. Others state that exposure times of around 10 hours[23] to 12 hours are needed.[24]

The absorption and emission spectra of a representative sample of the films that were tested are given in figure 5-3a, along with a fit to a spectrum with multiple Gaussian curves (figure 5-3b). The absorption clearly shows a strong peak at 434 nm, and the emission shows the sharp, well resolved emission spectrum characteristic of the beta phase.

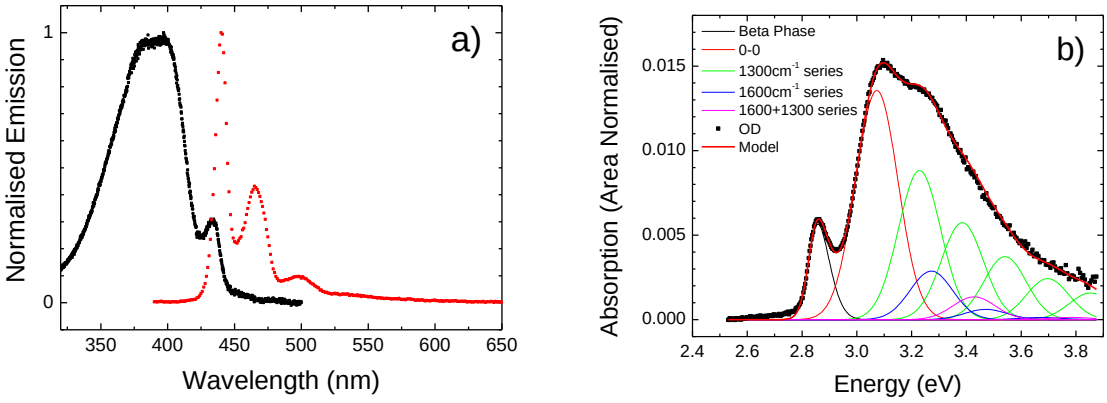

Figure 5-3: The normalised absorption and emission spectra of a sample exposed to toluene vapour for 1 minute (a) and a fit to a representative absorption spectrum on an energy scale using multiple Gaussian curves (b). See text for details.

The fractions of beta phase induced in a series of film samples of PF8 exposed to toluene vapour for different time intervals are given in figure 5-4a, using the area method described in chapter 4 to calculate the fraction of beta phase present. From the figure, the fraction of beta phase that can be formed in a pure PF8 film using this method saturates at about 9 %, and it does so within a minutes' exposure to warm toluene vapour. There is not a smooth trend in the data of increasing beta fraction at increasing exposure time, although where a smaller fraction of beta phase is formed this only occurs for very short exposure times (3 s to 15 s). This is in agreement with other work on solvent-swelling in PF8 films which discovered the transition to saturated beta-phase films occurred within five minutes at room temperature.[25] Chen et al. also found that the majority of the phase formation was completed within the first minute of vapour treatment.[15] Figure 5-4b shows the normalised emission spectra from various beta phase films, with an inset demonstrating that the variability in the relative magnitude of the first vibronic replica arises only from a variation in film optical density causing self-absorption of the main emission peak intensity, and is not correlated with the toluene exposure time.

However, there is also evidence of considerable variation in the data, which are mainly attributed to the simplicity of the method used, which did not effectively control the density of the toluene

vapour moving past the film surface, except that the hotplate was maintained at the same temperature to within 3K for all the samples. No attempt has been made to fit the trend since the variability of the data means that significant or more meaningful information could not be derived. From further examination of the data it appears that different samples may saturate at slightly different fractions of beta phase. The samples at 600 s and 1420 s exposure time are significantly below the level of the sample at 1200 s. This difference may be due to sample-to-sample differences in the as-spun film morphology.

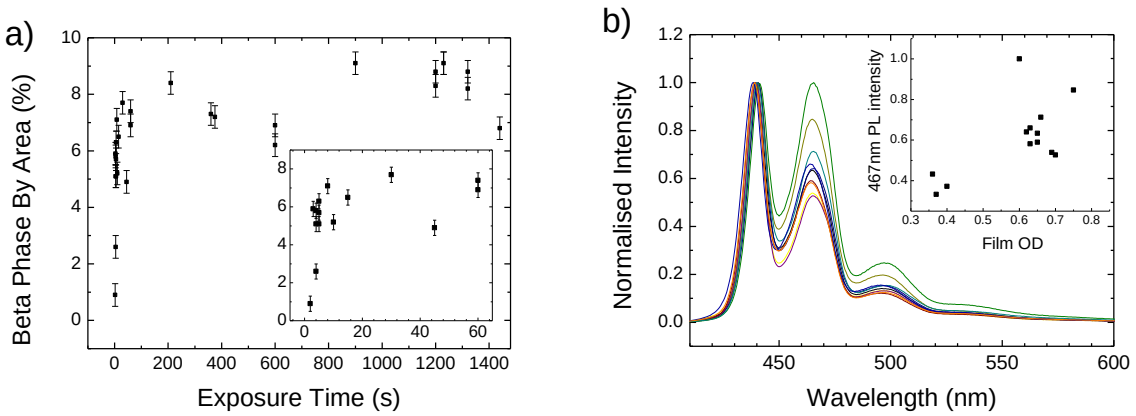

Figure 5-4: a) Beta phase fraction derived by peak fittting of the area of the main absorption bands. Inset: expanded scale of the first minute of exposure time. b) The emission spectra from the different samples. Inset: the correlation of the normalised film OD to the second vibronic PL intensity, showing that the spectral differences arise from self-absorption.

The differences between individual samples are therefore believed to be the result of some cases where the local film morphology can allow the movement of a larger number of chains in order to allow side chain interdigitation, or can accommodate the absorption of more solvent. However, it has been established that the samples are saturated within five minutes' exposure and that the sample variability is not sufficient to prevent the formation of the beta phase.

5.3.3 Thin Films of PF6-PF10 Exposed to Toluene Vapour

The polymers of the group PF6-PF10 were exposed to toluene vapour by the same method for 20 minutes to ensure the maximum phase shift had been induced. The corresponding absorption spectra are displayed as a series in figure 5-5. It is clear that the trend exhibited in chapter 4 for these polymers in solution is not fully replicated here, with far lower fractions of beta phase being formed. The as-spun alpha-phase film spectra are similar, as would be expected for the amorphous phase. The spectra of the films after vapour treatment all show significant changes, with a red-shift of the main absorption band, as was observed in the solutions, and there are varying degrees of shoulders apparent in the region of 430 nm. Although PF8 is still shown to be the optimal chain length of the group by exclusively exhibiting a second peak at 435 nm, there is not a clear absence of the phase in PF6. The PF6 film appears as if there may be traces of beta phase present. It is unclear if there is beta phase present in PF7, and the PF10 shows clear evidence of a strong shoulder at 430 nm, even more so than the PF9. This odd-even side chain length effect has previously been observed for this group of polymers by Knaapila et al.[26] and is known to affect the melting point of alkanes; even-numbered alkyl chains can achieve a higher packing density in the solid phase.[27]

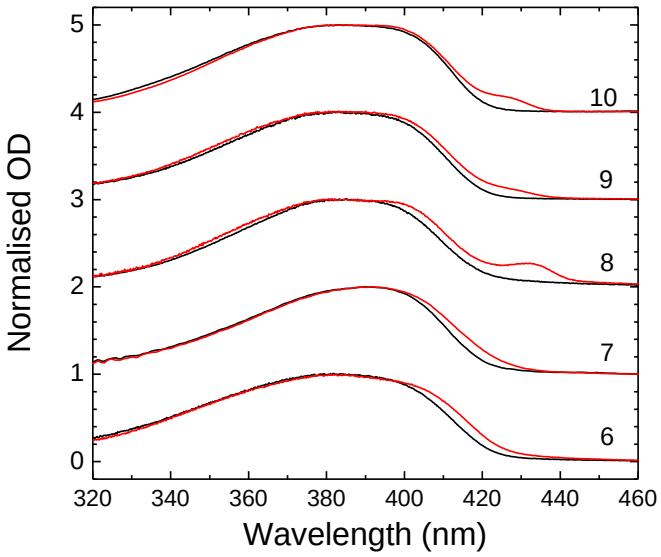

Figure 5-5: Room temperature absorption spectra before (black lines) and after 20 minutes' toluene vapour exposure (red lines) for PF6 to PF10 (marked 6-10).

The photoluminescence spectra for the corresponding films are given in figure 5-6. The main emission peaks of the as-spun films (black) are very similar, with minor differences in the wavelengths only. The emission spectra from the films after vapour treatment are far more informative. Firstly, the peak emission wavelengths show a trend from PF6 to PF8 of increasing redshift then decreasing redshift from PF8 to PF10, indicating that there is still an optimum chain length for maximum polymer backbone planarity. Second, the presence of the beta phase is confirmed in PF7 but not PF6; the beta phase entails a redshift of the energy levels of the system including the vibronics, which is shown in PF7 but not PF6. The change in the emission in PF6 is entirely due to self-absorption of the 0-0 emission by the film as a result of the absorption spectrum red-shift seen in figure 5-5. The vibronic replicas remain at the same wavelength as for the untreated film.

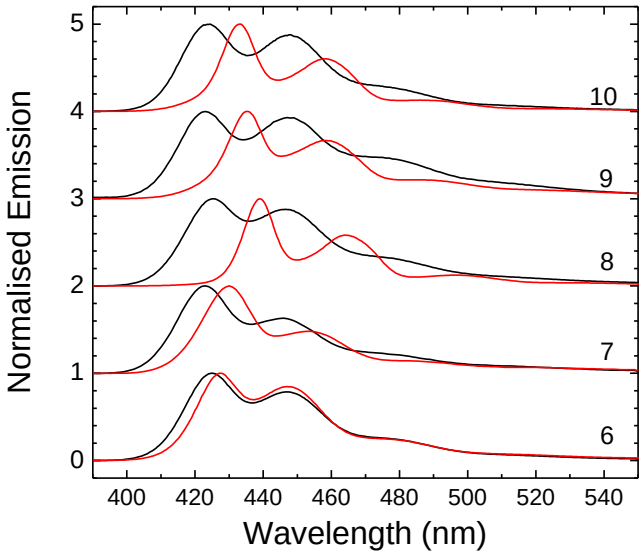

Figure 5-6: Room temperature photoluminescence spectra before (black lines) and after 20 minutes' toluene vapour exposure (red lines) for PF6 to PF10 (marked 6-10).

The toluene vapour method is apparently more effective than thermal cycling at producing the beta phase in the various side chain polymers that are capable of this phase change. For example, the

beta phase by area in the PF8 sample is 5.5 % for thermal cycling and in the region of 8 % for toluene exposure. However, it must be noted that there is considerable variability between samples, and it is possible that further thermal cycles may increase the beta phase fraction, although others have shown further cycles do not add significantly to the beta phase content.[28] It is, however, expected from the theory in chapter 5.2 that the solvent vapour method would be more effective. Thermal cycling provides the stress forces to rearrange the polymer chains, whilst the solvent vapour method both provides the stress forces from the film swelling and also reduces the local friction coefficient, increasing the chain mobility and allowing greater rearrangement of the polymer chains.

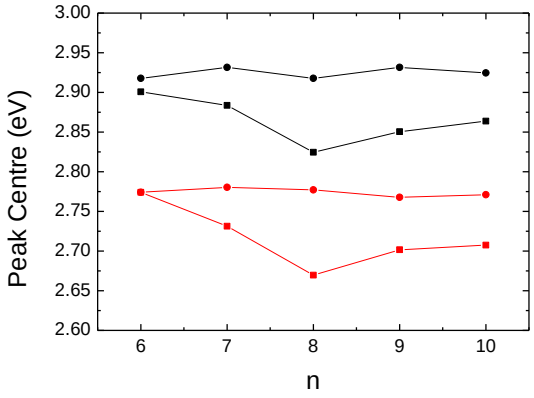

Figure 5-7: The 0-0 (black) and 0-1 (red) peak centres for the 290K emission spectra in figure 5-6 for as-spun samples (circles) and toluene vapour treated samples (squares) as a function of *n*-alkyl side chain length.

Figure 5-7 shows more clearly the energy stabilisation resulting from the beta phase by showing the shift of the emission peaks where the beta phase is formed in the toluene vapour treated films. PF6 shows no stabilisation of the 0-1 peak, confirming that the shift of the 0-0 peak is due to self-absorption. The other polymers all show a similar extent of stabilisation in both the 0-0 and 0-1 transitions; the peak shifts are are 49 meV, 108 meV, 66 meV and 63 meV for n=7, 8, 9 and 10 (data for the 0-1 transitions).

5.3.4 Low Temperature Emission Spectra

Further information may be gained from the films' emission spectra by observing the photoluminescence at very low temperatures, where the broadening due to low-energy ring torsion modes is greatly reduced and the vibronic replicas of the main emission wavelength can be resolved. The photoluminescence spectra of the films are shown in figure 5-6. These films have been saturated with toluene vapour and thermally cycled to ensure the maximum phase possible is present in each film and to prevent further beta phase formation influencing the results during the cooling. The spectra were taken during excitation to the alpha phase bulk at 380 nm.

The figure shows further evidence that the beta phase is formed in films of PF7 to PF10 but not in PF6. The main emission peak at 11K from PF6 is located at 430 nm rather than the range 438-442 nm for the other samples, and this emission band in PF6 is not spectrally narrowed to the extent seen in the others. The first vibronic replica is also a broad featureless peak centred at 458 nm, in contrast to the other polymers which all show a band composed of two or more sharper sub-peaks, although the structure in the emission of PF10 is not immediately apparent on first inspection. However, due to the similar molecular structure of the polymer PF6 to the other polymers it is likely that the same modes are present. But since the beta phase is not formed, the width of the density of states contributing to the emission is not reduced, and so the vibronic structure is not resolved.

In figures 5-8b and 5-8d there are still significant contributions to the spectrum from the α-phase components of the film for PF7 and PF9, which are absent from PF8 and PF10, again reinforcing the odd-even side chain length phenomenon.

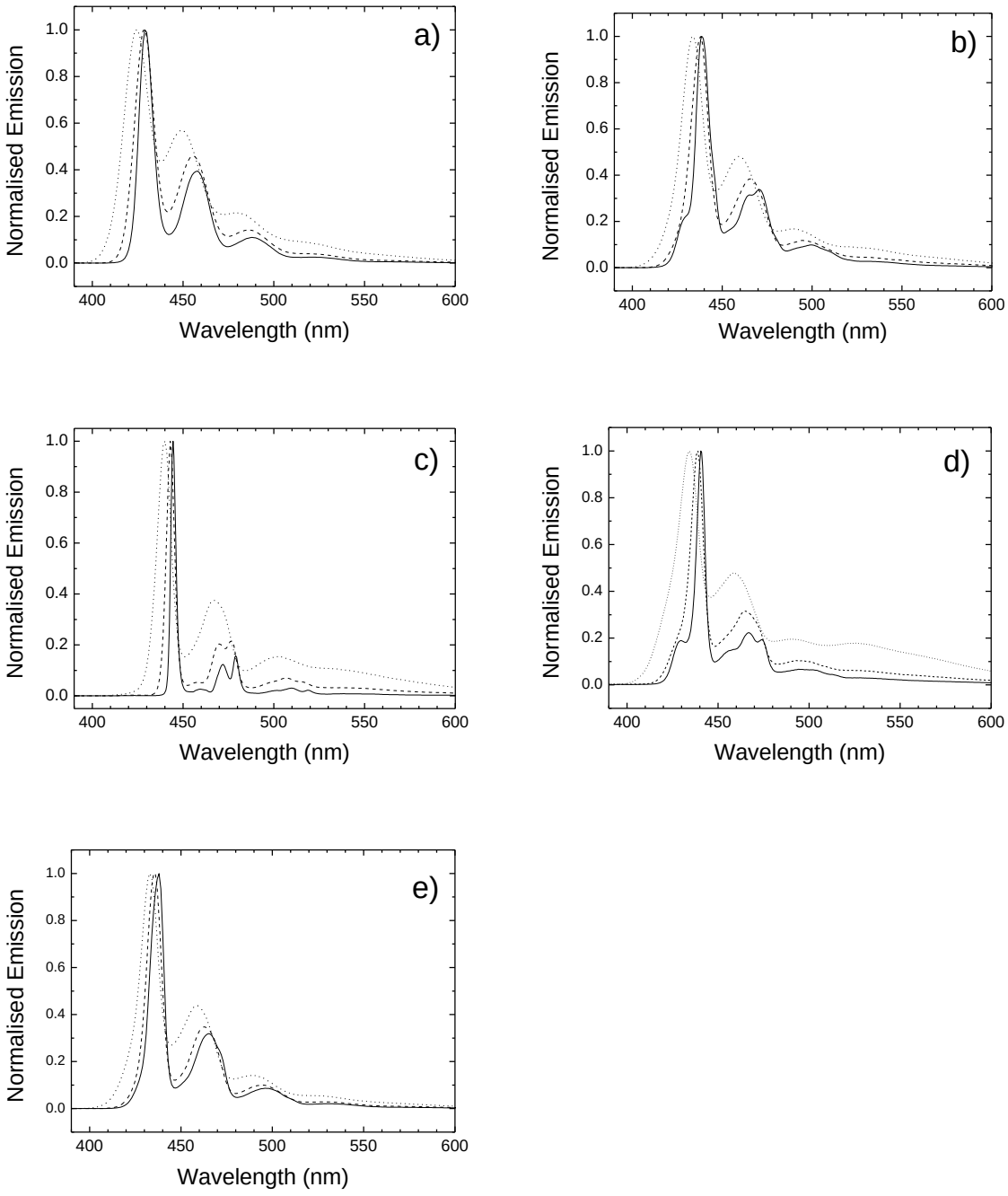

Figure 5-8: Emission spectra at 295K (dotted line) 150K (dashed line) and 11K (solid line) for PF6 (a) PF7 (b) PF8 (c) PF9 (d) and PF10 (e)

To accurately determine the emission spectrum from the beta phase components, site-selective spectroscopy was used.[29] By exciting the films at 432 nm, the incident radiation is absorbed by the beta phase (planarised) chain segments, which being at lower energy do not permit transfer of the

excitons back to the alpha phase. The spectra so produced should have far less contribution from the alpha phase components, although a very small fraction of the alpha phase chains in the low-energy tail of the absorption band may still be visible. However, these spectra can only be recorded from 438 nm upwards due to the scattered excitation beam obscuring the signal below this wavelength. The spectra are presented in figure 5-9.

The 11 K spectra excited on the beta phase chains show better resolution of the two features that form the first vibronic band that is seen at 295K in figure 5-8. Gaussian curves were used to fit each of these bands to derive the precise energy levels of the vibronics. All the bands were fitted well by two dominant Gaussians and a smaller band (that is only clearly resolved in PF8 and PF9). For PF7 a small remnant of alpha phase emission is seen, because it exhibits greater red-shift of the main band absorption (most clearly seen in figure 4-3f). The derived parameters are given in table 5-1.

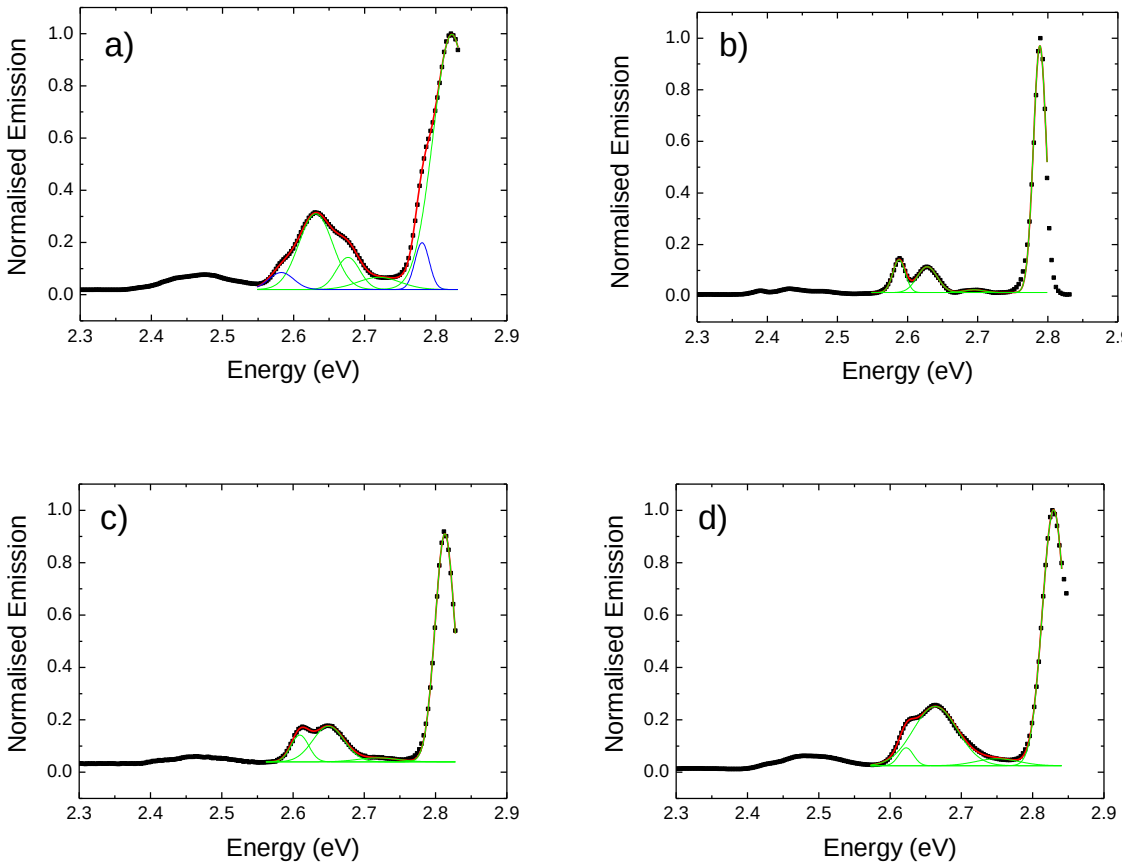

Figure 5-9: Site-selective photoluminescence spectra of PF7 (a) PF8 (b) PF9(c) and PF10 (d) at 11K using excitation at 432 nm (black squares). Fits to the data over the range 2.57 – 2.83 eV (red) are produced by summation of several Gaussian peaks (green). Extra peaks in 7a (blue) indicate remnants of the alpha phase emission and a vibronic mode.

Uncertainty in the wavelength of the peaks is 0.5 nm (from the fitting parameter uncertainties) which corresponds to an uncertainty in the energy of approximately 3 meV. Carrying this uncertainty through unit conversion yields an uncertainty in the wavenumber of approximately 25 cm^{-1}, indicating that the vibronic levels are approximately the same in each of the polymers to within experimental uncertainty for PF8, PF9 and PF10. The Gaussian fit to the PF8 0-0 band emission is rather poor due to self-absorption cutting out the high energy tail. The PF7 C-C stretching mode is only just significantly below the energy of the other polymers' C-C modes, perhaps suggesting a lesser extent of planarization in this case. This is corroborated by the energy level of the main band emission, which is the highest of the four which form the beta phase.

The PF6 data is included in the table with a single Gaussian fit to the 11K spectrum from figure 5-6a which fits very well to the spectrum shape. The vibrational contributions from the modes within this band cannot be resolved, indicating that the density of states in the polymer has not been narrowed by the presence of the more ordered beta phase, even at 11K. Attempts to fit the peak with two or more Gaussians resulted in a small improvement to the fit of the data but there was no convergence to a consistent fit from multiple starting points.

Table 5-1: Fit parameters of the Gaussian curves in figure 5-9a-d to the 11K emission spectra. Data for PF6 is taken from a fit to the 11K data shown in figure 5-8a. (n.r. = not resolved)

	Main Band			Vibronic Gap 1				Vibronic Gap 2				Vibronic Gap 3			
n	nm	eV	FWHM	nm	eV	cm^{-1}	FWHM	nm	eV	cm^{-1}	FWHM	nm	eV	cm^{-1}	FWHM
6	429.6	2.886	0.055	n.r.	n.r.	n.r.	n.r.	456.7	0.171	1379	0.100	n.r.	n.r.	n.r.	n.r.
7	439.5	2.821	0.053	455.9	0.101	818	0.060	463.2	0.144	1165	0.033	471.3	0.190	1536	0.048
8	444.5	2.790	0.017	459.8	0.093	747	0.028	471.8	0.162	1304	0.030	479.1	0.202	1626	0.018
9	440.5	2.815	0.027	456.1	0.096	774	0.057	467.9	0.165	1331	0.044	475.1	0.205	1653	0.025
10	438.5	2.828	0.031	450.7	0.077	620	0.060	465.6	0.165	1329	0.062	472.7	0.205	1652	0.021

The vibronic sublevels fall into three regions; 700-750 cm^{-1} (low intensity), corresponding to a stretch of the bridging carbon on the fluorene unit, 1250-1350 cm^{-1}, corresponding to a stretching vibration of the C-C bond between fluorene units, and 1600-1650 cm^{-1} which is in the region of the values for a symmetric benzene ring stretching mode (1595-1605 cm^{-1}).[30-31] The weaker mode around 730 cm^{-1} is subject to considerable position uncertainty in the fits, especially in the PF7 and PF10 where there is no definitive feature in the emission to constrain it effectively, and the uncertainty is estimated to be of the order of 20 meV or 160 cm^{-1}.

In PF7 the symmetric benzene ring stretching mode is the dominant vibration, with greater contribution to the photoluminescence spectrum. There is also a secondary contribution from emission from alpha phase regions, seen as a secondary peak in the main band emission at 2.781 eV and its vibronic contribution at 2.583 eV (1597 cm^{-1}). For PF8 the same applies, but the C-C stretch

has a greater relative intensity. In PF9 and PF10 the C-C stretch mode becomes the dominant contributor to the spectra. Looking at the vibronic energy levels, although the differences are mostly lower than the experimental uncertainty, there is a suggestion of a trend toward higher energy for longer side chain polymers. Taken with the trend of changing from aromatic ring-stretch to C-C stretch, this indicates an increase in stiffness of the beta phase conjugation lengths from PF7 to PF10.

5.3.5 Vibrational Modes in PF8 Emission

Further information can be drawn from an examination of the emission spectrum from PF8 at 11K (excitation at 380 nm), shown on a semi-logarithmic scale in figure 5-10. Many small features are observable at low energy, and their origins can be understood in terms of summation of three primary vibrational modes discussed previously. This process accounts for all of the features seen. Similar analysis for the other polymers is not possible due to greater broadening that prevents meaningful fitting of the higher-order modes.

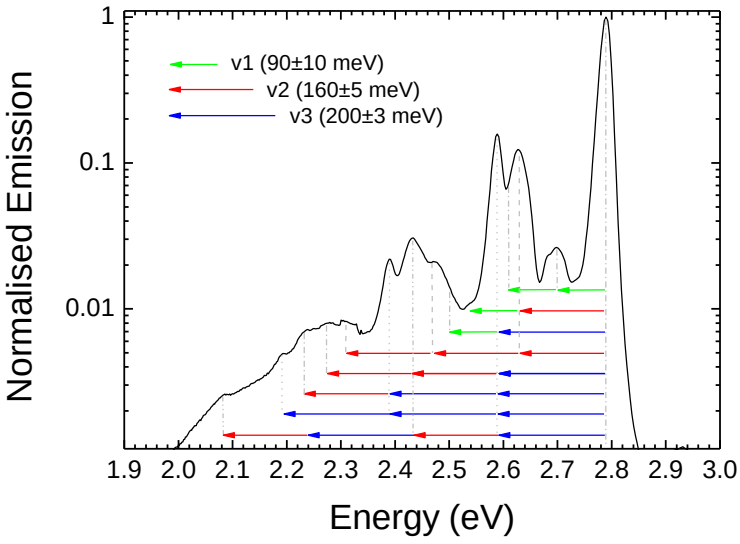

Figure 5-10: Beta phase emission from the PF8 toluene vapour exposed sample in figure 5-9b, on an energy x axis with logarithmic y axis, showing the large number of vibrational modes that can be resolved in the emission. Their origins are marked with arrows denoting overtones of three primary vibrational modes described earlier.

The low-energy mode at 90 meV is clearly comprised of several poorly resolvable smaller peaks, as it is broader than the other peaks and shows evidence of structure, in agreement with Raman spectra which show several vibrational modes around this energy.[31] Given the resolution of the spectrum it will be treated as a single mode, which is weakly coupled to the excited state, shown by the low amplitude of the vibronic replica in the emission and the presence of very few replicas in the lower energy range. Co-operative vibrations with the other modes are weak, indicated by mere suggestions of hidden features at the energies of v1+v2 and v1+v3.

The dominant vibrations at 160 meV and 200 meV are strongly coupled to the excited state, giving rise to clear features at twice and thrice the fundamental modes, as well as all the low-order linear combinations of these modes. The clearest sum mode in the spectra is v2+v3, which also exhibits a clear peak feature at the second replica of the sum. This shows that the v2+v3 mode is the most strongly coupled to the excited state, which supports the use of this mode in the fitting of the absorption spectra in chapter 4.3. The peak intensities show a good Huang-Rhys progression, indicated by the vibronic replicas of the 0-0 transitions of the v2 and v3 modes, which lie on a straight line through their peak intensities up to the second replica, after which the overlap with other summed modes shifts the intensity too high. Huang-Rhys values for the modes are 0.124 and 0.157 for v2 and v3.

5.4 Conclusions

Absorption spectra of thin films of the polyfluorene series show the effect of thermal cycling and toluene vapour exposure of amorphous films both induce the beta phase to form in PF7 to PF10. There is a similar trend in the capability of the polyfluorene group to form the beta phase, with the octyl side chains being the optimal length and a decrease in beta phase formation for longer or shorter side chains. In the case of the PF6 side chains there is once again insufficient energy to planarise the backbone despite the shorter side chains being easier to pack together within the densely packed solid state. The model that assumes solvent-absorption strain causes the

planarization is incomplete since the side chain dependence once again appears as a controlling factor. During toluene vapour exposure, the toluene molecules plasticise the film, reducing the local scale friction coefficient and allowing molecular reorganisation that permits side chain interdigitation. Fitting of the vibrational modes in the low-temperature site-selective emission spectra shows a trend in the coupling to the main vibrational modes; the dominant vibration changes from phenyl breathing (1600 cm^{-1}) to C-C stretch (1300 cm^{-1}) going from n=7 to n=10. Only one mode is resolved in PF6, again supporting the observation that no beta phase is formed in this case. The emission from PF8 is sufficiently well resolved that higher order vibrational modes can be observed on a semi-logarithmic plot.

5.5 References

1. Rubinstein, M.; Colby, R. H., *Polymer Physics*. Oxford University Press: New York, 2003; Vol. 1.
2. Rouse, P. E. *J. Chem. Phys.* **1953,** 21, (7), 1272-1280.
3. Zimm, B. H. *J. Chem. Phys.* **1956,** 24, (2), 269-278.
4. Degennes, P. G. *J. Chem. Phys.* **1971,** 55, (2), 572.
5. Doi, M.; Edwards, S. F. *J. Chem. Soc.-Faraday Trans. Ii* **1978,** 74, 560-570.
6. Doi, M.; Edwards, S. F. *J. Chem. Soc.-Faraday Trans. Ii* **1978,** 74, 918-932.
7. Grell, M.; Bradley, D. D. C.; Ungar, G.; Hill, J.; Whitehead, K. S. *Macromol.* **1999,** 32, 5810-5817.
8. Hintschich, S. I.; Rothe, C.; Sinha, S.; Monkman, A. P.; de Freitas, P. S.; Scherf, U. *J. Chem. Phys.* **2003,** 119, (22), 12017-12022.
9. Scheblykin, I. G.; Yartsev, A.; Pullerits, T.; Gulbinas, V.; Sundstrom, V. *J. Phys. Chem. B* **2007,** 111, (23), 6303-6321.
10. Khan, A. L. T.; Sreearunothai, P.; Herz, L. M.; Banach, M. J.; Kohler, A. *Phys. Rev. B* **2004,** 69, (8), 085201.
11. Rothe, C.; King, S. M.; Dias, F.; Monkman, A. P. *Phys. Rev. B* **2004,** 70, (19), 195213.
12. Dias, F. D.; Morgado, J.; Macanita, A. L.; Costa, F. P.; Burrows, H. D.; Monkman, A. P. *Macromol.* **2006,** 39, 5854-5864.
13. Lu, H. H.; Liu, C. Y.; Chang, C. H.; Chen, S. A. *Adv. Mater.* **2007,** 19, (18), 2574.
14. Ariu, M.; Lidzey, D. G.; Sims, M.; Cadby, A. J.; Lane, P. A.; Bradley, D. D. C. *J. Phys.-Conden. Matt.* **2002,** 14, (42), 9975--9986.
15. Chen, S. H.; Su, A. C.; Chen, S. A. *J. Phys. Chem. B* **2005,** 109, (20), 10067-10072.
16. Hayer, A.; Khan, A. L. T.; Friend, R. H.; Kohler, A. *Phys. Rev. B* **2005,** 71, (24), 241302.
17. Kitts, C. C.; Vanden-Boot, D. A. *Polymer* **2007,** 48, 2322-2330.
18. Khan, A. L. T.; Banach, M. J.; Kohler, A. *Synth. Met.* **2003,** 139, (3), 905-907.
19. Peet, J.; Brocker, E.; Xu, Y. H.; Bazan, G. C. *Adv. Mater.* **2008,** 20, (10), 1882.
20. Shaw, P. E.; Ruseckas, A.; Peet, J.; Bazan, G. C.; Samuel, I. D. W. *Adv. Funct. Mater.* **2010,** 20, (1), 155-161.
21. Bradley, D. D. C.; Grell, M.; Long, X.; Mellor, H.; Grice, A.; Inbasekaran, M.; Woo, E. P., Influence of aggregation on the optical properties of a polyfluorene. In *Optical Probes of*

Conjugated Polymers, Vardeny, Z. V.; Rothberg, L. J., Eds. Spie-Int Soc Optical Engineering: Bellingham, 1997; Vol. 3145, pp 254-259.
22. Cadby, A. J.; Lane, P. A.; Wohlgenannt, M.; An, C.; Vardeny, Z. V.; Bradley, D. D. C. *Synth. Met.* **2000,** 111, 515-518.
23. Da Como, E.; Scheler, E.; Strohriegl, P.; Lupton, J. M.; Feldmann, J. *Appl. Phys. A-Mater. Sci. Process.* **2009,** 95, (1), 61-66.
24. Endo, T.; Kobayashi, T.; Nagase, T.; Naito, H. *Jpn. J. Appl. Phys. Part 2 - Lett. Express Lett.* **2007,** 46, (45-49), L1093-L1095.
25. Caruso, M. E.; Anni, M. *Phys. Rev. B* **2007,** 76, (5), 054207.
26. Knaapila, M.; Dias, F. B.; Garamus, V. M.; Almasy, L.; Torkkeli, M.; Leppanen, K.; Galbrecht, F.; Preis, E.; Burrows, H. D.; Scherf, U.; Monkman, A. P. *Macromol.* **2007,** 26, 9398-9405.
27. Boese, R.; Weiss, H. C.; Blaser, D. *Angew. Chem.-Int. Edit.* **1999,** 38, (7), 988-992.
28. Hintschich, S. I. Picosecond Studies of Excited States in Conjugated Polymers. Durham University, Durham, 2007.
29. Bassler, H.; Schweitzer, B. *Accounts Chem. Res.* **1999,** 32, (2), 173-182.
30. Ariu, M.; Lidzey, D. G.; Bradley, D. D. C. *Synth. Met.* **2000,** 111, 607-610.
31. Ariu, M.; Sims, M.; Rahn, M. D.; Hill, J.; Fox, A. M.; Lidzey, D. G.; Oda, M.; Cabanillas-Gonzalez, J.; Bradley, D. D. C. *Phys. Rev. B* **2003,** 67, (19), 195333.

6 The Interaction between the Beta Phase and Keto Defects in Thin Films of PF8

6.1 Introduction

Having investigated the formation of beta phase in films of the polymers PF6 to PF10, the next chapter will investigate the interplay between the beta phase in PF8 and the keto defect. A review of the nature of the keto defect is given, and then results will be presented to show the effects of the keto defect on the emission spectrum at different concentrations of keto incorporated into the PF8 as a random co-monomer. The effect of inducing the beta phase in these polymer films is then examined through steady-state spectra and time-resolved spectra.

The spectral shifts for PF8 keto films that occur with changes in keto concentration and as a function of temperature will demonstrate that the energy transfer to the keto defect occurs by exciton migration, and that at low temperature this migration can be reduced to recover the emission of the PF8. Time resolved studies show the energy transfer taking place to the beta phase chains and to the keto sites, and for samples containing beta phase the excitons proceed to the keto sites via the beta phase regions by migration, which is consistent with beta phase domains rather than isolated chains, as would be expected for a side-chain driven beta phase formation mechanism.

6.1.1 The keto Defect

The keto defect is a point on the polymer chain where a fluorene unit has become oxidised, and the two alkyl chains bonded to the fluorene unit at the 9 position are replaced by an oxygen atom with a double bond to the carbon at the 9 position, forming fluorenone.[1] This keto unit is polar as a result of the highly electronegative oxygen atom, and as such it alters the nature of the associated conjugated region, and the emission spectrum is significantly changed.[2-6] The keto defect emits in a broad energy band with a peak near 530nm, so a small fraction of keto defects act as low-energy traps and can quench the polyfluorene fluorescence and change the emission from deep blue to

green-yellow. This is a major degradation pathway in the operation of PF8-based PLEDs,[3-4] as well as Poly(phenylene vinylene) based polymers.[7]

The beta phase of PF8 also acts as a low-energy trap, and so it may be expected that there will be a competition between the beta phase and the keto defect for the excitons that are created within the bulk alpha-phase material.

6.2 Results

6.2.1 Beta Phase Formation in PF8-Keto Copolymers

The first experiments are concerned with the examination of the formation of the beta phase in PF8-keto copolymer films. Toluene vapour exposure (see section 5.4) was used to induce different fractions of beta phase in the copolymer series containing 0.05%, 0.1%, 0.2%, 0.5%, 1% and 2% keto concentration. It was found that for all concentrations of the keto defect up to 2% (the highest concentration incorporated) the toluene vapour method successfully induced beta phase to a similar magnitude as it produced in the pure PF8 homopolymer (see chapter 7 for further investigations into the effect of the copolymer content on the maximum beta phase fraction).

A plot of beta phase fraction with toluene vapour exposure time is given in figure 6-1 for the 0.1% polymer. The figure shows similar results to the data in figure 5-4a in chapter 5, with a rapid increase in beta phase fraction after only seconds of exposure. The saturation level (of about 5%) is reached after only 5 minutes, in agreement with recent experiments by Caruso and Anni.[8] There is considerable variability in the data, which is attributed to variations in the vapour density flowing past the film surface during solvent exposure, and sample to sample differences in microscopic morphology in the as-spun films. This method therefore gives only an approximate level of control over the level of beta phase formed within the sample. However, there is a noticeably slower rate of toluene vapour uptake; there appears to be qualitatively more of a build-in time in this case, (the

data in figure 5-4a shows almost a step function) perhaps indicating that the keto monomers are reducing the propensity of the film to absorb the toluene molecules.

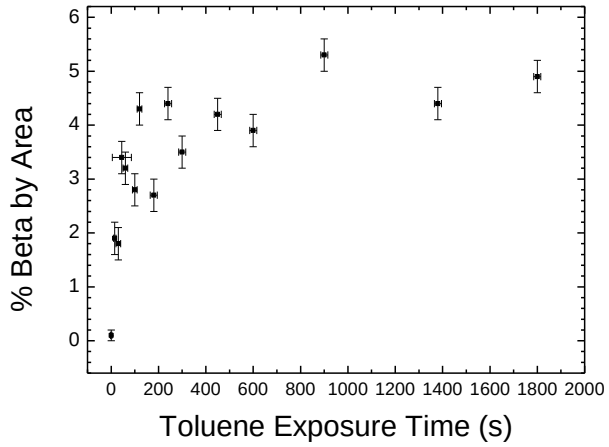

Figure 6-1: The fraction of beta phase induced in PF8-keto (0.1%) by different toluene vapour exposure times. Beta phase fractions are calculated by the fraction of the beta phase peak using multiple Gaussian curves to the absorption spectrum.

6.2.2 Optical Spectra of Alpha and Beta Phase Films

The first step is to consider the spectra of the film before and after beta phase formation, before examining changes as a function of keto defect content. The optical spectra for a PF8 0.1% keto film are given in figures 6-2a and b. Figure 6.2a shows the absorption and emission of the same film before and after exposure to toluene vapour for 20 minutes, whilst 6.2b directly compares the emission spectra before and after.

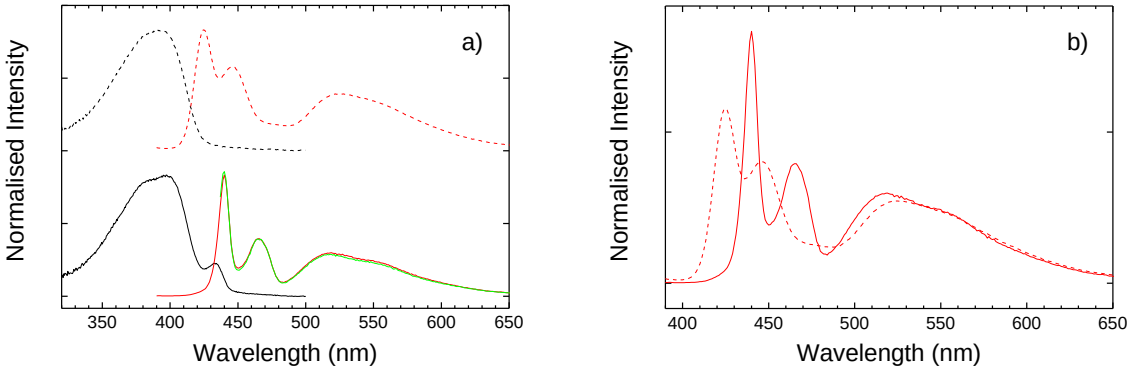

Figure 6-2: (a) absorption (black), emission excited at 380 nm (red) and 434 nm (green) of a PF8 0.1% film before (dashed line) and after toluene vapour exposure (solid line). The spectra are offset for clarity. (b) The emission spectra of the same film before and after toluene vapour exposure, normalised to the first vibronic replica.

It is clear that the absorption spectrum is unaffected by the presence of only 0.1 % keto monomers (figure 6-2a, black dashed line), as it is the same as seen for the PF8 film absorption spectra in chapter 5. The keto state in the copolymer absorbs at around 450 nm and is only observed at higher concentrations of around 25%.[1, 9-10] The exposure to toluene vapour causes the normal shift in the absorption spectrum that accompanies formation of the beta phase. In the emission spectra, however, stark changes are immediately apparent from the normal PF8 emission seen in the previous chapters. The emission is now dominated by a broad emission band around 530 nm, changing the colour of the sample emission from blue to green-white. As is the case for the beta phase, the energy transfer is apparently efficient given the scale of the spectral change produced by only one part in 1000 of keto monomers. However, it can also be seen that the intensity of the polyfluorene emission is greater for the sample containing the beta phase, possibly indicating a level of competition between the two energy traps for the excitons.

The data also show that in the beta phase sample, the majority of the energy transfer is occurring from the beta phase to the keto sites rather than directly from the alpha phase to the keto sites. This is supported by the spectrum produced by selective excitation of the beta phase chromophores

where the relative fraction of keto emission is the same as for excitation on the alpha phase (see later figure 6-6).

It is interesting to observe that the emission from the keto sites where beta phase is present (figure 6-2b) is significantly different from the emission measured from samples containing no beta phase. The smooth, broad band has now developed structure, indicating a more ordered system. Similar ordering of the keto emission has been observed for a system of copolymers with up to 25% keto with 9,9'-difarnesyl-fluorene in thin films at low temperature,[10] where the beta phase is prevented from forming in the polyfluorene due to side chain branching.[11] This structured emission is expected since the induction of the beta phase leads to a more planar arrangement of the polymer backbones,[12] with a far narrower density of states, and the on-chain keto defects will also be similarly affected. The structured emission is clearer for a sample of PF8 keto 0.5%, shown in figure 6-3 on an energy axis, allowing spectral deconvolution.

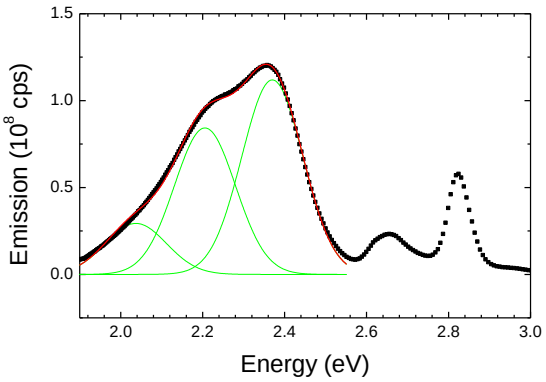

Figure 6-3: A three-Gaussian peak fit to keto emission of 0.5% keto with 5% beta phase at 290K

The keto emission is fitted with three Gaussian curves on the energy axis with the same FWHM of 149 meV, indicating a broad density of states, as expected for a charge-transfer emissive state.[20] The peak centres are at 1290 cm^{-1} and 2500 cm^{-1} and indicate that the two vibronic replicas are the v=1 and v=2 levels of the same dominant vibration mode with an energy of approximately 1290 cm^{-1}.

Interestingly, this does not correspond to the infrared absorption of the C=O bond of the fluorenone molecule (which would be expected in the region of 1700 cm^{-1}) but it is near to the 1300 cm^{-1} C-C inter-monomer stretch vibronic seen in PF8 and PF10.[13]

6.2.3 Emission Spectra with Changes in keto Content

The steady state photoluminescence spectra for the alpha-phase samples with varying keto concentrations are shown in figure 6-4, with the spectra normalised to the intensity of the keto emission peak around 540 nm. It can clearly be seen that the emission from the PF8 is reduced by the increasing keto concentration; for 0.05% keto content the keto emission intensity is only one third of that of the PF8, but at 2% keto content the PF8 emission is almost entirely quenched, at only 10% of the intensity of the keto emission. These spectra are similar to the spectra published by Hintschich et al. investigating alpha phase films of PF8 with keto,[3] and other data from Zojer et al. using poly(9,9'-difarnesyl-fluorene) with keto.[4] It can also be seen that the keto peak becomes red-shifted as the keto concentration increases. This is due to a drop in the PF8 (0-2) and (0-3) vibronic transitions that overlap with the keto emission at around 500 nm.

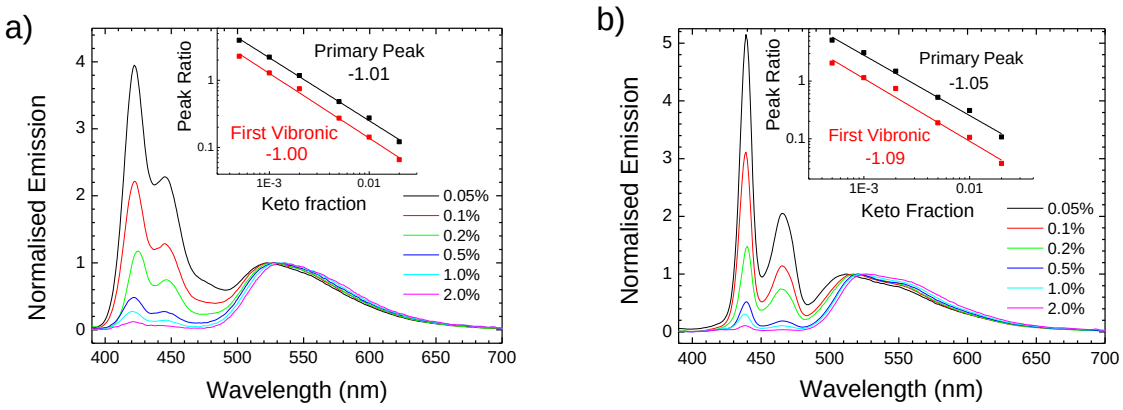

Figure 6-4: a) Steady state emission spectra excited at 380 nm of PF8 samples in the alpha phase with keto (fractions labelled) normalised to the peak of the keto emission band at around 540 nm. Inset: the ratio of the PF8 emission peak intensity to that of the keto (black) and the same ratio for the first vibronic (red) on a log-log scale with the keto fractions, and the best fits. b) the corresponding samples in the beta phase.

The inset shows the ratio of the PF8 emission peak intensity to that of the keto on a log-log scale with the keto fraction, with a power-law best fit to the data labelled with the gradient, using a fit weighting of y^{-2}. The data exhibits simple power-law dependence with a slope of almost precisely -1 to the keto concentration on the log-log scale for the main emission peak and the first vibronic peak intensity at 448 nm, although the uncertainty is of the order of 0.3. Significantly, the plots for the emission peak ratios for the beta phase samples give the same slope.

There are no significant differences in the fits to the (0-0) transitions or the (0-1) transitions, except for the smaller coefficient due to the lower intensity of the emission at the first vibronic replica. The alpha phase samples and the beta phase samples are quite similar; the main beta phase emission peak is larger than that of the alpha phase peak, resulting in a larger *a* coefficient, but the uncertainty on these coefficients is too large to draw further conclusions.

To further analyse the behaviour of the emission as a function of concentration, the keto-keto separation must be known. The distribution of the keto monomers is random within the polymer chains and therefore the distribution within the 3 dimensional film volume is also random, and so the mean separation can be approximated simply after making several assumptions. Firstly, the film will be modelled as a matrix of cubic volumes with side length r_k (the length of the keto unit) each of which may contain a monomer of F8 or keto (the keto units and the F8 units are assumed to be the same size). Since the concentrations of keto used in this work are low, keto-keto dipole interactions are neglected. All the cubes making up the bulk film are assumed to be occupied, although the constraining nature of the polymer chains in the real film will create vacant sites, but this effect is assumed to be insignificant for this simple level of model.

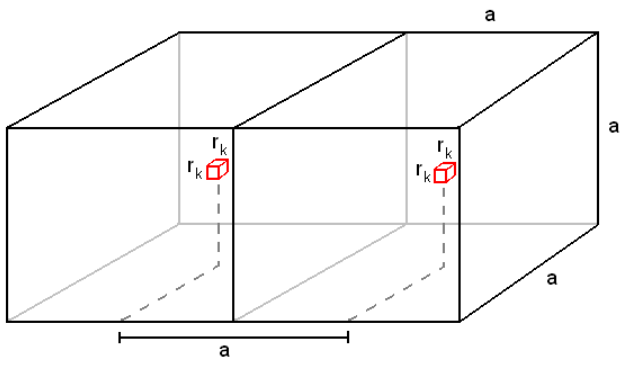

Figure 6-5: a simplified model to approximate the average separation between keto units for a given concentration. keto units (red cubes) are assumed to be distributed, on average, at the centres of cubes of polyfluorene units of side length *a*, and separated by an average distance *a*.

For a film of 0.1% concentration, there is one keto unit per 1000 total monomer units. The cube formed by this assembly of 1000 units is shown in figure 6-5, where $a=10 \cdot r_k$. If each keto unit is *on average* in the centre of such a cube, then the separation between keto units is the same as the side length, a, of this cube. For any given percentage concentration n_k, the side length is r_k multiplied by the the cube root of the number of units making up the cube in which one keto unit resides, giving the relation to the average distance between sites:

$$a = r_k \left(\frac{100}{n_k}\right)^{1/3} \qquad (6\text{-}1)$$

For concentrations of 0.05 % to 2 % this gives average separation between keto sites of between 10.5 nm and 3.1 nm respectively for r_k=0.83 nm, the width of the fluorene monomer along the backbone direction. For a real film where there are some vacant cube sites the average separation will be slightly underestimated. The keto unit separation at the lower concentrations (0.05% and 0.1%) is significantly greater than the range of values for the Förster radius for energy transfer from the alpha phase to the beta phase of polyfluorene, which has been estimated at 3 nm by simulation,[14] and measured to be 5.4 nm[15] and 8.2 nm.[16] The difficulty in estimating the precise beta phase content, and the inability to create a pure beta-phase film, have made it difficult to measure this accurately and these figures are all subject to considerable uncertainty.

This relation equates the -1 gradient of the graph fit with respect to keto concentration (figure 6-4 insets) to a -3 dependence of the beta-keto emission ratio on the mean separation between chromophores. This is entirely different to the -6 slope (on double-logarithmic axes) against chromophore separation that would be expected for a system where Förster transfer is the dominant process (including the line-dipole approximation)[15, 17] and so the data is more suggestive of 3-dimensional migration through the film.

If the quenching of the fluorescence from the polyfluorene is due to migration of the excitons to the keto sites, then there should be a clear change in the steady-state photoluminescence upon cooling to low temperature, since thermally assisted migration will be greatly reduced.

6.2.4 Temperature Dependent Emission Spectra

By measuring the emission spectra as a function of temperature, the nature of the energy transfer from the alpha phase to the beta phase and the keto defect may be better understood. Films of PF8 with different concentrations of keto were exposed to toluene vapour to saturate them with beta phase (all samples containing in the region of 6%) and their photoluminescence spectra were recorded at several temperatures down to 11K, the minimum available. Similar overall effects were observed in each case; a representative example is given in figure 6-6 for a film with 0.5% keto which best highlights these changes.

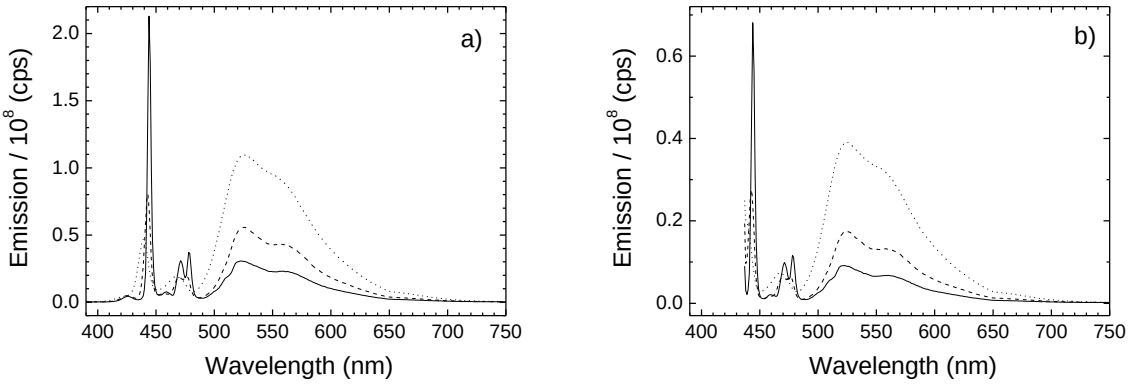

Figure 6-6: Steady-state emission spectra of 0.5% keto sample with saturated beta phase excited at 380 nm (a) and 434 nm (b), collected at 290K (dotted line) 100K (dash line) and 11K (solid line).

The data in figure 6-6 show the raw emission spectra as a function of temperature, with excitation on the alpha phase (a) and beta phase (b). The sample has 7% beta phase content by area of the absorption spectrum, induced by toluene vapour exposure. The raw spectra show that the intensity of the emission peak around 441 nm (v=0) increases as the temperature drops, with the result that the emission intensity at 11K is 3.5 times larger than at 290K. Note that emission spectra as a function of temperature for alpha phase samples containing keto are not possible, as a significant fraction of beta phase is induced upon cooling the sample, and the spectra at the different temperatures would not be comparable.

Correspondingly, the spectra over the range 500 to 600 nm show a clear and large drop in the emission from the keto. The keto emission is not prevented entirely, so not all of the emission at 540 nm is dependent upon migration. The spectra are identical whether excited at the alpha phase absorption peak (380 nm, figure 6-4a) or the beta phase absorption peak (434 nm, figure 6-4b), except that the intensity when excited on the beta phase is lower due to the lower optical density of this absorption peak. Therefore the following scheme is proposed for the transfer of excitons through the system in a film of PF8 containing beta phase and keto (Figure 6-7).

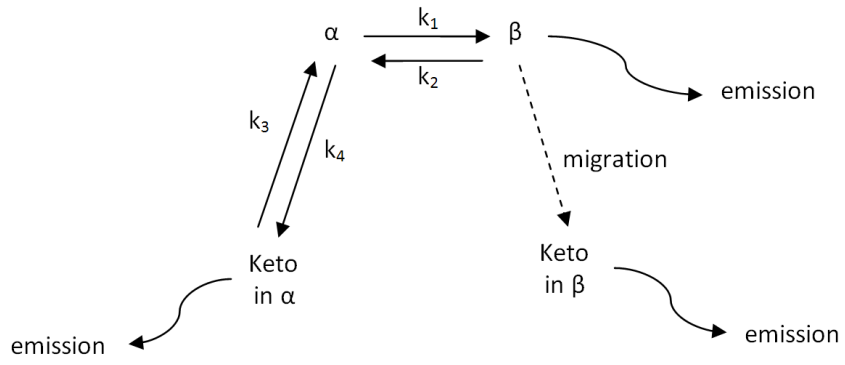

Figure 6-7: Scheme of exciton transfer processes in a film of PF8 containing both beta phase and keto. Energy level differences make the rate constants k_2 and k_3 extremely small with relation to k_1 and k_4. Note that migration is also included in k_1 and k_4.

The near-identical emission spectra from the PF8 keto 0.5% sample containing 7% beta phase in figure 2 show that k1 >> k4. This is unsurprising given the exceptional energy transfer efficiency from the alpha phase to the beta phase in PF8. If the counter example is considered where k1 < k4, then the emission spectrum for excitation on the alpha phase would show a relatively lower emission peak from the beta phase and a larger emission peak from the keto, since a smaller fraction of excitons would reach the beta phase regions to produce emission at 440 nm, and the excitons transferring to the keto in the alpha phase would not lose a fraction of their number to beta phase emission.

The energy transfer from the beta phase to the keto is clearly illustrated in figure 6-8, where 434 nm laser light is shown exciting a sample of PF8-keto 0.5% which has been vapour treated to induce beta phase formation, showing the yellow keto emission resulting from energy transfer from the beta phase to the keto. A blue tint is seen from the scattered excitation laser.

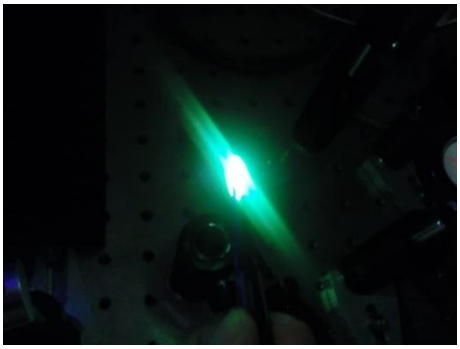

Figure 6-8: Laser excitation at 434nm of a PF8-keto 0.5% sample with 7% beta phase demonstrating energy transfer to the yellow-green keto sites. Note that the blue laser scatter is also visible.

The temperature dependent spectra observed for a sample containing 0.1% keto with saturated beta phase (figure 6-9) shows that the keto emission is reduced to below the measurement noise level at 11K, indicating that the emission from the keto states is limited by migration; the low concentration of keto defects necessitates migration in order for a significant rate of energy transfer to take place. By 0.5% keto concentration, there is enough keto present to make direct energy transfer contribute to the emission. In the 0.1% keto film there is also significant recovery of emission from the alpha phase seen as a resolved peak at 426 nm. This shows for a film containing 0.1% keto that there are a significant fraction of beta phase chromophores that are reached by migration through the alpha phase bulk at 7% beta phase concentration, and similarly that there are also a significant fraction keto sites reached only by migration though the alpha phase. When the temperature is reduced, thermally assisted exciton migration to either the beta phase or keto is reduced, and more emission occurs instead from alpha phase chromophores.

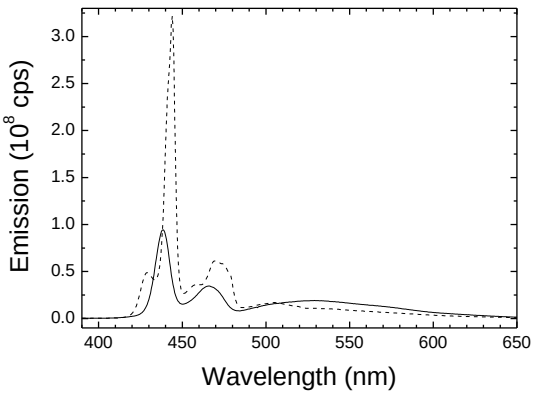

Figure 6-9: Emission spectra of PF8-keto 0.1% with 5% beta phase at 290K (solid line) and 11K (dashed line) using 380 nm excitation, showing the elimination of the keto emission and the recovery of both the beta phase emission and some alpha phase emission at 427 nm at low temperature.

6.2.5 Time Resolved Photoluminescence

The movement of excitons through the film to the keto sites via migration has been shown in the previous section, but this can be confirmed by observing the fluorescence decay from the films at different keto concentrations and as a function of temperature. Films of PF8 keto with 0%, 0.5% and 2% keto concentration were spun in the alpha phase state, with comparison samples saturated with beta phase using toluene vapour for 20 minutes. The Time-Correlated Single Photon Counting (TCSPC) method was used to measure the fluorescence intensity at several wavelengths across the emission spectrum with a bandpass window of approximately 5 nm. The exponential fluorescence lifetime components were deconvolved using GLOBALS software to model the decays.

For simple initial comparisons, the average lifetime was calculated.

$$\tau_{av} = \sum_i f_i \tau_i \qquad (6\text{-}2)$$

Where

$$f_i = \frac{a_i \tau_i}{\sum_j a_j \tau_j} \qquad (6\text{-}3)$$

The results as a function of keto concentration are shown in figure 6-10.

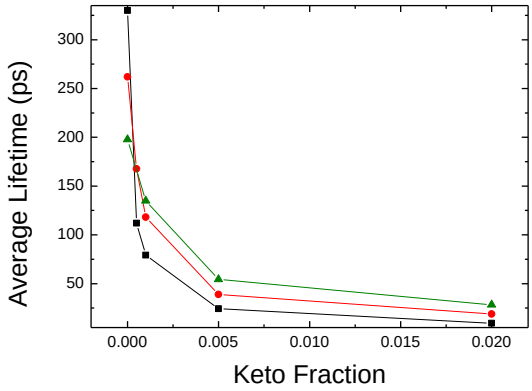

Figure 6-10: Average lifetimes fitted to TCSPC measurements as a function of keto concentration for alpha phase films excited at 390nm and measured at 425nm at 290K (black squares) and beta phase films excited at 434nm and measured at 442nm at 290K (red circles) and 77K (green triangles).

The overall trend shows strong quenching of the PF8 lifetime by the presence of the keto defect – a concentration of just 0.1% keto leads to an average lifetime drop of approximately 50%, which correlates with the significant changes in the emission spectra in figure 1 for even the 0.05% keto polymer. It is also clear that the direct energy transfer seen in the steady state spectra from the beta phase to the keto sites is confirmed again here. For the case of beta phase films excited at 434 nm, the data collected at 290K is compared with samples measured at 77K. There is a significant reduction in the lifetime quenching provided by the keto defect. At room temperature the average lifetime drops from 262 ps (no keto) to 9 ps (2% keto), whilst at 77K the drop is less severe; from 198 ps to 19 ps, again confirming the importance of migration in the energy transfer to the keto sites.

Given that the keto monomer is incorporated randomly within the polymer chains and the keto emission shows evidence of increased ordering, and that all the samples formed a similar fraction of beta phase upon toluene vapour exposure (beta phase can be formed with up to 20% co-monomer

content, see chapter 7), we can assume that the beta phase domains will contain the same concentration of keto sites as the alpha phase. Therefore, differences in the quenching of the PF8 emission by the keto are controlled by the differences in migration hopping rates to the keto sites within the alpha and beta phases of PF8. It may be expected that the narrower density of states within the beta phase (30 meV by a Gaussian fit to the beta phase emission spectrum) compared to the alpha phase (130 meV) would restrict the mobility of the excitons by reducing the number of downward energy sites available to hop to. The ratio of the 290K average lifetimes τ_β/τ_α at 0.05%, 0.1% and 0.5% keto concentrations gives a consistent fraction of 1.5, indicating that the mobility of the alpha phase excitons is 50% higher than those in the beta phase.

The individual lifetime components for a 0.1% keto sample with 7% beta phase are given as a function of temperature, excited at both 390 nm (table 6-1) and 434nm (table 6-2). The emission dynamics of the keto state are presented for a collection window at 565 nm, which is considerably to the right of the peak in the keto emission. This is the case because there is still significant overlap with the PF8 emission at the peak near 530-540 nm. Measurements at these wavelengths show a build-in of the beta phase fluorescence components lifetime at lower temperatures, which masks any build-in components in the keto states. Even at 565 nm, there is still a clear emergence of minor lifetime components at lower temperatures from the red tail of the beta phase emission of the order of 250-350 ps.

Table 6-1: Lifetime components from deconvolution of the emission from PF8-keto 0.1% with excitation at 390nm. Amplitudes are in parentheses, and lifetimes are in bold.

Component	290K			150K			77K		
ps	425nm	440nm	565nm	425nm	440nm	565nm	425nm	440nm	565nm
(a1) **t1**	(53) **9**	(-5.4) **6**	(-0.9) **7**	(43) **9**	(-11) **3**	(-1.2) **6**	(40) **9**	(5.3) **20**	(-1.8) **5**
(a2) **t2**	(7.3) **35**	(6.5) **67**	(0.1) **41**	(13) **31**	(7.1) **54**	(0.3) **71**	(13) **32**	(4.9) **62**	(0.5) **87**
(a3) **t3**	(1.5) **152**	(4.5)	(0.1)	(1.1)	(5.0)	(0.2)	(1.2)	(3.8)	(0.2)
		130	**361**	**176**	**129**	**297**	**172**	**153**	**480**
(a4) **t4**			(0.5)			(0.5)			(0.5)
			4245			**3950**			**3630**
Chi^2	1.56	1.19	0.98	1.50	1.23	1.03	1.33	1.17	1.06

Table 6-2: Lifetime components from deconvolution of the emission from PF8-keto 0.1% with excitation at 434nm.

Component	290K		150K		77K	
ps	442nm	565nm	442nm	565nm	442nm	565nm
(a1) **t1**	(6.4) **57**	(-0.2) **3**	(3.4) **56**	(-0.3) **6**	(4.5) **38**	--
(a2) **t2**	(5.4)	--	(6.3)	(0.2) **66**	(5.3)	(0.5) **82**
	116		**127**		**155**	
(a3) **t3**		--	(0.03)	(0.1)		(0.4)
			274	**252**		**232**
(a4) **t4**		(0.5)		(0.5)		(0.5)
		4530		**4240**		**3680**
Chi^2	1.23	1.50	1.19	1.04	1.46	1.04

The strong scatter from the cryostat windows impairs the quality of the fits somewhat, especially where all the lifetime components are short, resulting in reduced chi-squared values of up to 1.56. The uncertainty is estimated at 5ps for the fast lifetime components and approximately 10% for the other components, based on sample-to-sample variations which are larger than the fitting uncertainty, which is of the order of 2 ps for the mid-range (200 ps) components. It should also be noted that the build-in lifetime components are only just within the resolution of the deconvolution, both in terms of the lifetime magnitude and its relative contribution to the fluorescence. However, they are consistently found by the deconvolution software from several different sets of initial

parameters, and the build-ins are a reasonable match to the fastest lifetime component from the fluorescence at the alpha phase peak. This build-in component ceases to make a sufficiently large contribution to the emission to be resolved at 77K, in agreement with the reduction of the keto emission seen in the spectrum at low temperature in figure 6-9. This indicates exciton migration from the alpha phase emission to the beta phase and from the beta phase to the keto being impeded through a reduction in thermally assisted hopping, since the fast decay and build-ins are of the expected time scale. This is further confirmed when viewed in conjunction with the evidence from the steady-state spectra.

It is difficult to definitively assign origins to all the lifetime components seen in the data. Fast lifetime components in the region of 50 ps are attributed to the quenched emission from the beta phase PF8 chains within sufficient proximity to transfer energy by migration. Components at 130 ps are seen in nominally pure PF8 reference films in the beta phase when excited at 390 nm, which contribute significantly to the steady state fluorescence (up to 30%), and are tenuously attributed to slight quenching of the emission due to undetectably low concentrations of keto. It may be expected that a distribution of lifetime fits using the Maximum Entropy Method might yield a distribution of lifetimes corresponding to chromophores in a range of different nanoscale environments.[18] The components at 250-300 ps are confidently assigned to the beta phase fluorescence lifetime as this is the sole component for the fluorescence of pure PF8 saturated beta phase reference films excited at 434 nm.

Studies of 0.5% and 2% keto films show similar patterns, but the higher quenching leads to fast mono-exponential decays of the 425 nm and 440 nm emission at room temperature, whilst the keto lifetimes are dominated by single components of the order of 4000 ps. Upon cooling, there is again a slight recovery of longer lifetime components in the region of 150-250 ps for 0.5% keto films, but at 2% keto concentration the majority of beta phase chromophores are within direct energy transfer range of a keto site and few changes occur.

The existence of lifetime components indicating migration in beta phase samples excited directly at 434 nm is an indication of domains of beta phase present in the film. The beta phase singlet level is 90 meV below that of the alpha phase, which localises the excitons to beta phase chromophores once they have transferred across, since thermally assisted hopping is limited to upwards steps of K_BT (25 meV). Therefore, excitons excited directly on the beta phase cannot migrate except to other beta phase chromophores or the even lower energy keto chromophore, which must be in close proximity in order to allow exciton to transfer. This requires that the beta phase chains be located within domains or the migration-mediated energy transfer would not be observed. This is in agreement with confocal microscopy measurements by Caruso et al.[8] and Anni et al.[19] which showed beta phase emission from specific domains within the film. The structure of the beta phase aggregates in MCH solution have been studied by X-ray scattering,[20] indicating that sheet-like domains are built up during the aggregation process. These results, in conjunction with the data in chapter 4 which show that the beta phase is mediated by side-chain interactions, all correspond to beta phase domains rather than isolated chains.

The finding that the energy transfer from the alpha phase to the beta phase is highly efficient in all the concentrations studied suggests there is an upper limit on the possible size of the beta phase domains (through which migration to the keto then takes place). The majority of the alpha phase bulk material can be no further from a beta phase domain than the sum of the exciton diffusion length plus the Förster radius, so the beta phase must be occurring as many small domains (tens of nanometres) rather than several very large domains.

6.3 Conclusions

Photoluminescence spectra of pure PF8 films and films of PF8-keto copolymers with varied keto concentrations show that: the polyfluorene emission intensity is higher when the beta phase is formed, and excitons created in the alpha phase regions transfer rapidly to the beta phase and are then localised on the beta phase chromophores. Energy transfer from beta phase to the keto defect at concentrations of less than 2% (which is sufficient to quench the PF8 emission almost entirely) primarily occurs via migration. This is supported by a -1 slope of the emission ratio with keto concentration on a double-logarithmic scale, the reduction of keto emission in steady-state photoluminescence at 77K, and freezing out of lifetime quenching in TCSPC measurements at 77K.

Energy transfer takes place directly from beta phase to keto when excited at 434 nm. This process is still migration dependent and is reduced at low temperature, and is the result of keto sites dispersed within the beta phase domains. This is further supported by the clearly vibrationally resolved keto emission indicative of keto defects within well ordered regions. Migration from the beta phase chromophores to keto sites within the alpha phase bulk is not energetically possible, and for evenly dispersed beta phase chains there would be no migration observed as either fast energy transfer would occur directly to the keto or no transfer would take place. This indicates that the beta phase occurs in aggregated regions rather that dispersed chains, as expected for the process driven by side-chain interactions.[13, 21]

6.4 References

1. List, E. J. W.; Guentner, R.; de Freitas, P. S.; Scherf, U. *Adv. Mater.* **2002,** 14, (5), 374-378.
2. Scherf, U.; List, E. J. W. *Adv. Mater.* **2002,** 14, (7), 477.
3. Hintschich, S. I.; Rothe, C.; Sinha, S.; Monkman, A. P.; de Freitas, P. S.; Scherf, U. *J. Chem. Phys.* **2003,** 119, (22), 12017-12022.
4. Zojer, E.; Pogantsch, A.; Hennebicq, E.; Beljonne, D.; Bredas, J. L.; de Freitas, P. S.; Scherf, U.; List, E. J. W. *J. Chem.Phys.* **2002,** 117, (14), 6794-6802.
5. Chan, K. L.; Sims, M.; Pascu, S. I.; Ariu, M.; Holmes, A. B.; Bradley, D. D. C. *Adv. Funct. Mater.* **2009,** 19, (13), 2147-2154.
6. Lupton, J. M.; Craig, M. R.; Meijer, E. W. *Appl. Phys. Lett.* **2002,** 80, (24), 4489-4491.
7. Yan, M.; Rothberg, L. J.; Papadimitrakopoulos, F.; Galvin, M. E.; Miller, T. M. *Phys. Rev. Lett.* **1994,** 73, (5), 744-747.
8. Caruso, M. E.; Anni, M. *Phys. Rev. B* **2007,** 76, (5), 054207.
9. Dias, F. B.; Maiti, M.; Hintschich, S. I.; Monkman, A. P. *J. Chem.Phys.* **2005,** 122, (5), 054904.
10. Romaner, L.; Pogantsch, A.; de Freitas, P. S.; Scherf, U.; Gaal, M.; Zojer, E.; List, E. J. W. *Adv. Funct. Mater.***2003,** 13, (8), 597-601.
11. Knaapila, M.; Garamus, V. M.; Dias, F. B.; Almasy, L.; Galbrecht, F.; Charas, A.; Morgado, J.; Burrows, H. D.; Scherf, U.; Monkman, A. P. *Macromol.* **2006,** 39, (19), 6505-6512.
12. Chunwaschirasiri, W.; Tanto, B.; Huber, D. L.; Winokur, M. J. *Phys.Rev. Lett.* **2005,** 94, (10), 107402.
13. Bright, D. W.; Galbrecht, F.; Scherf, U.; Monkman, A. *Macromol.* **2010,** 43, (18), 7860-7863.
14. Meskers, S. C. J.; Hubner, J.; Oestreich, M.; Bassler, H. *J. Phys. Chem. B* **2001,** 105, (38), 9139-9149.
15. Shaw, P. E.; Ruseckas, A.; Peet, J.; Bazan, G. C.; Samuel, I. D. W. *Adv. Funct. Mater.* **2010,** 20, (1), 155-161.
16. Khan, A. L. T.; Sreearunothai, P.; Herz, L. M.; Banach, M. J.; Kohler, A. *Phys.Rev. B* **2004,** 69, (8), 085201.
17. Beenken, W. J. D.; Pullerits, T. *J. Chem. Phys.* **2004,** 120, (5), 2490-2495.
18. Alcala, J. R.; Gratton, E.; Prendergast, F. G. *Biophys. J.* **1987,** 51, (4), 597-604.
19. Anni, M.; Caruso, M. E.; Lattante, S. *J. Phys. Chem. C* **2008,** 112, (8), 2958-2963.
20. Knaapila, M.; Dias, F. B.; Garamus, V. M.; Almasy, L.; Torkkeli, M.; Leppanen, K.; Galbrecht, F.; Preis, E.; Burrows, H. D.; Scherf, U.; Monkman, A. P. *Macromol.* **2007,** 26, 9398 -9405.
21. Bright, D. W.; Dias, F. B.; Galbrecht, F.; Scherf, U.; Monkman, A. P. *Adv. Funct. Mater.* **2009,** 19, (1), 67-73.

7 The Beta Phase Formation Limit in Poly(9,9-dioctylfluorene) Copolymers

7.1 Introduction

It has been shown in chapter 6 that the beta phase can be formed in PF8-Keto copolymers in thin film with 2% co-monomer content. Increasingly PF8 is being used as a unit for copolymerising with a variety of other monomer units to enhance the charge-transport properties for more efficient devices, or to adjust the emission colour.[1] It is also used for more fundamental studies such as the study of charge-transfer states.[2] It is currently used as a solubilising blue light-emitting monomer unit as part of a single-polymer white-light emitting diode.[3-4] It is therefore of interest to understand the limits at which the beta phase can occur, since the presence of the beta phase has been used as an advantage to produce more efficient LEDs.[4-6] This chapter will investigate the formation of the beta phase via the solvent vapour method in two different series of copolymers to show the limit at which the beta phase can be formed, finding the result that there is a linear decrease in the beta phase fraction as the number of F8 side chains are reduced. A statistical model of the dibenzothiophene (DBT) units in the polymer chains is used with the measured beta phase cut-off limit of 20% DBT content to estimate a beta phase conjugation length of 9±1 monomer units. Further investigations of a charge-transfer type copolymer appear to show a lower limit of 12%, but the precise limit is masked by the build-in of new spectral features.

7.2 Previous Studies of Related PF8 Copolymers

The incorporation of dibenzothiophene-S,S-dioxide (here referred to as S unit) as a co-monomer in oligo-/polyfluorene backbones (figure 7-1) is a system currently under investigation for creating systems which show high luminescence efficiency and increased electron-accepting properties.[7-8] The copolymer system of PF8 with S unit has also shown promise as a system for producing white light.[2] The emission spectrum from short alternating oligomers is dependent upon solvent polarity, and in a polar solvent an intramolecular charge-transfer state is stabilised by solvent interactions. In this case, the emission consists of a broad featureless band centred on 460 nm.[9] Studies on the random copolymers of this system found that a similar charge-transfer state is formed in thin films of this polymer, with the same broad emission band observed for 30% S-unit content.[10] It was concluded that the dipole-dipole interactions with neighbouring molecules led to molecular rearrangement that stabilised the charge-transfer state. Further work found that the S-unit incorporated into the chain produced improved electroluminescent device efficiency relative to PF8 alone due to modification of the charge transport properties, and near-white light was produced.[11]

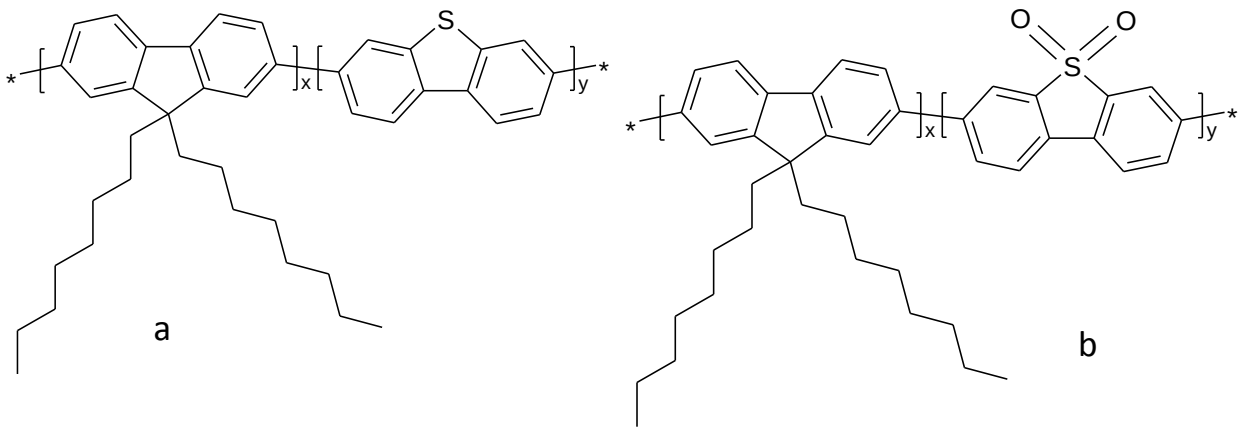

Figure 7-1:Molecular structure of the two copolymers of PF8 with a) dibenzothiophene (DBT) and b) dibenzothiophene-S,S-dioxide (S unit) used in this work.

In another study of PF8 copolymers, it has been suggested from x-ray studies that in the case of solutions in poor solvents that for the copolymer of PF8 with poly(9,9-bis(2-ethylhexyl)fluorene)

(PF2/6) the beta phase is inhibited once the co-monomer content reaches 10%.[12] Work by Knaapila et al. observed that 5% and 10% PF2/6 copolymers formed a viscous gel in the same manner as pure PF8 upon aggregation after a cooling-heating cycle, whilst a 50% copolymer remained as a transparent liquid, indicating that the beta phase transition did not occur. However, this is not a result that was highlighted in that study, and there are often strong differences in the behaviour between polymers in solution and the solid state. This work demonstrates the result that there is a limit within this range in the solid state for the PF8-DBT system, and the PF8-S copolymer system which is the subject of current study for the physics of charge-transfer dynamics.[2] This limit is important in situations where there is a wish to prevent beta phase formation, or if there is a wish to use the presence of the beta phase in conjunction with a co-monomer to enhance charge mobility.

7.3 Results

The first series of copolymers incorporate 0%, 8%, 12%, 15%, and 20% of dibenzothiophene (DBT) as a simple co-monomer unit, which is analogous to the fluorene unit but with a sulphur atom at the 9 position and no side chains present (the un-substituted fluorene unit is not sufficiently soluble to create high molecular weight copolymers for study). This series of polymers is useful since the DBT unit does not induce any modifications of the normal energy levels of the PF8 system, which may hide the changes to the optical spectra by the beta phase chain conformation, especially at higher concentrations of co-monomer where only small spectral changes are expected from low fractions of beta phase.

Random copolymers of poly(9,9-dioctylfluorene) (PF8) with 0%, 2%, 5%, 8%, 12% and 15% with the co-monomer dibenzothiophene-S,S-dioxide were also synthesised by the chemistry department at Durham University. Copolymer film samples were spun from warm solution producing clear colourless amorphous films with a peak optical density of approximately 0.3. The films were then exposed to toluene vapour for 15 minutes to attempt to induce the beta phase.

7.3.1 PF8-DBT copolymers

The area-normalised absorption spectra of the PF8-DBT copolymers after toluene vapour treatment are shown in figure 7-2a. The as-spun films all give the same absorption spectrum, which approximately overlays the trace of the 20% DBT copolymer. Upon vapour treatment, the resulting films give absorption spectra that show a clear trend of smoothly decreasing beta phase content which can be formed in these films as the fraction of DBT is increased.

These spectra were further analysed by multiple-peak fitting, as described in chapter 4.4.1. The beta phase fractions derived from the peak fitting are plotted in Figure 7-2b. There is a clear linear reduction in the fraction of beta phase formed by vapour treatment, with the 20% showing that almost no beta phase is formed. This is supported by the emission spectra in figure 7-2c, where the emission spectra are characteristic of the beta phase of PF8 for all the films up to 15%, and in the 20% sample there is evidence of trace amounts of beta phase from a small peak in the emission at 440 nm.

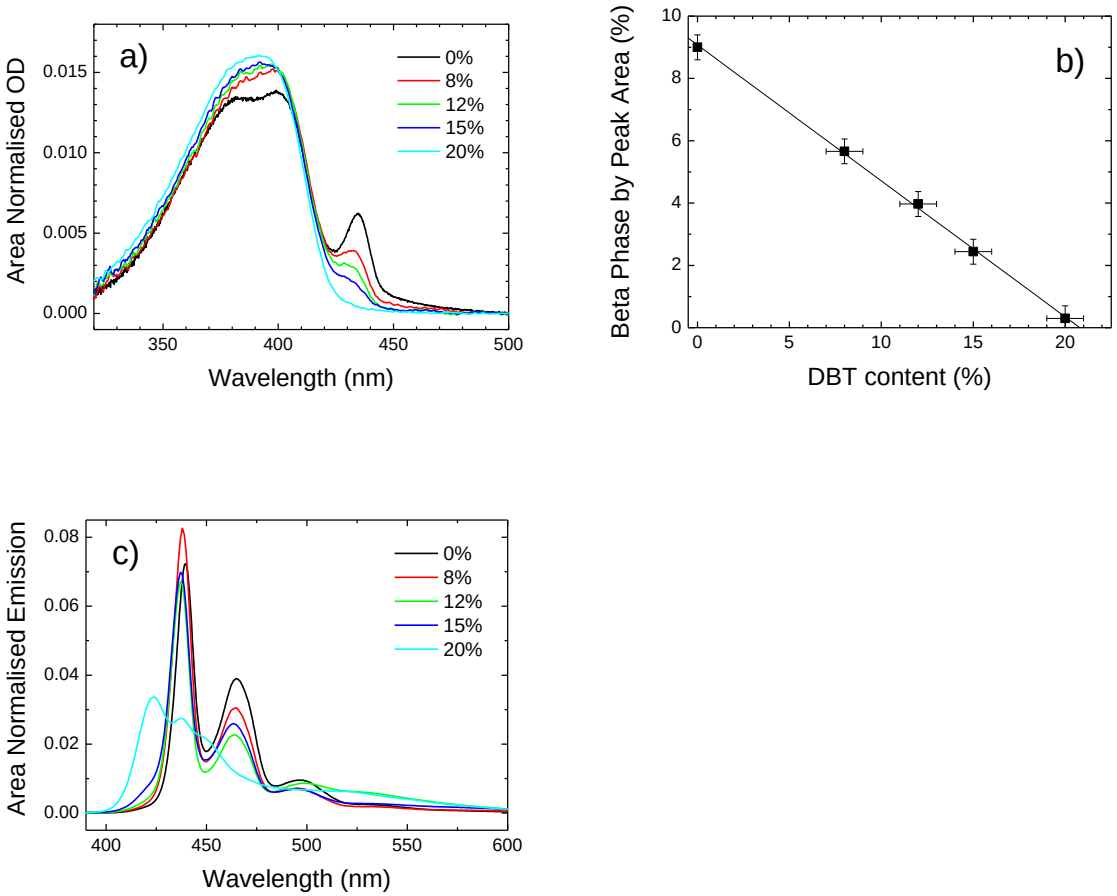

Figure 7-2: a) Absorption of the PF8-DBT copolymer films (content of DBT unit marked) for toluene vapour exposed films. The traces of the as-spun films (not shown) follow the spectrum of the 20% film. b) Beta phase by area of the fitted beta phase peak as a function of DBT co-momomer with a linear fit. c) Area normalized emission spectra of the same samples shown in a).

7.3.2 Modelling of the Beta Phase Cut-Off Limit and Conjugation Length

The conjugation length of the beta phase is not known. It has been estimated approximately as 30±12 monomer units by Tsoi et al.[13] using samples of different lengths of oligomers. However, the samples measured were not mono-disperse, and the uncertainty in the method is significant. By modelling the cut-off DBT fraction, this conjugation length can be approximated by making the assumption that the beta phase requires a continuous segment of F8 units across an entire conjugated region.

For a molecular weight M_w of 100 kDa, the average monomer will reside in a chain length of approximately 250 units. A copolymer chain of *n*=170 monomers in length is modelled using Bernoulli statistics; each monomer in the chain is either F8 or DBT, with the probability *p* of it being a DBT monomer given by the concentration of the random co-monomer in the sample. The Binomial distribution is then employed to calculate the probability that the chain contains a certain number *X* of DBT units according to equation 7-1.

$$p(x = X) = \binom{n}{X} p^X (1-p)^{n-X} \qquad X \in (0,1,2,\dots n) \tag{7-1}$$

The value of *n* used in this model is limited by the use of the factorial functions in calculating the number of combinations of each value of *X*, which exceeds the range of double-precision numbers ($>10^{308}$) at $n > 170$. The distribution *p(x)* peaks at a value determined by the DBT unit concentration, *p*, shown for example in figure 7-3a for $n = 170$, $p = 0.10$. For each value *x* of monomers in the modelled chain, the DBT units therein will be separated on average by a distance <*s*>, plotted in 7-3b. For each value of $X > 2$, the "expectation" value of the separation between monomer units can be calculated simply as $\langle s \rangle = 170 / X$ monomers. The parameter *s* takes values separated by large intervals at low *X*, and since the domain is discrete this leads to the rather quantised plot for larger values of <s> in figure 7-3b. The total of the probabilities for the cases where <*s*> is greater than *A* (where *A* is the conjugation length) can then be summed.

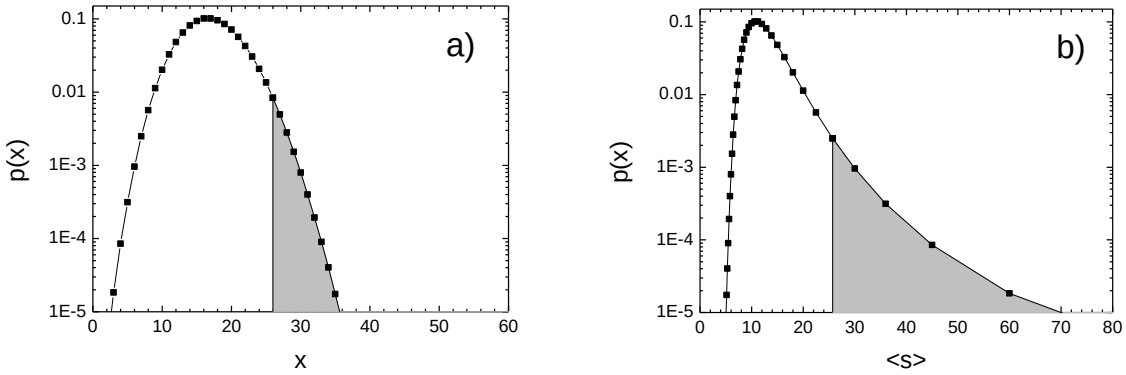

Figure 7-3: a) Binomial distribution *p(x)* for *n*=170, *p*=0.10 using equation 7-2, showing the probability p(*x*>26) as a filled area, and b) the same distribution plotted against the expectation value *s* (the number of F8 monomers separating the DBT units). The shaded area in b) is the fraction of chains in a 10% DBT content sample of chains of length 170 units that have 26 or more F8 units in a continuous sequence (0.39%).

By iterating this calculation of *p(s>A)* for an array of values of *A* and *p*, an area plot of the dependence of the fraction of chains greater than an arbitrary conjugation length can be built up. This is shown in figure 7-4, where the experimentally measured cut-off concentration is marked. The minimum beta phase fraction that can be experimentally resolved in the absorption spectrum is estimated at 0.5%, which indicates an estimated conjugation length of 9±1 monomer units. This is significantly shorter than the estimated value of 30±12 mentioned earlier, but is close to the persistence length of fully dissolved PF8 "worm-like" chains in toluene solution of around 9 nm.[14-15] This may indicate that the significant polydispersity of the samples used by Tsio et al. affected their measurement, or equally that there are inaccurate assumptions in the model. Inaccuracy in the model is likely to occur from: assuming a single DBT monomer will inhibit beta phase formation, not taking into account a distribution of values of *s* resulting from each number of DBT units in the chain, or from the consideration of only one chain length.

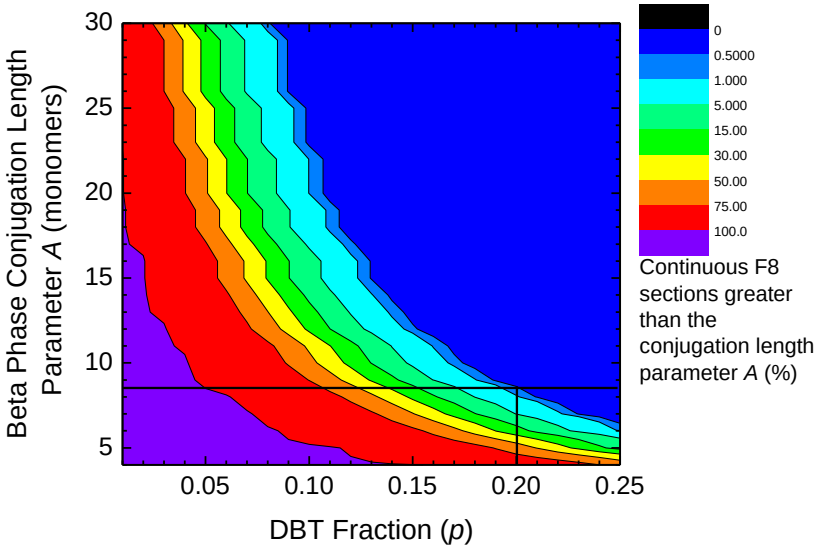

Figure 7-4: Area plot of *p(s>A)* for a range of values of *A* and *p*, showing that the experimentally determined cut-off value of *p*=0.2 corresponds to a value of *A*= 9±1 monomer units for a beta phase content detection limit in the absorption spectrum of 0.5%.

7.3.3 PF8-S Copolymers

The normalised absorption spectra of the S-unit copolymers in as-spun films and vapour treated films are shown in Figure 7-5 (the traces are offset for clarity). Two trends are found in the series of films; the absorption band of the as-spun films becomes broader and slightly red-shifted with increasing S unit content, and the characteristic absorption band of the beta phase at 435 nm ceases to be induced by vapour treatment at an S unit concentration between 8% and 12%. It can be seen that there is still a change in the absorption spectrum at these higher concentrations, but it is more similar to the main band structure observed previously in poly(9,9-di-n-hexylfluorene) (PF6) when it aggregates and becomes more ordered.[11, 16] There is sufficient broadening in the absorption band that it is uncertain at which S unit concentration the beta phase is formed. Given the result found for the DBT copolymers, it is likely that there is a small fraction of beta phase formed in the 12% S unit

copolymer but that the characteristic spectral shifts are hidden by the CT state. This also prevents the fitting of these spectra in the manner used for the PF8-DBT copolymers.

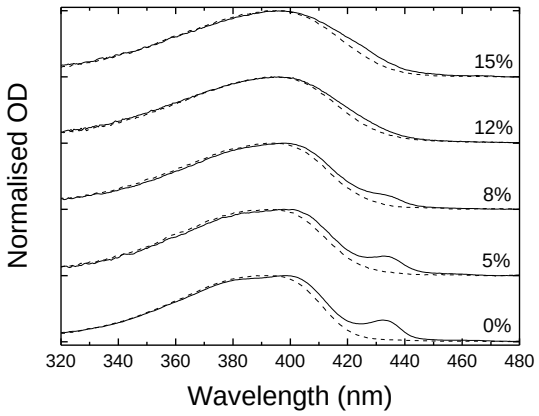

Figure 7-5: Absorption of the PF8-S copolymer films (co-monomer content marked) for amorphous (dashed line) and toluene vapour exposed films (solid line). The 2% film is excluded for clarity but follows the trend shown. Traces are offset.

In chapter 4 and previous work,[16-17] x-ray and optical experiments showed that similarly structured aggregates are formed in concentrated solutions of polyfluorenes with two linear alkyl side chains of 6, 7, 8 and 9 carbons. In the case of PF6 the aggregates are present but PF6 does not form the beta phase: the characteristic spectral changes are not observed. It was proposed that the side chain interactions provided the necessary energy to overcome the steric hindrance of the fluorene units, and that insufficient side chain length was the cause of this failure to planarise the backbone once the same structured aggregates have been formed. A similar cause is at work here for PF8-DBT and PF8-S, and that there are insufficient side chain interactions within each chromophore due to fewer side chains being present as the DBT or S content increases. As a result, the polymer backbone does not become fully planarised.

The earlier work (mentioned previously) by Knaapila et al. on solutions of PF8-F2/6 copolymers in a poor solvent predicted that there is an upper limit of ca. 10% F2/6 co-monomer content that enables

beta phase formation to occur.[12] They found that gelation, characteristic of beta phase formation in moderate concentrations of solution, occurred in copolymers of PF8-PF2/6 at 5% and 10% PF2/6 but not for 50%. They presented an in-depth theoretical description taking into account free energy changes, phase transition temperatures and polymer-solvent de-mixing. The finding of a similar limit in PF8-S copolymers may have been unexpected, as the theoretical description of Knaapila et al. was limited to the case of solutions only, and the polar S-unit may also be expected to interfere with the side chain interactions of the F8 monomer needed to planarise the polyfluorene backbone and form the beta phase.

It is possible that the solvent vapour treatment method used here to induce the beta phase may be responsible for the similar results. The presence of a high concentration of solvent molecules in the film during the swelling process makes it possible that similar energetic considerations are applicable during the beta phase formation, although greater physical constraint will restrict the chain rearrangement in the film.

The photoluminescence spectra of the same films are presented in figure 7-6a (amorphous films) and b (vapour treated films). The emission in the amorphous films is far more easily influenced by the presence of the polar S-unit as the spectral change is continuous for the amorphous films. Indeed, in films with 30% S-unit content, a charge-transfer state is the dominant species at room temperature.[10]

The charge transfer state is produced from the separation of the exciton charges by the polarity of the S-units, and the charge-transfer exciton energy level is significantly lower than the Frenkel exciton level. Large variations in local molecular environment and a lack of fixed electron-hole separation produced by the polar monomer units also leads to a broad density of states, producing a broad featureless emission band that quenches the polyfluorene emission at 30% S-unit concentration.[10] The absorption bands of the F8 and S units overlap, making Förster transfer

between them unlikely, and the electron is directly excited into either an exciton state or a charge transfer state depending upon the local environment.[9-10]

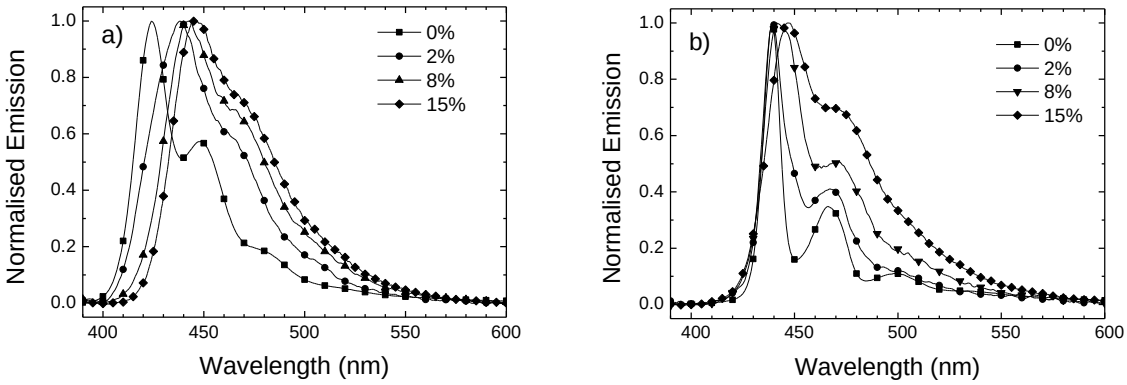

Figure 7-6: Photoluminescence spectra of the 0%, 2%, 8% and 15% copolymer films excited at 380nm, showing the smooth change in the emission for amorphous films (a) and beta phase films (b). The 5% and 12% films are excluded for clarity but follow the trends shown.

The spectra of 2%, 5%, and 8% toluene treated copolymer films show a smooth shift to an emission peak at 448 nm that is the peak emission wavelength of the 15% copolymer, which is also the peak wavelength of the broad charge transfer emission band that appears at 30% S-unit concentration.[10] The presence of the beta phase, which is itself a low-energy trap, inhibits the charge transfer emission even at 8% S-unit content, and the emission is spectrally narrowed and retains sharp well-resolved vibronic replicas characteristic of the beta phase emission. The gradual loss of spectral narrowing with increasing S-unit concentrations is attributed to the lower beta phase content for these films.

For the vapour treated films, the emission spectrum shifts with increasing S-unit content are far less significant, but when comparing the effect of inducing the beta phase for a fixed S-unit concentration from figure 7-6a to b, in every case there is a significant sharpening of the vibronic

replicas, indicating an increase in the ordering of the polymer chains in every case where vapour treatment is applied to these films.

In conjunction with the work presented in the earlier chapters, it is proposed that at F8 unit concentrations of less than about 85% there are not enough side chain interactions per chromophore to overcome the steric hindrance of the adjacent fluorene units and planarise the polymer backbone. The increasing fraction of co-monomers reduces the number of sections of continuous F8 units greater than or equal to the conjugation length of the beta phase, eventually preventing its formation.

Photoluminescence from the vapour treated films at all S-unit concentrations with excitation at 434 nm (not shown) are identical to the results in figure 7-6b, showing that when the samples are excited at 380 nm on the main absorption band of the amorphous polymer, there is a similar fraction of electrons excited into either an exciton state or a charge transfer state.

7.4 Conclusions

It has been demonstrated for PF8-DBT and PF8-S copolymer systems, which are used in current investigations into white LEDs and charge-transfer states, the formation of the beta phase can be achieved for copolymers with up to 20% of DBT or 12% S units in the chain. The fraction of beta phase formed also decreases linearly with increasing co-monomer content. This is in agreement with theoretical and experimental results for MCH solutions of PF8 copolymers incorporating F2/6 co-monomers studied by Knaapila et al.[11] This may due to F8 unit incorporation ratios of less than approximately 80% providing insufficient side chain interactions per chromophore to overcome the steric hindrance of the adjacent fluorene units, which is a requirement for planarising the polymer backbone. These new results may point to the universality of this limit, indicative of a trade-off between the specific side chain interactions which favour the beta phase and thermal disruption of this highly ordered phase. These results contribute to the understanding of the factors which control morphological states in polyfluorenes and provide guidelines for the design of new PF8 copolymers

with tailored structural hierarchy and emissive properties. A statistical model of the DBT units in the polymer chains is used with the measured beta phase cut-off limit of 20% DBT content to estimate a beta phase conjugation length of 9±1 monomer units, which is significantly shorter than an earlier estimate value of 30±12 monomers, but the same as the persistence length of PF8 in toluene at 9nm or 9-10 monomer units.

7.5 References

1. Leclerc, M. *J. Polym. Sci. A-Polym. Chem.* **2001,** 39, (17), 2867-2873.
2. Dias, F. B.; Kamtekar, K. T.; Cazati, T.; Williams, G.; Bryce, M. R.; Monkman, A. P. *ChemPhysChem* **2009,** 10, (12), 2096-2104.
3. Wu, H. B.; Ying, L.; Yang, W.; Cao, Y. *Chem. Soc. Rev.* **2009,** 38, (12), 3391-3400.
4. Niu, X. D.; Liu, J. B.; Xie, Z. Y. *Organ. Electron.* **2010,** 11, (7), 1273-1276.
5. Lu, H. H.; Liu, C. Y.; Chang, C. H.; Chen, S. A. *Adv. Mater.* **2007,** 19, (18), 2574.
6. Lee, S. K.; Ahn, T.; Park, J. H.; Jung, Y. K.; Chung, D. S.; Park, C. E.; Shim, H. K. *J. Mater. Chem.* **2009,** 19, (38), 7062-7069.
7. Perepichka, I. I.; Perepichka, I. F.; Bryce, M. R.; Palsson, L.-O. *Chem. Commun.* **2005**, (27), 3397-3399.
8. Li, H.; Batsanov, A. S.; Moss, K. C.; Vaughan, H. L.; Dias, F. B.; Kamtekar, K. T.; Bryce, M. R.; Monkman, A. P. *Chem. Commun.* **2010,** 46, (26), 4812-4814.
9. Dias, F. B.; Pollock, S.; Hedley, G.; Palsson, L. O.; Monkman, A.; Perepichka, II; Perepichka, I. F.; Tavasli, M.; Bryce, M. R. *J. Phys. Chem. B* **2006,** 110, (39), 19329-19339.
10. Dias, F. B.; King, S.; Monkman, A. P.; Perepichka, II; Kryuchkov, M. A.; Perepichka, I. F.; Bryce, M. R. *J. Phys. Chem. B* **2008,** 112, (21), 6557-6566.
11. King, S. M.; Perepichka, II; Perepichka, I. F.; Dias, F. B.; Bryce, M. R.; Monkman, A. P. *Adv. Funct. Mater.* **2009,** 19, (4), 586-591.
12. Knaapila, M.; Stepanyan, R.; Torkkeli, M.; Garamus, V. M.; Galbrecht, F.; Nehls, B. S.; Preis, E.; Scherf, U.; Monkman, A. R. *Phys. Rev. E* **2008,** 77, (5), 14.
13. Tsoi, W. C.; Charas, A.; Cadby, A. J.; Khalil, G.; Adawi, A. M.; Iraqi, A.; Hunt, B.; Morgado, J.; Lidzey, D. E. *Adv. Funct. Mater.* **2008,** 18, 600-606.
14. Grell, M.; Bradley, D. D. C.; Long, X.; Chamberlain, T.; Inbasekaran, M.; Woo, E. P.; Soliman, M. *Acta Polym.* **1998,** 49, (8), 439-444.
15. Chen, J. H.; Chang, C. S.; Chang, Y. X.; Chen, C. Y.; Chen, H. L.; Chen, S. A. *Macromol.* **2009,** 42, (4), 1306-1314.
16. Bright, D. W.; Dias, F. B.; Galbrecht, F.; Scherf, U.; Monkman, A. P. *Adv. Funct. Mater.* **2009,** 19, (1), 67-73.
17. Knaapila, M.; Dias, F. B.; Garamus, V. M.; Almasy, L.; Torkkeli, M.; Leppanen, K.; Galbrecht, F.; Preis, E.; Burrows, H. D.; Scherf, U.; Monkman, A. P. *Macromol.* **2007,** 26, 9398 -9405.

8 Conclusions

Chapter 4 presents the results of temperature dependent absorption spectra of PF6 to PF10 in MCH at around 5 µg mL^{-1} along with the emission and excitation spectra of very dilute solutions in the range of 10 µg mL^{-1} over time after returning to room temperature from low temperature. These results show the trend in beta phase formation as a function of side chain length, with no beta phase in PF6, slight evidence for beta phase formation in PF7, optimal beta phase content in PF8 and a decreasing fraction being formed in PF9 and PF10. The results make clear that the beta phase formation process is distinct from simple aggregation driven by changes in solubility across the group, as the heavily aggregating PF6 does not form the beta phase, whilst also showing that the 410nm peak that has been associated with the beta phase is the result of aggregation, but not of beta phase formation. It is proposed that the mechanism of beta phase formation is therefore driven by side chain interactions, where van der Waals interactions between the alkyl chains provide the energy to planarise the polymer backbone, and that the shorter alkyl chains of PF6 do not provide sufficient energy to complete the process despite strong aggregation. Alkyl chains longer than PF8 are less able to form the beta phase in MCH solution because the increasing solubility reduces the extent of aggregation and the longer, more disordered side chains are less likely to form the ordered interacting domains of polymer chains that lead to the formation of the beta phase. The spectra of the dilute solutions show that chain folding in poor solvents can also provide the necessary interactions to form the beta phase. Analysis of the absorption spectra shows a trend of lower transition temperatures with increasing side chain lengths for PF8 to PF10, indicating the effect of increasing solubility. The aggregation model of Dias et al. is applied to PF8, PF9 and F10 but the data does not produce convincing results, although the derived enthalpy change is within the range of realistic values for PF8.

Chapter 5 shows optical spectra of thin films of PF6 to PF10 after thermal cycling and toluene vapour exposure. The thin films show a similar trend in beta phase formation tendency as the solutions in MCH of chapter 4. This indicates that the beta phase is still dependent upon a similar mechanism for beta phase formation in the solid state, where side chain interdigitation is required to drive the polymer backbone planarization. This adds to the currently held concept that the phase change is driven only by local strain, induced by either the differences in thermal expansion coefficients of the polymer and substrate acting during thermal cycling, or by the film swelling during solvent exposure. This data shows that the strain effects may instead induce changes in the ordering of the polymer chains in the film, but that side chain interactions are still necessary for beta phase formation. The PF8 is again shown to be the optimal side chain length, and in the solid state it is proposed that the reduction in beta phase formation tendency is limited in the longer side chain polymers by the more difficult requirements of polymer chain rearrangement for longer side chains within the confines of a solid film. Finally, site-selective PL spectra of the films at 11 K are deconvolved to characterise the beta phase formed in PF7 to PF10, showing that in all cases similar dominant vibrational modes are produced, and also that the PF6 does not show the narrow linewidth or resolved vibronic bands that occur in the other polymers.

Chapter 6 uses steady state spectra and TCSPC to investigate the effect of the keto defect on the emission of beta phase in PF8. A series of films with known concentrations of keto monomer incorporated into random copolymers, with impurity-level concentrations in the range 0.05% to 2% show in the emission spectra a clear variation in the emission peak quenching ratio as a function of keto content. This fits accurately to a -1 power law on a double-logarithmic plot for both the alpha phase and beta phase films with respect to keto content, equating to a -3 power law with separation between the keto defects. This is clearly in contrast to the -6 power law expected for Förster transfer or the exponential variation expected for Dexter transfer, so it is proposed that the energy transfer process is migration limited. This is confirmed by temperature dependent emission spectra that show a sharp reduction in keto emission at lower temperatures, confirming the migration-limited

transfer step. Global fitting of the TCSPC emission decays was used to derive up to 4 lifetime components for a series of alpha and beta phase samples with the same keto content as the steady state measurements. The results show low amplitude short lifetime components that show Forster transfer taking place from alpha phase to beta phase chromophores, as well as some transfer from beta phase chromophores to keto defects. The more dominant effect is a quenching of the fluorescence lifetime that increases with keto content, which is reduced at low temperature again confirming its migration-mediated origin. A scheme for the exciton migration within a PF8 alpha-beta keto system is proposed, where energy transfer from the alpha phase to the beta phase dominates over energy transfer from the alpha phase to keto. Energy transfer to the beta phase is followed by migration from the beta phase to keto. The presence of a migration controlled step confirms the presence of beta phase domains rather than isolated chains, a result which is again consistent with a side-chain driven process for beta phase formation.

Chapter 7 provides absorption and emission spectra of two series of PF8-based copolymers to examine the limit of co-monomer content at which beta phase can be formed. Thin films of PF8-DBT copolymers with 0%, 8%, 12%, 15% and 20% show a clear trend of decreasing beta phase being formed after being saturated with toluene vapour, with only traces of beta phase being formed at 20% co-monomer. Spectral deconvolution to derive the beta phase content yields a clear linear decrease of beta phase content with increasing DBT monomer, a result which is consistent with the side-chain driven model of beta phase formation. Reducing the octyl side chain density along the polymer chain reduces the number of conjugated chain segments which have sufficient side chain interactions to drive the polymer backbone planarization. The distribution of DBT units within the polymer chain was modelled to find the conjugation length of the beta phase chromophore, giving a value of 9±1 monomers, which is significantly shorter than a published value of 30±12 monomers but the same as the persistence length of alpha phase PF8 in toluene of 9-10 monomer units. Optical spectra were then measured for thin films of PF8 copolymers with 5%, 8%, 12% and 15% S-unit content, which is a co-monomer of current research interest to investigate charge-transfer states.

These films show a similar reduction in beta phase formation with increasing co-monomer, but the gradual encroachment of the charge-transfer state makes it difficult to either deconvolve the absorption spectra or to be certain of the point at which the beta phase is no longer being formed.

These results together show a consistent picture of beta phase formation driven by the interactions between the alkyl side chains, in both solution and solid state. This adds to the fundamental understanding of how this phase change occurs, and demonstrates that the beta phase can be induced in a wide range of copolymer systems being researched for more efficient PLED devices, both in the areas of blue emitters for display pixels and for white-light emitting devices.